ULTIMA Computing

Jurnal Sistem Komputer

RICHAT PAHLEPI, SANTOSO SOEKIRNO, HARYAS SUBYANTARA WICAKSANA

Solar Radiation Intensity Imputation in Pyranometer of Automatic Weather Station Based on Long Short Term Memory

BAYU SANTOSO, MUHAMMAD RYAN, HARYAS SUBYANTARA WICAKSANA, NAUFAL ANANDA, IRVAN BUDIAWAN, FAQIHZA MUKHLISH, DEDDY KURNIADI

Predictive Maintenance: Automatic Weather Station Sensors Error Detection using Long Short-Term Memory

ANDRIAN KHARISMA WIJAYA, ANDINI SINTAWATI

An Automatic Internet Of Things-Based System For Breeding Rabbit in Cage

MEGANTARA PURA, CHARLES H. LANGKO, JASON KHO

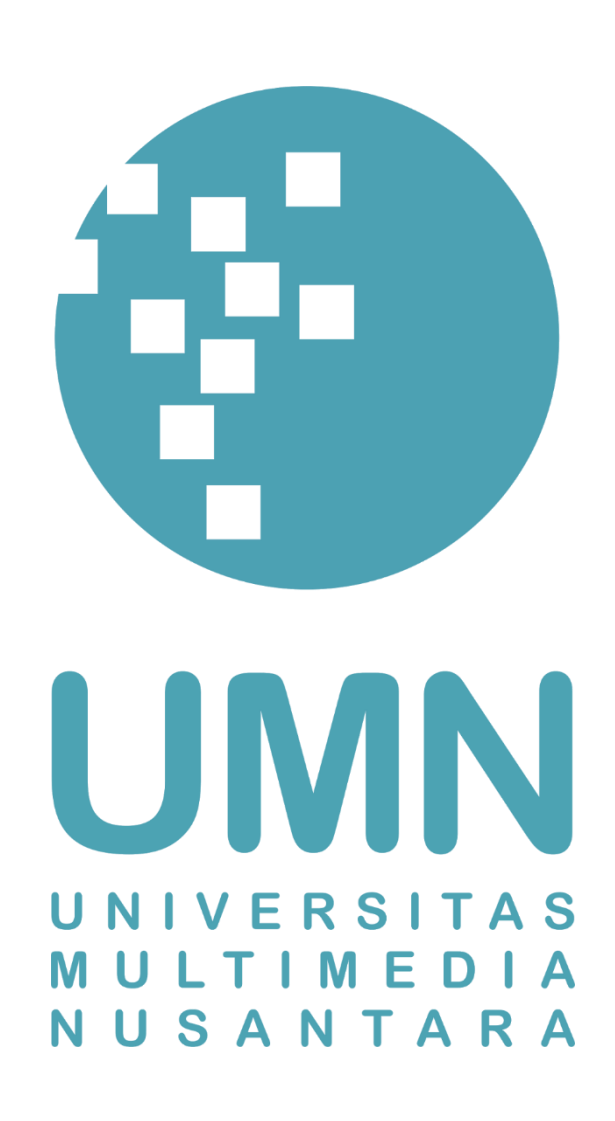
Automatic Mass Waste Sorting System Using Inductive Proximity Sensor, Water Level Sensor and Image Processing using MobileNet Algorithm

INDAH RADITYO PUTRI, ESTIYANTI EKAWATI, EKO MURSITO BUDI, ALFISENA JUWANDANA, NAUFAN AUREZAN MULYAWAN, PHILIP INARTA KHO, KOMARUDIN KUDIYA

Trajectory Planning of Spherical Pendulum Pattern for Application in Creating Batik Patterns

MONICA PRATIWI

EEG-Based Depression Detection in the Prefrontal Cortex Lobe using mRMR Feature Selection and Bidirectional LSTM



EDITORIAL BOARD

Editor-in-Chief

M.B.Nugraha, S.T., M.T.

Managing Editor

Megantara Pura, S.T., M.T. Nabila Husna Shabrina, S.T., M.T. Monica Pratiwi, S.S.T., M.T. Fakhruddin M., S.T., M.T. (Undip) Dede Furqon N., S.T., M.T. (Unjani) Imam Taufiqurrahman, S.Pd., M.T. (Unsil) Iqbal Ahmad Dahlan, S.T., M.T. (Unhan)

Designer & LayouterDimas Farid Arief Putra

Members

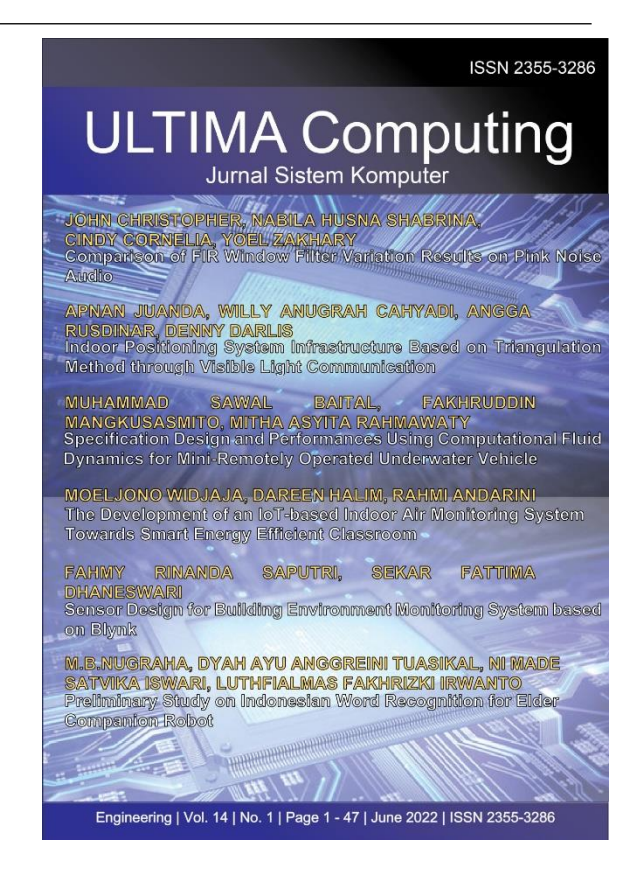
Dista Yoel Tadeus, S.T., M.T. (Undip)
Denny Darlis, S.Si., M.T. (Telkom University)
Ariana Tulus Purnomo, Ph.D. (NTUST)
Silmi At Thahirah, S.T., M.T. (UPI)
Nurul Fahmi Arief Hakim, S.Pd., M.T. (UPI)
Moeljono Widjaja, Ph.D. (UMN)
Dareen Halim, S.T., M.Sc. (UMN)
Fenina Adline Twince Tobing, M.Kom. (UMN)
Ahmad Syahril Muharom, S.Pd., M.T. (UMN)
Samuel Hutagalung, M.T.I (UMN)

EDITORIAL ADDRESS

Universitas Multimedia Nusantara (UMN)
Jl. Scientia Boulevard
Gading Serpong
Tangerang, Banten - 15811
Indonesia
Phone. (021) 5422 0808

Email: ultimacomputing@umn.ac.id

Fax. (021) 5422 0800



Ultima Computing: Jurnal Sistem Komputer is a Journal of Computer Engineering Study Program, Universitas Multimedia Nusantara which presents scientific research articles in the field of Computer Engineering and Electrical Engineering as well as current theoretical and practical issues, including Edge Computing, Internet-of-Things, Embedded Systems, Robotics, Control System, Network and Communication, System Integration, as well as other topics in the field of Computer Engineering and Electrical Engineering. The Ultima Computing: Jurnal Sistem Komputer is published regularly twice a year (June and December) and is jointly managed by the Computer Engineering and Electrical Engineering Study Program at Universitas Multimedia Nusantara.

Call for Papers



International Journal of New Media Technology (IJNMT) is a scholarly open access, peer-reviewed, and interdisciplinary journal focusing on theories, methods and implementations of new media technology. Topics include, but not limited to digital technology for creative industry, infrastructure technology, computing communication and networking, signal and image processing, intelligent system, control and embedded system, mobile and web based system, and robotics. IJNMT is published twice a year by Faculty of Engineering and Informatics of Universitas Multimedia Nusantara in cooperation with UMN Press.



Jurnal Informatika is the Journal of the Informatics Study Program Universitas Multimedia Nusantara which presents scientific research articles in the fields of Analysis and Design of Algorithm, Software Engineering, System and Network security, as well as the latest theoretical and practical issues, including Ubiquitous and Mobile Computing, Artificial Intelligence and Machine Learning, Algorithm Theory. World Wide Web, Cryptography, as well as other topics in the field of Informatics.



Ultima Computing: Jurnal Sistem Komputer is a Journal of Computer Engineering Study Program, Universitas Multimedia Nusantara which presents scientific research articles in the field of Computer Engineering and Electrical Engineering as well as current theoretical and practical issues, including Edge Computing, Internetof-Things, Embedded Systems, Robotics, Control System, Network and Communication, System Integration, as well as other topics in the field of Computer Engineering and Electrical Engineering.



Ultima InfoSvs : Jurnal Ilmu Sistem Informasi is a Journal of Information Systems Study Program at Universitas Multimedia Nusantara which presents scientific research articles in the field of Information Systems, as well as the latest theoretical and practical issues, including database systems, management information systems, system analysis and development, svstem project management information, programming, mobile information system, and other topics related to Information Systems.

FOREWORD

ULTIMA Greetings!

Ultima Computing: Jurnal Sistem Komputer is a Journal of Computer Engineering and Electrical Engineering at Multimedia Nusantara University which presents scientific research articles in the field of Computer Systems as well as the latest theoretical and practical issues, including Edge Computing, Internet-of-Things, Embedded Systems, Robotics, Control Systems, Network and Communication, System Integration, and other topics in the field of Computer Engineering and Electrical Engineering.

In this December 2023 edition, Ultima Computing enters the 2nd Edition of Volume 15. In this edition there are six scientific papers from researchers, academics and practitioners in the fields of Computer Engineering and Electrical Engineering. Some of the topics raised in this journal are: Solar Radiation Intensity Imputation in Pyranometer of Automatic Weather Station Based on Long Short Term Memory, Predictive Maintenance: Automatic Weather Station Sensors Error Detection using Long Short-Term Memory, An Automatic Internet Of Things-Based System For Breeding Rabbit in Cage, Automatic Mass Waste Sorting System Using Inductive Proximity Sensor, Water Level Sensor and Image Processing using MobileNet Algorithm, Trajectory Planning of Spherical Pendulum Pattern for Application in Creating Batik Patterns and EEG-Based Depression Detection in the Prefrontal Cortex Lobe using mRMR Feature Selection and Bidirectional LSTM.

On this occasion we would also like to invite the participation of our dear readers, researchers, academics, and practitioners, in the field of Engineering and Informatics, to submit quality scientific papers to: International Journal of New Media Technology (IJNMT), Ultimatics: Jurnal Teknik Informatics, Ultima Infosys: Journal of Information Systems and Ultima Computing: Journal of Computer Systems. Information regarding writing guidelines and templates, as well as other related information can be obtained through the email address ultimacomputing@umn.ac.id and the web page of our Journal here.

Finally, we would like to thank all contributors to this December 2023 Edition of Ultima Computing. We hope that scientific articles from research in this journal can be useful and contribute to the development of research and science in Indonesia.

December 2023,

M.B.Nugraha, S.T., M.T. Editor-in-Chief

TABLE OF CONTENT

Solar Radiation Intensity Imputation in Pyranometer of Automatic Weather Station	
Based on Long Short Term Memory	
Richat Pahlepi, Santoso Soekirno, Haryas Subyantara Wicaksana	35-40
Predictive Maintenance: Automatic Weather Station Sensors Error Detection using	
Long Short-Term Memory	
Bayu Santoso, Muhammad Ryan, Haryas Subyantara Wicaksana, Naufal Ananda, Irvan	
Budiawan, Faqihza Mukhlish, Deddy Kurniadi	41-51
An Automatic Internet Of Things-Based System For Breeding Rabbit in Cage	
Andrian Kharisma Wijaya, Andini Sintawati	52-57
Automatic Mass Waste Sorting System Using Inductive Proximity Sensor, Water	
Level Sensor and Image Processing using MobileNet Algorithm	
Megantara Pura, Charles H. Langko, Jason Kho	58-64
Trajectory Planning of Spherical Pendulum Pattern for Application in Creating	
Batik Patterns	
Indah Radityo Putri, Estiyanti Ekawati, Eko Mursito Budi, Alfisena Juwandana, Naufan	
Aurezan Mulyawan, Philip Inarta Kho, Komarudin Kudiya	65-70
EEG-Based Depression Detection in the Prefrontal Cortex Lobe using mRMR Feature	
Selection and Bidirectional LSTM Monica Pratiwi	71-78
Wionica Fratiwi	,1 ,0

Solar Radiation Intensity Imputation in Pyranometer of Automatic Weather Station Based on Long Short Term Memory

Richat Pahlepi^{1,3}, Santoso Soekirno¹, Haryas Subyantara Wicaksana^{2,4}

¹Department of Physics, Faculty of Mathematics and Science, Universitas Indonesia, Depok, Indonesia

²Faculty of Industrial Technology, Institut Teknologi Bandung, Bandung, Indonesia

³Climatology Station of West Java, BMKG, Bogor, Indonesia

⁴Center of Instrumentation, Calibration and Engineering, BMKG, Jakarta, Indonesia

¹richat.pahlepi@ui.ac.id, ²santoso.s@sci.ui.ac.id, ³haryas.wicaksana@bmkg.go.id

Accepted on 17 October 2023 Approved on 06 November 2023

Automatic Weather Station experienced problems in the form of component damage and communication system failure, resulting in incomplete parameter data. Component damage also occurs in pyranometers. Decreased pyranometer performance results in deviations, uncertainty in measuring solar radiation intensity, and data gaps. Data imputation is one solution to minimize measurement deviations and the occurrence of missing AWS pyranometer data. This research aims to design and analyze the accuracy performance of the multisite AWS pyranometer solar radiation intensity data imputation model when a data gap occurs. This research attempts to utilize the spatio-temporal relationship of multisite AWS solar radiation intensity in the imputation model. Long-Short Term Memory (LSTM) algorithm is used as an estimator in the multisite AWS pyranometer network. Data imputation modeling stage includes data collection, data pre-processing, creating missing data scenarios, LSTM design and model testing. Overall, LSTM-based imputation model has ability of filling gap data on AWS Cikancung pyranometer with maximum missing sequence of 12 hours. Imputation model has MAPE 1.76% - 5.26% for missing duration 30 minutes-12 hours. It still it meet World Meteorological Organization (WMO) requirement for solar radiation intensity measurement with mean absolute percentage error (MAPE) < 8%.

Index Terms— imputation; pyranometer; Long Short Term Memory

I. INTRODUCTION

Solar radiation is electromagnetic energy emitted by the sun as a result of nuclear fusion in the sun's core. Solar radiation is one of the elements of weather and climate. Solar radiation parameter measurements are mainly used in seasonal forecast modeling [1]. Apart from that, measuring this parameter is also useful for the energy, architecture, astronomy and environmental sectors. Almost all companies and manufacturers related to solar power generation use solar radiation measurement data to plan generating system mechanisms [2].

Shortwave solar radiation with a spectrum range from 290 to 3000 nm. One of automatic digital instruments for measuring shortwave solar radiation is pyranometer. Pyranometers use photodiode or thermophile type sensors [3]. This instrument is installed on the Automatic Weather Station (AWS) and Automatic Solar Radiation Station (ASRS) [4]. Photodiode type pyranometers use photodiodes to detect the intensity of sunlight. Photodiodes convert changes in light intensity values into changes in electric current values. Thermophile type pyranometer uses a thermophile detector. Thermophile element is able to convert changes in temperature values into changes in electrical voltage values. The thermophile consists of a black layer and a reference layer [5].

The decline in pyranometer performance is characterized by degradation changes in sensor sensitivity values. Degradation of pyranometer sensitivity is caused by drift of internal components, leveling shifts, changes in spectral response, presence of scratches, as well as installation environmental conditions [6]. Decreased pyranometer performance results in deviations, uncertainty in measuring solar radiation intensity, and data gaps. This reduces the accuracy of synoptic surface weather analyzes [7]. Imputation is able to minimize the occurrence of missing data on pyranometer.

Several previous studies have been carried out regarding the imputation of meteorological data including the intensity of solar radiation. Turrado et al. designed a model for estimating the intensity of solar radiation per 10 minutes using the Multivariate

Imputation by Chained Equation (MICE) algorithm based on the spatial links between 9 ground station pyranometers in Galicia, Spain [8]. This algorithm has an RMSE performance of 13.37% and is lower than multilinear regression and interpolation methods based on Inverse Distance Weighting (IDW).

Karaman et al. used Extreme Learning Machine (ELM) to estimate daily solar radiation with inputs including sun duration, air temperature and wind speed in Turkey [9]. This algorithm shows better performance than ANN with an RMSE of 0.0297 kJ/m². ELM also has a shorter computing time than ANN. Yamoah et al. applied the multilinear regression (MLR) method to impute hourly wind speed data. Regression predictor variables include temperature, humidity, air pressure and rainfall [10]. The multilinear regression method produces an average error of 2.38 m/s. This method has better performance than ARIMA and Kalman filter. The limitations of the methods are risks related to incomplete availability of multivariable inputs.

Previous studies have not involved spatial and temporal links simultaneously. This research attempts to utilize the spatio-temporal relationship of solar radiation intensity in the imputation model. Multisite AWS has advantages on imputes pyranometer data spatially. Long short term memory algorithm is chosen based on its capability of extracting long term temporal features on time series data [11].

II. DATA

Physical AWS pyranometer used for modeling is located in West Java Province. These sensors are spread across 3 AWS locations in Sumedang Regency and Tasikmalaya Regency. AWS locations include AWS Cipasung, AWS Cikancung and AWS Cimalaka. Figure 1 shows AWS pyranometer location map in the research area.



Fig. 1. Sites of AWS pyranometer

Figure 1 shows that all sites are covered adjacently area. Physical AWS pyranometer used for modeling is located in West Java Province. Table 1 describes site coordinates in more detail.

TABLE I. SITES COORDINATES

No	Site	Latitude	Longitude	Elevation
1	AWS Cikancung	-6,9988	107,8168	680 m
2	AWS Cimalaka	-6,8154	107,9475	545 m
3	AWS Cipasung	-7,3416	108,1280	417 m

Table 1 states study area based on label number of Figure 1 respectively. Variations in distance and elevation is possibly produce further analysis related to the results of spatial imputation model for the three pyranometer data [12]. AWS pyranometer data is generated and sent every 10 minutes. This data is collected from the BMKG Database Center via the BMKG AWS Center website. Three AWS pyranometers data was taken in the period 2021 – 2022.

III. METHODS

Imputation modeling stage includes literature study, data collection, data pre-processing, creating missing data scenarios, Long Short Term Memory (LSTM) design and model testing. Figure 2 shows imputation modeling flowchart.

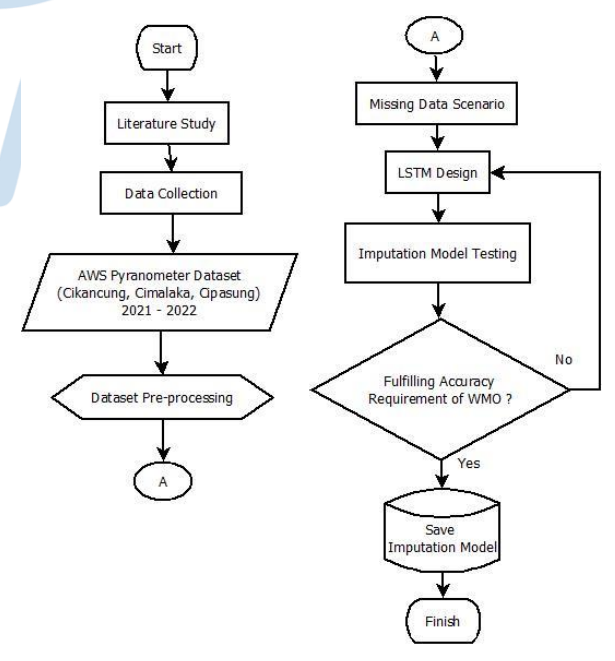


Fig. 2. Imputation Modeling Flowchart

Based on Figure 2, a literature study was carried out on literature reviews of previous research. Data collection is carried out by downloading AWS data on

Badan Meteotologi Klimatologi dan Geofisika (BMKG) Database Center page. Before the imputation model is designed, the dataset needs to be preprocessed to select well-qualified data. Missing data simulations were implemented on normal datasets. The imputation model is designed using LSTM algorithm, then tested on the missing data scenario that has been created. If the test imputation model does not meet the World Meteorological Organization (WMO) accuracy criteria, then the LSTM imputation model is redesigned until the accuracy criteria are achieved.

A. Dataset Pre-processing

Pre-processing functions to prepare modeling data. Data pre-processing was carried out to remove outliers in the AWS pyranometer raw data. Outliers are deviations from normal data values according to certain criteria.

Outliers are identified through data quality control (QC) based on range check and step check. Range check is checking data based on the historical range per parameter. If the data is not within the normal range, then it becomes suspect based on the range check. A normal range of solar radiation intensity data is 0-1500 W/m^2 [12].

Step check is a check based on the temporal relationship of current data to previous data. If the difference between the current data and previous data exceeds a certain threshold, then the data becomes suspect based on the step check [13]. Step check threshold value for solar radiation intensity data is that there is no change in the value exceeding 800 W/m² for a period of 5 minutes. Outliers are removed via a listwise deletion mechanism. Listwise deletion is the process of deleting all outlier data [14]. This mechanism is carried out at the three AWS pyranometer locations.

B. Missing Data Scenario

Missing data scenario is simulated to AWS Cikancung pyranometer data. AWS pyranometer dataset is only taken from 07.00 - 19.00 Local Time according to sunshine hours in Indonesia [15]. Pyranometer dataset on 2021-2022 is divided into two parts. The 2021 dataset is the imputation model data and the 2022 dataset is the test data. Missing data scenario is only carried out on the 2022 AWS pyranometer dataset. There are 5 missing data scenarios:

- i. For every 3 days, pyranometer data are missing for 30 minutes respectively;
- ii. For every 6 days, pyranometer data are missing for 60 minutes respectively;
- iii. For every 18 days, pyranometer data are missing for 3 hours respectively;

- iv. For every 36 days, pyranometer data are missing for 6 hours respectively;
- v. For every 72 days, pyranometer data are missing for 12 hours respectively.

All of these missing data are then saved as actual data for testing stage. These scenarios produces balance number of missing data. It purposes to perform imputation model on vary missing data possibilities in one day.

C. Imputation Model Based on LSTM

Imputation techniques fill in empty data based on available data using certain methods [16]. LSTM is one method of imputation technique. LSTM has a memory cell in each neuron. LSTM model consists of connections between cells in three gates: input gate, forget gate and output gate. Forget gate has a role to regulate flow of information, so that LSTM has management of cell memory [17]. Table II shows LSTM algorithm.

TABLE II. LSTM ALGORITHM

Input:	Input (x_t) , previous cell state (c_{t-1}) , and previous hidden state (s_{t-1})			
Output :	Current cell state (c_t) and current hidden state (s_t)			
1	Initialization $x,c_{t-1},s_{t-1} \rightarrow ReLU(x) = max(0,1)$			
2	n = epoch			
3	For $i = 0,1,n$, do:			
4	$f_t = \sigma(W_f.[s_{t-1}, x_t] + b_f)$			
5	$i_t = \sigma(W_f.[s_{t-1}, x_t] + b_i)$			
6	$c_t = \tanh(W_c. [s_{t-1}, x_t] + b_c)$			
7	$c_t = f_t * c_{t-1} + i_t * c_t$			
8	$o_t = \sigma(W_o.[s_{t-1}, x_t] + b_o)$			
9	$s_t = o_t * \tanh(c_t)$			
10	Calculate RMSE of c _t and c _{actual}			
11	End of iteration			

Design of LSTM-based imputation model aims to determine the structural configuration of LSTM algorithm. This design consists of preparation stages, data transformation, data segmentation, hyperparameter design, training and model validation. Model design uses the 2021 dataset.

Preparation stage for LSTM design is determining input and output of the model. Imputation of AWS pyranometer data is carried out spatially. LSTM input is data from two pyranometers around target pyranometer: AWS Cipasung and AWS Cimalaka. Meanwhile, LSTM output is data from one target pyranometer: AWS Cikancung.

Input and output data are then transformed. Data transformation functions to simplify computational learning. Input and output are transformed into variables on a smaller scale range. Transformation equation is stated as follows [18]:

$$Z_{norm} = \frac{z_i - z}{stdev(z)} \tag{1}$$

Each input and output value (Z_i) is reduced to its average value (Z), then divided by its standard deviation, to obtain a new variable as a result of the transformation. Next, the input and output data of the 2021 dataset are segmented into 80% training data and 20% validation data. Testing data are taken from the 2022 dataset based on missing data scenarios.

LSTM hyperparameter design is adopted from previous literature. In 2022, Parasyris et.al. developed an LSTM model for estimating temperature, humidity and wind speed. This time, the model is applied to impute solar radiation intensity of pyranometer [11]. Table III shows hyperparameter design of LSTM for imputation model

TABLE III. LSTM HYPERPARAMETER DESIGN

Hyperparameter	Value				
Hidden Layer	2				
Neuron Number	[40,40]				
Activation Function	Rectified Linear Unit				
Batch Size	32				
Epoch	100				
Number of inputs	2 (pyranometers of AWS Cimalaka and AWS Cipasung)				
Number of output	1 (pyranometer of AWS Cikancung)				

Value of hidden layer and neuron number are determined by best trial process during training. Validation aims to review model training performance on a smaller number of data distributions. This process ensures that the model experience no underfitting or overfitting [19]. Validation results are then compared against modeling performance criteria based on the WMO requirements for solar radiation intensity measurement, namely a maximum of 8% error [20].

D. Model Testing

AWS pyranometer imputation model needs to be tested to determine the level of LSTM accuracy performance. Model is tested against the 2022 dataset. The imputed data is compared to actual AWS pyranometer data. Accuracy performance of the imputation model is measured using 3 parameters, namely correlation coefficient (R), root mean square error (RMSE) and mean average percentage error (MAPE). These equations are stated respectively as follows [21]:

$$R = \frac{\sum_{i=1}^{m} (x_i - \bar{x}) \sum_{i=1}^{m} (y_i - \bar{y})}{\sqrt{\sum_{i=1}^{m} (x_i - \bar{x})^2 \sum_{i=1}^{m} (y_i - \bar{y})^2}}$$
(2)

$$RMSE = \sqrt{\frac{1}{m} \sum_{i=1}^{m} (y_i - x_i)^2}$$

$$MAPE = \frac{100\%}{m} \sum_{i=1}^{m} \left| \frac{x_i - y_i}{y_i} \right|$$
(3)

MAPE =
$$\frac{100\%}{m} \sum_{i=1}^{m} \left| \frac{x_i - y_i}{y_i} \right|$$
 (4)

y is denoted for actual data, while x is denoted as imputed data. correlation coefficient states the relationship between the imputed data variables and the actual data on a scale of 0-1. RMSE states the error value in units of solar radiation intensity. MAPE expresses the error value in percentage form.

IV. RESULT AND ANALYSIS

Initial total raw dataset for AWS Cikancung, AWS Cipasung and AWS Cimalaka are respectively 49,817; 49,697; and 49,820 for 2021, then 51,278; 51,318; and 50,130 for 2022. AWS Cimalaka contains 10 outliers in 2021 and 5 outliers in 2022, so it remains 49,810 in 2021 and 50,125 in 2022. AWS Cipasung contains only 2 outliers in 2022, so it remains 51,316 data in 2022. AWS Cimalaka contains no outliers in 2021 and 2022. Next, a listwise deletion is performed on the outlier. This process removes all raw data in the same sampling time when there are outliers.

Data are only selected at 07.00 - 19.00 Local Time or 00.00 - 12.00 am UTC. Hence, total raw selected dataset are 26,280 data for every sites, whether in 2021 or 2022. There are no outlier inside the selected dataset. Simulation is performed on Spyder application. Spyder utilizes Python 3.9 programming language. Library used in compiling LSTM algorithm is keras-tensorflow.

Missing data scenarios are carried out in AWS Cikancung 2022 dataset, then they are saved as actual data for testing. LSTM is trained utilizing 80% of 2021 dataset. Training stage duration spends 305 s and yields 374.40 W/m² of RMSE. Table IV shows validation result of LSTM algorithm.

TABLE IV. VALIDATION RESULT OF LSTM

Total Missing	Validation					
Missing Data	R RMSE (W/m²) MAPE (%)					
5256	0.763	194.04	5.13			

LSTM is validated using 20% of 2021 dataset. According to Table IV, validation RMSE has insignificant difference compared to training result. It means LSTM model experience no underfitting or overfitting. Imputed data in validation process has moderate correlation against actual data with R > 0.7. MAPE value is less than 8%, so it indicates that LSTM model fulfill WMO requierement for solar radiation intensity measurement. LSTM is then tested using 2022 dataset based on arranged scenarios. There are 5 variations of missing data scenarios in different duration. Table V shows model testing results.

TABLE V. TEST RESULT OF LSTM

Total	Missing	Testing				
Missing Data	Data Scenario	R	RMSE (W/m²)	MAPE (%)		
1095	30 minutes	0.868	243.90	5.26		
1098	60 minutes	0.894	235.85	4.14		
1098	3 hours	0.915	222.05	3.32		
1116	6 hours	0.910	208.48	2.93		
1152	12 hours	0.911	176.18	1.76		

Based on Table V, all imputed data ara strongly correlated to actual data, because R>0.85 in overall scenarios. RMSE testing values are still in range of training and validation results. Meanwhile, MAPE values are <8%, so it meet WMO requirement for solar radiation intensity measurement. In accordance with missing data duration, longer imputed values produces higher accuracy. It is proven by an increase of R values, and a decrease of RMSE and MAPE values. It shows that LSTM has capability on long term data imputation, because it has forget gate as memory holder in each neuron [22].

Figure 3 shows imputed data versus actual data with 60 minutes of missing data. Missing data occurs on January 1, 2022 at 04.30 - 05.30 UTC. Solar radiation intensity may reach zenith point on this period. Figure 3 determines that imputed data has difference compared to actual data, but it follows the fluctuation adjacently.

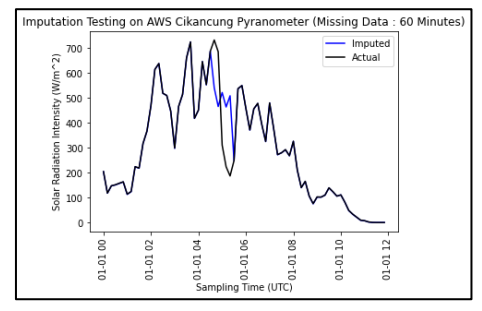


Fig. 3. Imputation testing plot with 60 minutes of missing data

Figure 4 shows imputed data versus actual data with 12 hours of missing data. Missing data occurs on January 1, 2022 at 00.00 - 12.00 UTC. It happens on one day of sunshine duration.. Figure 4 determines that

imputed data is able to coincide actual data patterns adjacently. However, it has weakness on mid day of solar time, because actual data is tend to higher than imputed data.



Fig. 4. Imputation testing plot with 60 minutes of missing data

Table VI describes statistical components of imputed data versus actual data. Imputed data give no significant changes to actual statistical components value based on its mean, median, maximum, minimum and standar deviation. Imputation affects only standar deviation. Greater missing data sequences yield a little decrease on deviation. It becomes a limitation of any imputation model.

TABLE VI. TEST RESULT OF LSTM

Compo	Actual	Imputed Data (W/m²)				
nent	Data W/m ²	30 min	60 min	3 hours	6 hours	12 hours
Mean	284	285	285	284	284	284
Median	214	217	217	216	216	217
Max	1141	1141	1141	1141	1141	1141
Min	0	0	0	0	0	0
Stdev	255	254	254	254	253	253

Based on Figure 5, distribution of pyranometer data is a normal distribution type with a certain skewness. Results of imputation in all missing data scenarios have trivial impact on data variability, so it unchange distribution shape.

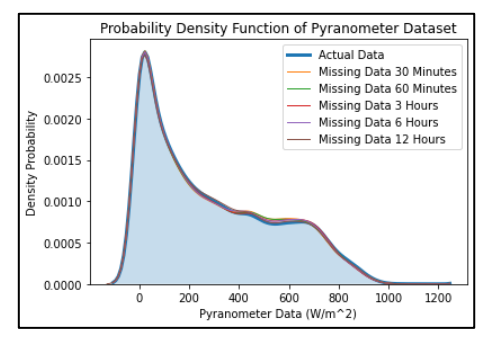


Fig. 5. Imputation testing plot with 60 minutes of missing data

Nonetheless, LSTM-based imputation model needs improvement in order to minimize bias. Difference of imputed versus actual data is caused by input compability, hyperparameter setting and internal bias of the algorithm. Solar radiation intensity measurement is also affected by cloud cover. Spatial relationship among three sites of pyranometer may be interrupted by different total cloud cover value at same time. Cloud has irregular shape and area, meanwhile pyranometer site has fixed position and elevation. Hyperparameter setting of LSTM also contributes bias of imputation model [23]. Optimal number of hidden layers and neuron should be tuned in future works.

V. CONCLUSION

Overall, LSTM-based imputation model has ability of filling gap data on AWS Cikancung pyranometer with maximum missing sequence of 12 hours. It yields strong correlation to actual data with R>0.85. Imputation model has MAPE 1.76% - 5.26% for missing duration 30 minutes-12 hours. It still it meet WMO requirement for solar radiation intensity measurement with MAPE<8%. Difference of imputed versus actual data is caused by input compability, hyperparameter setting and internal bias of the algorithm.

REFERENCES

- [1] L. Wald, Fundamentals of Solar Radiation. CRC Press, 2021. https://doi.org/10.1201/9781003155454.
- [2] J. Haigh, Solar influences on Climate. Grantham Institute for Climate Change Briefing paper No 5. Imperial College London. 2011
- [3] J. Fraden, Handbook of Modern Sensors. Cham: Springer International Publishing, 2016. https://doi.org/10.1007/978-3-319-19303-8
- [4] Badan Meteorologi Klimatologi dan Geofisika, Peraturan Kepala BMKG Nomor 7 Tahun 2014 tentang Standar Teknis dan Operasional Pemeliharaan Peralatan Pengamatan Meteorologi, Klimatologi dan Geofisika. 2014.
- [5] M. Al-Rasheedi, Gueymard, A. Ismail, , & T. Hussain, Comparison of two sensor technologies for solar irradiance measurement in a desert environment. Solar Energy, 161, 194– 206, 2018. https://doi.org/10.1016/j.solener.2017.12.058
- [6] J. D. Wood, T. J. Griffis, & J. M. Baker, Detecting drift bias and exposure errors in solar and photosynthetically active radiation data. Agricultural and Forest Meteorology, 206 33– 44, 2015. https://doi.org/10.1016/j.agrformet.2015.02.015
- [7] Manfred Georg Kratzenberg, Hans Georg Beyer, S. Colle, and A. Albertazzi, "Uncertainty Calculations in Pyranometer Measurements and Application," Solar Energy, Jan. 2006, https://doi.org/10.1115/ISEC2006-99168
- [8] C. Turrado, M. López, F. Lasheras, B. Gómez, J. Rollé, and F. Juez, "Missing Data Imputation of Solar Radiation Data under Different Atmospheric Conditions," Sensors, vol. 14, no. 11,

- pp. 20382–20399, Oct. 2014, https://doi.org/10.3390/s141120382
- [9] Ö. A. Karaman, T. Tanyıldızı Ağır, and İ. Arsel, "Estimation of solar radiation using modern methods," Alexandria Engineering Journal, vol. 60, no. 2, pp. 2447–2455, Apr. 2021, https://doi.org/10.1016/j.aej.2020.12.048
- [10] E. Afrifa-Yamoah, U. A. Mueller, S. M. Taylor, and A. J. Fisher, "Missing data imputation of high-resolution temporal climate time series data," Meteorological Applications, vol. 27, no. 1, Jan. 2020, https://doi.org/10.1002/met.1873
- [11] A. Parasyris, G. Alexandrakis, G. V. Kozyrakis, K. Spanoudaki, and N. A. Kampanis, "Predicting Meteorological Variables on Local Level with SARIMA, LSTM and Hybrid Techniques," Atmosphere, vol. 13, no. 6, p. 878, May 2022, https://doi.org/10.3390/atmos13060878
- [12] C. A. Fiebrich, C. R. Morgan, A. G. McCombs, P. K. Hall, and R. A. McPherson, "Quality Assurance Procedures for Mesoscale Meteorological Data," Journal of Atmospheric and Oceanic Technology, vol. 27, no. 10, pp. 1565–1582, Oct. 2010, https://doi.org/10.1175/2010JTECHA1433.1
- [13] F. Vejen, C. Jacobsson, U. Fredriksson, M. Moe, L. Andresen, E. Hellsten, P. Rissanen, Þ. Pálsdóttir, & Þ. Arason, Quality Control of Meteorological Observations Automatic Methods Used in the Nordic Countries. KLIMA Report. 2002.
- [14] T. B. Pepinsky, "A Note on Listwise Deletion versus Multiple Imputation," Political Analysis, vol. 26, no. 4, pp. 480–488, Aug. 2018, https://doi.org/10.1017/pan.2018.18
- [15] S. Hamdi, "Mengenal Lama Penyinaran Matahari Sebagai Salah Satu Parameter Klimatologi," Berita Dirgantara, vol. 15, no. 1, 2014, https://jurnal.lapan.go.id/index.php/berita_dirgantara/article/view/2068.
- [16] T. Emmanuel, T. Maupong, D. Mpoeleng, T. Semong, B. Mphago, and O. Tabona, "A survey on missing data in machine learning," Journal of Big Data, vol. 8, no. 1, Oct. 2021, https://doi.org/10.1186/s40537-021-00516-9
- [17] S. Hochreiter and J. Schmidhuber, "Long Short-Term Memory," Neural Computation, vol. 9, no. 8, pp. 1735–1780, Nov. 1997, doi: https://doi.org/10.1162/neco.1997.9.8.1735.
- [18] F. L. Gewers et al., "Principal Component Analysis," ACM Computing Surveys, vol. 54, no. 4, pp. 1–34, May 2022, https://doi.org/10.1145/3447755
- [19] M. Kubat, An Introduction to Machine Learning. Cham: Springer International Publishing, 2017. https://doi.org/10.1007/978-3-319-63913-0
- [20] "Guide to Instruments and Methods of Observation (WMO-No. 8) | World Meteorological Organization," community.wmo.int. https://community.wmo.int/en/activity-areas/imop/wmo-no_8
- [21] D. Chicco, M. J. Warrens, and G. Jurman, "The coefficient of determination R-squared is more informative than SMAPE, MAE, MAPE, MSE and RMSE in regression analysis evaluation," PeerJ Computer Science, vol. 7, no. 5, p. e623, Jul. 2021, https://doi.org/10.7717/PEERJ-CS.623
- [22] T. T. K. Tran, S. M. Bateni, S. J. Ki, and H. Vosoughifar, "A Review of Neural Networks for Air Temperature Forecasting," Water, vol. 13, no. 9, p. 1294, May 2021, doi: https://doi.org/10.3390/w13091294.
- [23] J. Kalliola, J. Kapočiūtė-Dzikienė, and R. Damaševičius, "Neural network hyperparameter optimization for prediction of real estate prices in Helsinki," PeerJ Computer Science, vol. 7, p. e444, Apr. 2021, https://doi.org/10.7717/peerj-cs.444

Predictive Maintenance: Automatic Weather Station Sensors Error Detection using Long Short-Term Memory

Bayu Santoso^{1,2}, Muhammad Ryan³, Haryas Subyantara Wicaksana¹, Naufal Ananda¹, Irvan Budiawan⁴, Faqihza Mukhlish⁴, Deddy Kurniadi¹

¹ Instrumentation and Control Study Program, ITB, Bandung, Indonesia
² Department of Instrumentation and Calibration, BMKG, Medan, Indonesia
³ Center of Aviation Meteorology, BMKG, Jakarta, Indonesia
⁴Engineering Physics Study Program, ITB, Bandung, Indonesia
¹bayu.santoso@bmkg.go.id, ²muhammad.ryan@bmkg.go.id, ³haryas.wicaksana@bmkg.go.id,
⁴naufal.ananda@bmkg.go.id, ⁵budiawan.irvan@gmail.com, ⁶faqihza.m@itb.ac.id, ⁷kurniadi@itb.ac.id

Accepted on 13 November 2023 Approved on 04 December 2023

Abstract— Weather information plays a crucial role in various sectors due to Indonesia's wide range of weather and extreme climate phenomena. Automatic Weather Stations (AWS) are automated equipment designed to measure and collect meteorological parameters such as atmospheric pressure, rainfall, relative humidity, atmospheric temperature, wind speed, and wind direction. Occasionally, AWS sensors may produce erroneous values without the technicians' awareness. This study aims to develop sensors error detection system for predictive maintenance on AWS using the Long Short-Term Memory (LSTM) model. The AWS dataset from Jatiwangi, West Java, covering the period from 2017 to 2021, will be utilized in the study. The study revolves around developing and testing four distinct LSTM models dedicated to each sensor: RR, TT, RH, and PP. The research methodology involves a phased approach, encompassing model training on 70% of the available dataset, subsequent validation using 25% of the data, and finally, testing on 5% of the dataset alongside the calibration dataset. Research outcomes demonstrate notably high accuracy, exceeding 90% for the RR, TT, and PP models, while the RH model achieves above 85%. Moreover, the research highlights that Probability of Detection (POD) values generally trend high, surpassing 0.8, with a low False Alarm Rate (FAR), typically below 0.1, except for the RH model. Sensor condition requirements will adhere to the rules set by World Meteorological Organization (WMO) and adhere to the permitted tolerance limits for each weather parameter.

Index Terms— automatic weather station; long short-term memory; predictive maintenance; sensor error detection

I. INTRODUCTION

Indonesia exhibits a wide array of weather and extreme climate phenomena [1]. Weather information plays a pivotal role across various sectors, serving as

the cornerstone for policymaking by the central government, local authorities, and other stakeholders in infrastructure development, transportation, agriculture, tourism, energy, industry, and more. In the year 2021, the National Disaster Management Agency (BNPB) recorded that a striking 99.5% of the disasters occurring in Indonesia were of hydrometeorological nature. The top three prevailing events were floods, extreme weather, and landslides [2].

Automatic Weather Stations (AWS) are automated equipment utilized for observing meteorological parameters, including atmospheric pressure, rainfall, relative humidity, atmospheric temperature, wind speed, and wind direction. The Meteorology, Climatology, and Geophysics Agency (BMKG) currently operates 368 AWS units distributed across Indonesia, both within and outside the vicinity of Meteorological Station Management Units (UPT) (BMKG, 2023). **BMKG** currently conducts maintenance activities, which encompass both corrective and predictive maintenance [4]. Corrective maintenance involves actions taken when AWS sensors are damaged, necessitating replacement or repair. Preventive maintenance, on the other hand, is a routine maintenance activity performed at scheduled intervals. But maintenance is not limited to corrective and preventive maintenance alone but also includes predictive maintenance [5].

Predictive maintenance can be classified into three primary approaches: knowledge-based, physics-based, and data-based methods [6]. The knowledge-based method leverages the expertise and experience of specialists to diagnose equipment failures. The physics-based method employs mathematical or physical comprehension of the system to assess the

remaining useful life of the machinery. The data-based method makes use of historical data collected by sensors on the equipment to make failure predictions. Of the three approaches mentioned, the most suitable predictive maintenance model for AWS sensors is the data-based approach. This is because AWS generates data for each interconnected meteorological parameter, and this data is critical for detecting the sensor's condition.

The study aims to develop a system that can monitor sensor output values and detect AWS sensor errors based on historical sensor data as a pivotal step in predictive maintenance. The sensor parameters used in this study include pressure atmospheric pressure, rainfall, relative humidity, and atmospheric temperature. The machine learning algorithm chosen for this study is Long Short-Term Memory (LSTM). Sensor condition requirements will align with the World Meteorological Organization (WMO) standards concerning measurement tolerance for meteorological parameters, which specify maximum allowable deviations as follows: 5% for rainfall, 0.2°C for atmospheric temperature, 3% for relative humidity, 0.15 hPa for atmospheric pressure [7].

Within the realm of predictive maintenance, the LSTM (Long Short-Term Memory) algorithm outperforms other machine learning algorithms. The LSTM algorithm, classified within the neural network model category, possesses exceptional capabilities in understanding long-term relationships sequential data. Additionally, it adeptly captures temporal relationships within data, exhibiting a high level of accuracy and facilitating the generation of exceptionally precise predictions regarding the future state of equipment. Oh and Kim obtained results indicating that predictions developed the LSTM model mirror the trends present in actual values. This model is applied to predictive maintenance for real-time equipment status diagnosis. Nevertheless, the LSTM model's accuracy is significantly compromised owing to an insufficiency of training data [8].

Jiang, et.al conclude that the proposed A²-LSTM method outperforms other existing techniques in the prediction of remaining useful life (RUL). The comparative results illustrate that the A²-LSTM method can proficiently identify critical attributes and temporal dependencies within manufacturing system, offering valuable assistance to maintenance personnel in their duties [9]. Dey and Jana have obtained results indicating that the proposed LSTM model surpasses the KernelRidge regression model in RMSE values, making it a viable choice for effectively conducting predictive maintenance on rotating machinery [10]. Ruhiyat, et.al conclude that the LSTM algorithm can be utilized for predictive maintenance of a ventilator system. The most

significant result indicates a 98.4% probability of failure within 50 cycles with an 82% accuracy [11].

II. BASIC CONCEPTS

A. Predictive Maintenance

Predictive maintenance involves the utilization of condition monitoring technology to observe the deterioration of components, predict their future status, and consistently revise maintenance plans in accordance with the predictive outcomes [5]. The primary objectives of predictive maintenance are to diagnose the current condition (diagnostic) and forecast future conditions (prognostic). Predictive maintenance can be classified into three approaches: knowledge-based, physics-based, and data-based methods [6], as illustrated in Figure 1.

The knowledge-based method is employed for diagnosing and prognosticating failures, primarily relying on expert knowledge and experience. This approach utilizes historical failure data as a primary tool for prediction. Within the knowledge-based method, three model categories can be identified: rule-based models, case-based models, and fuzzy logic-based models. The physics-based approach leverages the physical understanding of the system to assess the remaining useful life of machinery. This method is divided into several models, including mathematical models, Hidden Markov models, and filtering models such as the Kalman Filter, Extended Kalman Filter, and others.

The data-based approach utilizes data collected from sensors on equipment, components, and machinery to predict failures. This data is extracted to process, analyze, and derive degradation information from it. Choosing the suitable machine learning or deep learning algorithms should align with the pertinent parameters of the equipment. This method provides the benefit of not depending on the precision of mathematical and physical models or intricate expert rule formulation.

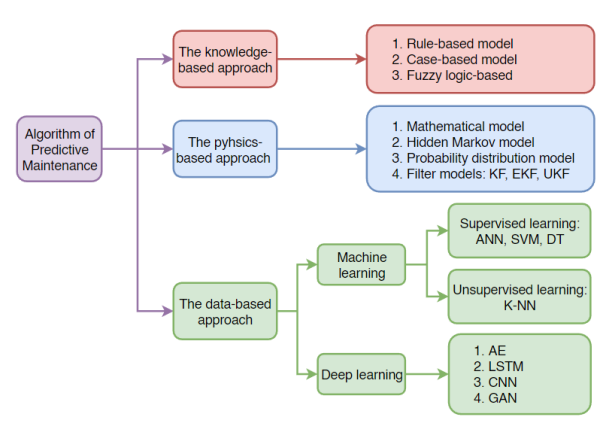


Fig. 1. Algorithm of predictive maintenance

The data-based approach utilizes data collected from sensors on equipment, components, and machinery to predict failures. This data is extracted to process, analyze, and derive degradation information from it. Choosing the suitable machine learning or deep learning algorithms should align with the pertinent parameters of the equipment. This method provides the benefit of not depending on the precision of mathematical and physical models or intricate expert rule formulation.

B. Automatic Weather Station

Weather Station Automatic (AWS) is meteorological station responsible for conducting observations and transmitting data automatically [12]. The primary measurements performed by an AWS include essential weather parameters, such as pressure atmospheric pressure, rainfall, relative humidity, atmospheric temperature, wind speed, and wind direction. In maritime environments, additional parameters such as evaporation, water temperature. and water level are incorporated. Automatic Agroclimate Weather System (AAWS) is implemented in agroclimatology, which encompasses sensors for solar radiation, soil temperature, and soil moisture [13].

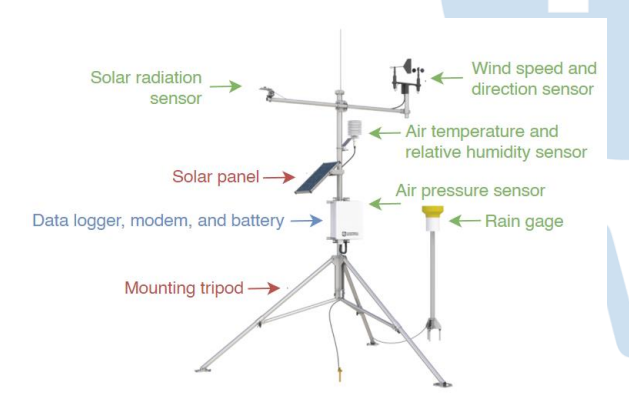


Fig. 2. Components of AWS

AWS is categorized into two groups based on data presentation: AWS real-time and offline. AWS real-time refers to meteorological stations that offer real-time data to users, featuring communication systems and alert mechanisms for extreme weather conditions like storms, heavy rain, high temperatures, and more. On the other hand, AWS offline refers to weather stations that focus on data recording, storing it in storage media, and displaying the current data. The stored data can be downloaded as required at any time. Sensor condition requirements will adhere to the rules set by World Meteorological Organization (WMO). Measurement tolerances that meet the requirements are presented in Table I.

TABLE I. WMO REGULATION

Parameter	Range	Achievable measurement tolerance
Rainfall	0 ~ 500 mm	higher 5% or 0.1 mm
Atmospheric temperature	-80 ~ 60 °C	0.2 °C
Relative humidity	0 ~ 100%	3%
Atmospheric pressure	500 ~ 1080 hPa	0.15 hPa

C. Long Short-Term Memory

Long Short-Term Memory (LSTM) is an improvement on the Recurrent Neural Network (RNN). Its main objective is to create models with the ability to retain long-term memory, while also having the capacity to filter out irrelevant information in the training data.

LSTM utilizes a combination of two activation functions: the hyperbolic tangent (tanh) and the sigmoid functions [14]. In the tanh function, the output values are bounded within the (-1,1) range, facilitating the regulation of data flow through the network and preventing the vanishing gradient issue. Additionally, the sigmoid activation function is also incorporated into LSTM. It confines the output values to the (0,1) range, enabling the neural network to filter out unrelated data. When the output value approaches zero, it essentially becomes zero. The tanh and sigmoid activation function are defined as follows:

$$tanh(x) = \frac{e^{x} - e^{-x}}{e^{x} + e^{-x}}$$
(1)
$$\sigma(x) = \frac{1}{e^{x} + e^{-x}}$$
(2)

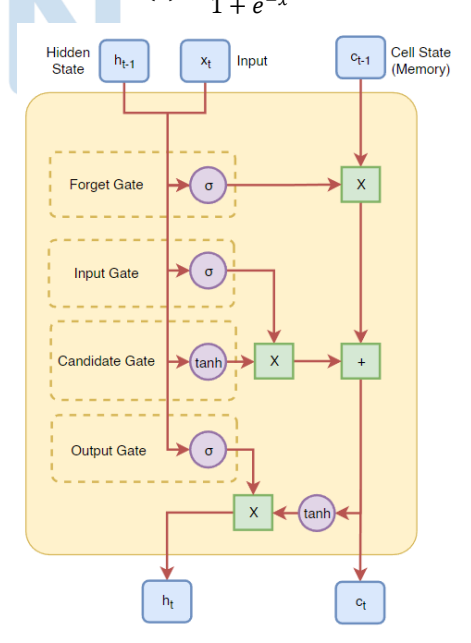


Fig. 3. LSTM architecture

LSTM introduces a cell state, which is a crucial component of the algorithm. The hidden state functions as short-term working memory, while the cell state is employed as long-term memory to retain important information from previous data. LSTM possesses the ability to modify cell state values using a mechanism called Gates. LSTM incorporates four gates, as illustrated in Figure 3:

- The Forget Gate decides which values from the preceding cell state to discard and which ones to preserve.
- The Input Gate picks values from the prior hidden state and the present input for updating by subjecting them to a sigmoid function. The output of this function is subsequently multiplied by the previous cell state.
- The Cell State Candidate Gate initially governs the flow of information within the network by using a tanh function on the prior hidden state and the present input. The resultant of the tanh function is then multiplied by the output of the Input gate to compute the candidate for the current cell state. This candidate is then added to the previous cell state.
- The Output Gate calculates the current hidden state by employing a sigmoid function to decide which new information is crucial to consider. This is accomplished by applying the sigmoid function to the previous hidden state and the current input. The current cell state value is then processed by a tanh function. Finally, the results of these two functions are multiplied together.

III. METHODS

The study relies on recorded sensor data for rainfall, relative humidity, atmospheric temperature, and atmospheric pressure. This data was obtained from the AWS Jatiwangi site, which is situated at the Class III Meteorological Station in Kertajati, Majalengka Regency, West Java Province. Data records were obtained from the BMKG Central Office in Jakarta, accessible through the website https://awscenter.bmkg.go.id/.



Fig. 4. AWS Jatiwangi site

The study covers a time frame starting on January 1, 2017 and concluding on December 31, 2021 with data recorded at 10-minute intervals. The entire study flowchart is depicted in Figure 5.

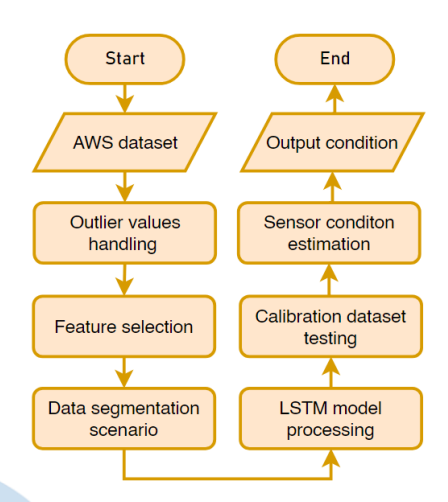


Fig. 5. Study flowchart

A. Outlier Values Handling

Handling outlier values aims to ensure that they do not exert an excessive influence on the outcomes and interpretations of the forthcoming LSTM model. The BMKG Central Database sets forth criteria concerning the quality of AWS data. These guidelines, presented in Table II, represent general requirements applied by BMKG to enforce quality control for AWS data throughout Indonesia.

TABLE II. QUALITY CONTROL AWS DATA

Sensor	Minimum Threshold	Maximum Threshold	Stepcheck Threshold
Rainfall (mm)	0	300	30
Atmospheric temperature (°C)	5	45	3
Relative humidity (%)	5	100	15
Atmospheric pressure (hPa)	800	1050	2

B. Feature Selection

Feature selection is conducted to recognize the most significant and informative parameters among the features available in the dataset. This process involves the elimination of features that do not make a substantial contribution to the model under development. Feature selection encompasses several methods, including filtering methods, wrapper methods, and embedded methods [15]. In this study, feature selection is conducted using the embedded

method, specifically the Random Forest Importance Feature technique.

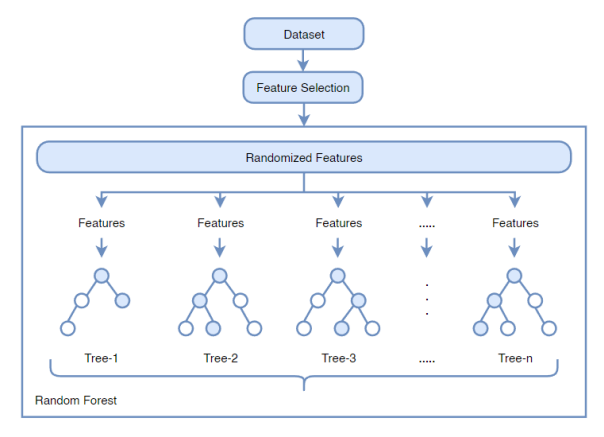


Fig. 6. Random forest architecture

Random Forest is a machine learning algorithm that amalgamates numerous decision trees to generate more precise and robust predictions [16]. Features with a greater impact on the model's predictions will exhibit higher degrees of importance in the feature importance metric. This technique includes permuting feature values to evaluate their influence on the model's performance. Features that have a significant impact on the model will result in a notable decrease in accuracy when their values are shuffled. According to [17], their study results showed that the Random Forest algorithm attained an accuracy exceeding 90% for feature selection within a dataset.

C. Data Segmentation

The data segmentation scenario is split into two conditions: the normal dataset and the synthetic dataset [18]. The normal dataset contains the original parameter values, signifying sensors operating under standard conditions. Meanwhile, the synthetic dataset is created by adjusting parameter values beyond the normal sensor tolerance limits in compliance with the 2021 WMO No. 8 standard, indicating sensors in an erroneous state.

The AWS dataset is segmented into three components: dataset fo the training process, validation process, and testing process. The training dataset is utilized to train the LSTM algorithm and generate training models for each sensor parameter. The validation dataset is employed to assess the performance of the model on data that it has not encountered during the training process. Finally, the testing dataset is prepared to assess the LSTM models that have been built, comparing their results with the calibration dataset from AWS Jatiwangi.

The AWS dataset will be distributed as follows: 70% will be used for the LSTM training process, 25% will be reserved for validation the LSTM model, and

5% will be allocated for testing against the AWS Jatiwangi calibration dataset. Within each process, 50% will be derived from the normal dataset, while 50% will be synthesized. Synthetic data generated from data transformation scenarios will be randomly inserted into the dataset. This random scenario is intended to make the error patterns of sensor readings resemble real-world occurrences during operations.



Fig. 7. Segmentation dataset process

D. LSTM Model

The dataset processed in the LSTM algorithm consists of AWS Jatiwangi data from January 2017 to December 2021. The LSTM model is implemented in Python using the PyTorch library. The LSTM design used in this study is presented in Table III.

TABLE III. DESIGN OF LSTM MODEL

Parameterization	RR	TT	RH	PP	
Unit	mm	°C	%	hPa	
Input Layer (I)	3	3	3	3	
Hidden Layer (H)	2	2	2	2	
Output Layer (O)	RR	TT	RH	PP	
Epoch	100				
Hidden Size	64				
Optimizer		Ad	am		

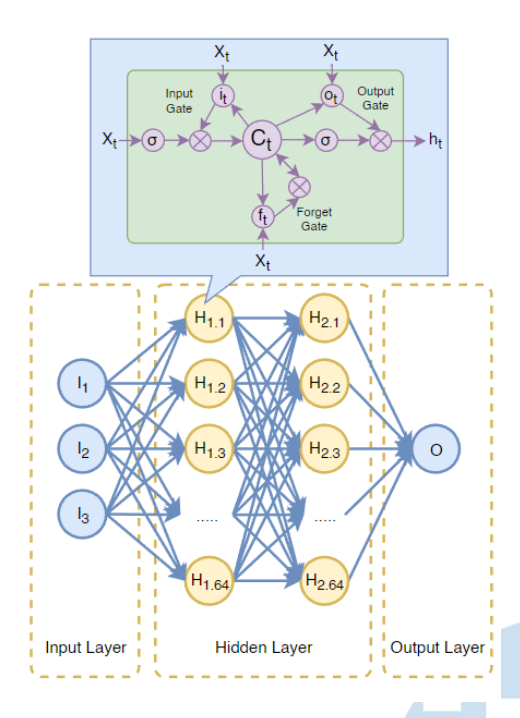


Fig. 8. Architecture LSTM sensor model

The LSTM model design for rain gauge sensors uses three input parameters: rainfall, atmospheric temperature, and relative humidity. The structure comprises a single input layer, two hidden layers, and single output layer. For synthetic data, the scenario includes randomly introducing damage values ranging from +5% to +400% and 0.1 to 100 for 0 mm from the normal values.

The LSTM model design for atmospheric temperature sensors uses three input parameters: atmospheric temperature, relative humidity, and rainfall. The structure comprises a single input layer, two hidden layers, and single output layer. For synthetic data, the scenario involves randomly introducing damage values ranging from $\pm 2\%$ to $\pm 50\%$ from the normal values.

The LSTM model design for relative humidity sensors uses three input parameters: relative humidity value, atmospheric temperature, and rainfall. The structure comprises a single input layer, two hidden layers, and single output layer. For synthetic data, the scenario involves randomly introducing damage values ranging from -9% to -60% and +9% to +70% from the normal values.

The LSTM model design for atmospheric pressure sensors uses two input parameters: atmospheric pressure value and atmospheric temperature. The structure comprises a single input layer, two hidden layers, and single output layer. For synthetic data, the scenario includes randomly introducing damage values ranging from $\pm 0.04\%$ to 10% from the normal values.

LSTM sensor model architecture is depicted in Figure 8.

E. Performance Evaluation

The Confusion Matrix is employed as an evaluation tool for assessing the classification model's performance in the LSTM algorithm [19]. This evaluation method measures how accurately the classification model predicts the class or label of the data. The confusion matrix comprises four main cells: *True Positives (TP)* are the data points correctly identified as positive by the model, while *True Negatives (TN)* are the data points correctly identified as negative. *False Positives (FP)*, or Type I Errors, are the data points inaccurately identified as positive, and *False Negatives (FN)*, or Type II Errors, are the data points inaccurately identified as negative.

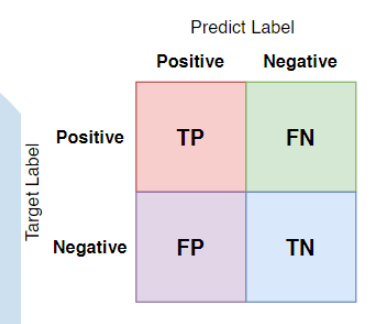


Fig. 9. Confusion matrix

The confusion matrix additionally enables the computation of various performance evaluation metrics, detailed as follows:

 Accuracy: Measures how well correct classifications are made compared to the total predictions. In pattern recognition, accuracy assesses how well a system can correctly identify patterns.

$$Accuracy = \frac{TP + TN}{TP + TN + FP + FN} \tag{3}$$

 Probability of Detection (POD): Measures how well the model can detect actual positive data.
 POD is a vital component of the confusion matrix as it specifically highlights the system's success in detecting actual occurrences.

$$POD = \frac{TP}{TP + FN} \tag{4}$$

• False Alarm Rate (FAR): Measures how often the model generates false positive signals, indicating instances where the system incorrectly identifies negatives as positives. FAR provides insights into the system's reliability in identifying negative events, serving as a crucial measure of its trustworthiness.

$$FAR = \frac{FP}{FP + TN} \tag{5}$$

IV. RESULT AND DISCUSSION

The dataset comprises 5 columns: the "tanggal" column indicates the date and time, the "rr" column represents the rainfall sensor values in mm, the "tt_air_avg" column denotes the atmospheric temperature sensor values in oC, the "rh_avg" column signifies the relative humidity sensor values in %, and the "pp_air" column displays the atmospheric pressure sensor values in hPa.

	tanggal	rr	tt_air_avg	rh_avg	pp_air
0	2017-01-01 00:00:00+00	0.0	20.4	100.0	1003.7
1	2017-01-01 00:10:00+00	0.0	20.8	100.0	1004.3
2	2017-01-01 00:20:00+00	0.0	21.6	99.9	1005.1
3	2017-01-01 00:30:00+00	0.0	23.3	96.0	1006.2
4	2017-01-01 00:40:00+00	0.0	25.0	90.5	1006.4
	•••				
186737	2021-12-31 23:10:00+00	0.5	25.0	96.6	1005.0
186738	2021-12-31 23:20:00+00	0.5	25.0	96.4	1005.1
186739	2021-12-31 23:30:00+00	0.5	25.2	95.8	1005.1
186740	2021-12-31 23:40:00+00	0.5	25.4	95.0	1005.1
186741	2021-12-31 23:50:00+00	0.5	25.6	94.1	1005.3

Fig. 10. AWS dataset

A. Handling outlier values

According to the BMKG Central Database requirements, outliers are removed by excluding them from the dataset. TABLE IV displays the dataset attributes after going through data preprocessing. Each column shows a reduction in data count due to the removal of outliers. The minimum and maximum values for each sensor attribute have been adjusted to align with BMKG's AWS data quality control standards.

TABLE IV. AFTER HANDLING OUTLIER VALUES

Attribute	RR	TT	RH	PP
Total data	175,787	175,787	175,787	175,787
Minimum	0.0	17.5	15.9	994.5
Maximum	276.0	38.6	100.0	1011.1
Mean	4.2	27.5	75.7	1004.6
Std	15.2	3.4	18.2	1.9

Figure 11 displays a sample dataset from December 29th to December 31st, 2021, where all parameters have values of 0. A sensor recording a value of 0 is interpreted as an indication of a malfunction in other components of the AWS, such as power supply issues or data transmission failures to the Central Database. This inference is drawn from the consistent occurrence of 0 values for each parameter within the same minute. It is also predicated on the absence of direct checks on the datalogger at the AWS Jatiwangi site, as the dataset

was solely obtained from the AWS Center BMKG website. Consequently, the 0 values can be disregarded, as the failures are attributed to other components, rendering the sensors inactive or switched off.

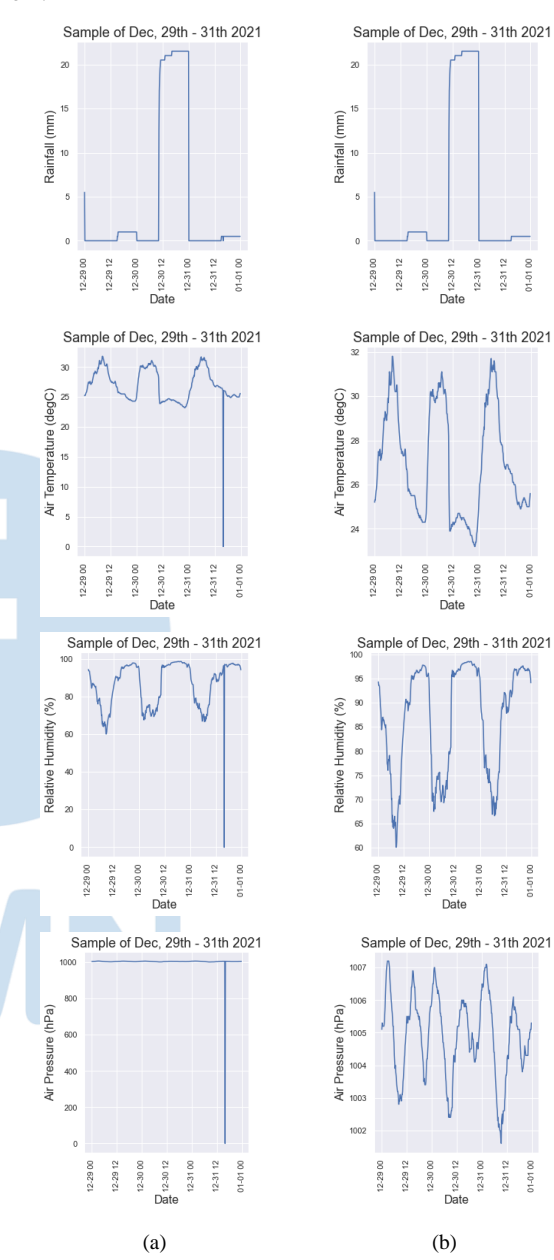


Fig. 11. Imputation testing plot with 60 minutes of missing data

B. Feature Selection

The feature importance for the relative humidity sensor is 0.43, for the atmospheric pressure sensor is 0.29, and for the atmospheric temperature sensor is 0.27 in relation to the rainfall sensor. Regarding the atmospheric temperature sensor, the relative humidity sensor holds a feature importance of 0.86, while the atmospheric pressure sensor has 0.12, and the rainfall

sensor has 0.02. As for the relative humidity sensor, the atmospheric temperature sensor holds a feature importance of 0.82, the rainfall sensor has 0.12, and the atmospheric pressure sensor has 0.05. In the context of the atmospheric pressure sensor, the relative humidity sensor has a feature importance of 0.48, the atmospheric temperature sensor has 0.39, and the rainfall sensor has 0.12.

The LSTM model employs the two most prominent feature importance values as inputs from the other sensors. Therefore, it was found that the RR model utilizes inputs from RR, RH, and PP, the TT model uses inputs from TT, RH, and PP, the RH model employs inputs from RH, TT, and RR, and the PP model takes inputs from PP, RH, and TT.

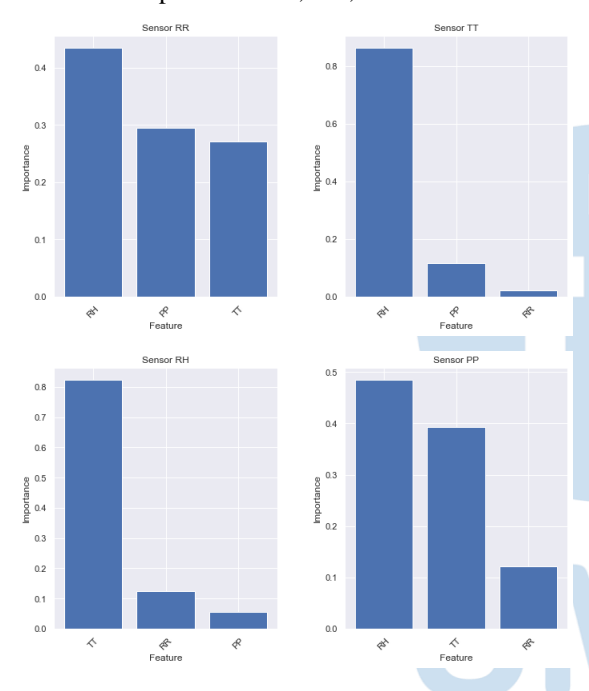


Fig. 12. Sensor feature selection

C. Data Segmentation

The dataset composition used for the LSTM model training process is 70% of the data, which amounts to 123,051 data points. The dataset used for the LSTM model validation process is 25%, which equals 43,947 data points. Additionally, the dataset used for the testing process with the AWS Jatiwangi calibration dataset is 5%, totaling 8,789 data points. Visualization of randomize synthetic data shown in Figure 13. Label 1 indicates synthetic values within the dataset, while label 0 represents normal values within the dataset.

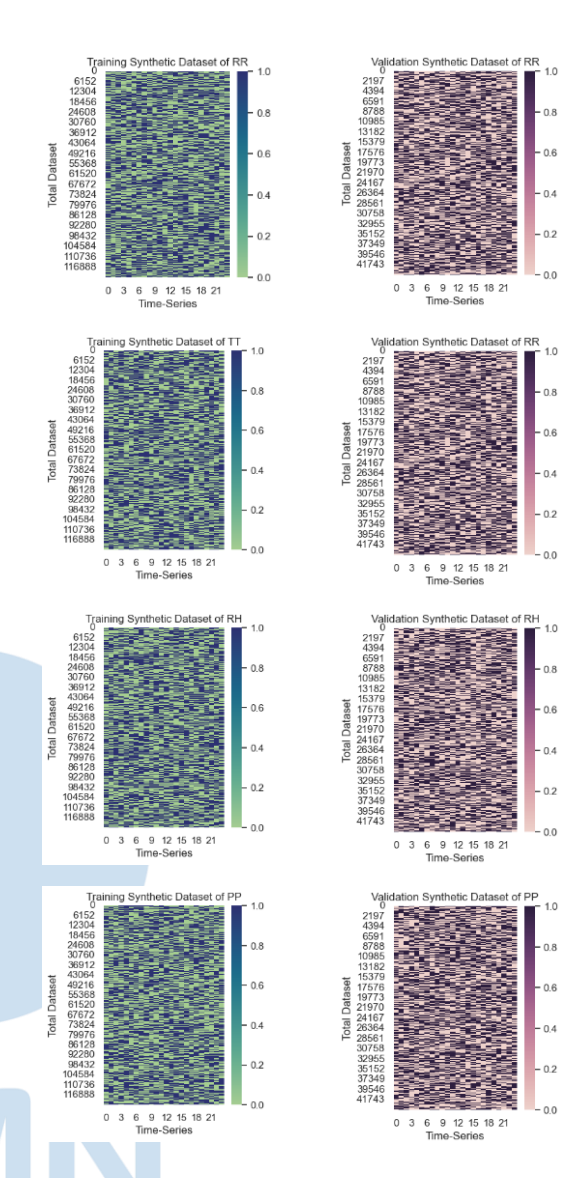


Fig. 13. Imputation testing plot with 60 minutes of missing data

In handling time series data, converting the data into matrices for Python processing using vectorization can greatly improve the speed and efficiency of the process compared to employing for or while loops that on individual elements separately. operate Vectorization. utilizing NumPy's broadcasting operations, enables mass array operations, allowing for parallel processing and optimization by the library. This leads to a significant performance enhancement, especially when dealing with extensive datasets.

D. Evaluation of LSTM Model

Training is conducted to enable the model to discern patterns within both the input and output data from the training dataset. In this process, four LSTM architecture models are constructed, namely the RR model, TT model, RH model, and PP model. Each of these models is designed to handle specific aspects or parameters of the data. The information provided

describes the architecture and training progress for four different LSTM models, each with 2 hidden layers consisting of 64 neurons:

- Model RR for estimating the condition of rainfall sensors: Loss at epoch 1: 0.2384 and Loss at epoch 100: 0.0269.
- Model TT for estimating the condition of atmospheric temperature sensors: Loss at epoch 1: 0.2904 and Loss at epoch 100: 0.0322.
- Model RH for estimating the condition of relative humidity sensors: Loss at epoch 1: 0.3636 and Loss at epoch 100: 0.0981.
- Model PP for estimating the condition of atmospheric pressure sensors: Loss at epoch 1: 0.1766 and Loss at epoch 100: 0.0098.

These models are used to estimate the condition of sensors for different environmental parameters based on the given training data. The loss values at different epochs indicate how well the models are performing during the training process, with lower loss values typically indicating better model performance. Among these four LSTM models, the PP model has the lowest loss, suggesting that it is the most predictable pattern when there are reading errors by the PP sensor. In other words, the PP model exhibits a higher degree of

94.0

94.0

94.0

89.5

89.4

95.8

95.8

95.8

t + 21

t + 2.2

t+23

98.9

98.9

0.962

0.962

0.962

accuracy in estimating the condition of the atmospheric pressure sensor when compared to the other sensor models.

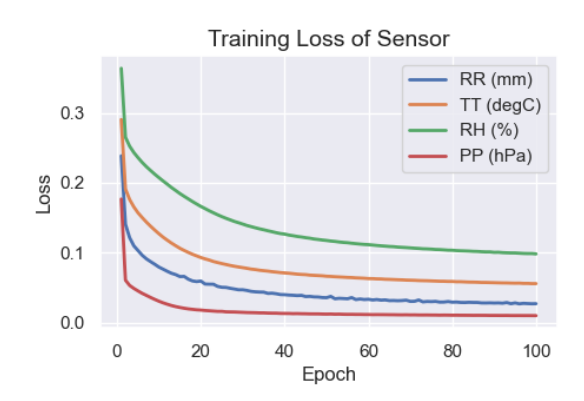


Fig. 14. Sensor loss

During the validation of the sensor dataset, the LSTM model demonstrates an accuracy above 85%, with POD exceeding 0.85 and FAR below 0.15. These metrics signify the model's proficiency in accurately recognizing the status of AWS sensors. Enclosed is the distribution table illustrating evaluation metrics during the 4-hour time-series validation in Table V.

		A 001	INO OV									
Time-	Accuracy (%)			POD				FAR				
Series	RR	TT	RH	PP	RR	TT	RH	PP	RR	TT	RH	PP
t+0	85.1	86.4	77.1	97.3	0.812	0.963	0.811	0.996	0.099	0.200	0.260	0.047
t+1	91.2	89.4	82.3	97.9	0.906	0.927	0.835	0.992	0.082	0.133	0.189	0.033
t+2	93.3	91.0	86.3	98.2	0.942	0.927	0.878	0.990	0.076	0.106	0.151	0.025
t+3	94.0	92.0	87.5	98.3	0.944	0.930	0.887	0.988	0.064	0.090	0.136	0.021
t+4	94.5	92.6	88.1	98.5	0.948	0.932	0.887	0.989	0.058	0.080	0.126	0.019
t+5	94.8	92.9	88.6	98.6	0.950	0.934	0.890	0.991	0.054	0.077	0.119	0.019
t+6	95.0	93.3	88.7	98.8	0.951	0.939	0.890	0.993	0.050	0.073	0.117	0.018
t+7	95.2	93.5	88.8	98.8	0.954	0.942	0.891	0.993	0.049	0.071	0.114	0.017
t+8	95.3	93.7	89.1	98.8	0.954	0.943	0.893	0.994	0.048	0.069	0.111	0.017
t+9	95.4	93.8	89.2	98.9	0.956	0.944	0.894	0.995	0.047	0.069	0.110	0.017
t+10	95.5	93.8	89.3	98.9	0.957	0.945	0.895	0.995	0.046	0.068	0.110	0.017
t+11	95.6	93.9	89.2	98.9	0.959	0.946	0.895	0.995	0.047	0.068	0.111	0.017
t+12	95.7	93.9	89.3	98.9	0.960	0.946	0.896	0.995	0.046	0.068	0.109	0.017
t+13	95.7	93.9	89.4	98.9	0.960	0.946	0.896	0.994	0.046	0.068	0.109	0.017
t+14	95.7	93.9	89.5	98.9	0.960	0.947	0.897	0.995	0.046	0.068	0.108	0.017
t+15	95.7	93.9	89.4	98.9	0.960	0.946	0.896	0.995	0.046	0.069	0.108	0.017
t+16	95.7	93.9	89.5	98.9	0.960	0.947	0.897	0.995	0.046	0.068	0.107	0.017
t+17	95.8	93.9	89.4	98.9	0.961	0.946	0.897	0.995	0.045	0.068	0.108	0.017
t+18	95.8	93.9	89.4	98.9	0.961	0.946	0.896	0.995	0.045	0.067	0.108	0.017
t+19	95.8	94.0	89.4	98.9	0.962	0.947	0.897	0.995	0.045	0.067	0.109	0.017
t+20	95.8	94.0	89.5	98.9	0.962	0.947	0.898	0.995	0.045	0.067	0.108	0.017

0.947

0.948

0.947

TABLE V. PERFORMANCE EVALUATION OF SENSORS IN VALIDATION PROCESS

0.898

0.898

0.897

0.995

0.995

0.995

0.045

0.045

0.045

0.067

0.067

0.109

0.109

0.108

0.017

0.017

Data	Data TT		R	Н	P	P	;	Status
point-	STD	UUT	STD	UUT	STD	UUT	STD	UUT
1	28,41	28,19	80,94	79,00	1007,68	1007,92	normal	normal
2	28,46	28,09	80,33	81,00	1007,67	1007,92	normal	normal
3	28,48	28,04	80,86	80,30	1007,65	1007,92	normal	normal
4	28,50	28,04	78,42	80,80	1007,63	1007,89	normal	normal
5	28,55	28,07	79,87	78,84	1007,62	1007,88	normal	TT Error
6	28,56	28,16	79,05	79,91	1007,60	1007,86	normal	normal
7	28,61	28,17	80,81	80,10	1007,58	1007,83	normal	normal
8	28,66	28,15	80,29	81,60	1007,54	1007,81	normal	normal
9	28,64	28,11	78,17	80,10	1007,53	1007,79	normal	normal
10	28,67	28,04	78,85	79,36	1007,50	1007,77	normal	normal
11	28,72	28,06	76,82	79,77	1007,48	1007,74	normal	normal
12	28,79	28,09	77,30	78,75	1007,47	1007,73	normal	normal
13	28,91	28,14	77,19	78,26	1007,45	1007,72	normal	normal
14	29,05	28,26	79,75	79,39	1007,44	1007,70	normal	normal
15	29,12	28,42	76,16	79,98	1007,42	1007,69	normal	normal
16	29,23	28,53	76,14	77,90	1007,39	1007,66	normal	normal
17	29,34	28,68	76,54	77,07	1007,38	1007,64	normal	normal
18	29,48	28,79	76,49	77,58	1007,38	1007,64	normal	normal
19	29,58	28,93	75,64	77,22	1007,38	1007,64	normal	normal
20	29,55	29,01	74,01	75,73	1007,39	1007,64	normal	normal
21	29,46	28,99	73,74	73,01	1007,38	1007,64	normal	normal
22	29,47	29,01	72,13	74,49	1007,39	1007,65	normal	normal
23	29,46	29,00	71,68	72,94	1007,39	1007,65	normal	normal
24	29,45	29,03	72,40	71,80	1007,41	1007,67	normal	normal
25	29,47	29,08	73,24	74,14	1007,42	1007,68	normal	normal
26	29,53	29,10	74,55	73,34	1007,44	1007,70	normal	normal

TABLE VI. CALIBRATION DATASET TESTING

The increase in accuracy, such as the lower accuracy at t+0 compared to t+1, stems from several factors:

- Short-term detections (t+1) are simpler due to the availability of information from t+0, which can be used for t+1 detections. This added information can enhance accuracy by providing the model access to more current data.
- The known data at t+0 enables clearer pattern recognition, aiding the model in identifying patterns for t+1 detections.
- The potential lack of relevant features or necessary data for t+0 detections might lead to reduced accuracy in precisely detection at t+0.

Testing was conducted on the calibration dataset from AWS Jatiwangi. This dataset was acquired from the calibration activities performed by BBMKG Wilayah II Tangerang Selatan on August 22, 2022. The calibration dataset comprises parameters TT, RH, and PP with normal values labeled as 0. During the testing using the calibration dataset, the models tested were restricted to TT and PP sensors as input data for sensor RR was not available. Hence, the RH and RR models could not be tested due to the absence of RR sensor data as input for the model. This limitation in testing the calibration dataset stems from the lack of RR sensor input, as the calibration method for RR sensors by BBMKG Wilayah 2 Tangerang Selatan differs from

the calibration method used for TT, RH, and PP sensors. Result of testing is shown in Table VI.

The STD column contains values from the standard calibration sensor for each parameter, while the UUT column displays values from the AWS Jatiwangi sensor. The testing results reveal the model's proficiency in identifying patterns within the standard calibration sensor values, confirming the normal state of this sensor. However, within the AWS Jatiwangi sensor, the model detected an abnormal pattern in a single data point, particularly in the 5th entry, where the temperature (TT) measured 28.05°C.

Although an anomaly was detected in one data point, overall assessments still categorize the TT and PP sensors from AWS Jatiwangi as within the normal range. The model's analysis indicates that this anomaly was only observed in one data point, resulting in the general conclusion that both sensors remain considered stable and normal.

V. CONCLUSION

The paper presents a technique for detecting sensor errors in AWS using LSTM algorithms. The method produces four sensor models: RR, TT, RH, and PP models. These models predict by identifying patterns of reading errors within synthetic data scenarios in the training dataset. There's a notable decrease in loss values as the number of epochs increases. Individual sensor performance evaluations show that the models

can detect sensor reading errors with high average accuracy (>90%, except for RH), high POD, and low FAR. The proposed sensor error detection can serve as a prospective method for predictive maintenance, offering potential implementation for future AWS maintenance procedures. The predictive maintenance framework comprises critical stages related to sensor anomalies in both primary and secondary processes. In this study, the commencement of future work on developing algorithms for estimating remaining useful life should be grounded in the detection of errors.

ACKNOWLEDGMENT

The authors extend their gratitude to the Indonesia Lembaga Pengelola Dana Pendidikan (LPDP) Grant 202109110107819 for offering partial funding support for this research and also express their appreciation to Badan Meteorologi, Klimatologi, dan Geofisika for granting access to the AWS Jatiwangi dataset and calibration dataset, which significantly contributed to this study.

REFERENCES

- [1] BMKG, "Peraturan Badan Meteorologi, Klimatologi, Dan Geofisika Republik Indonesia Nomor 4 Tahun 2020 Tentang Rencana Strategis Badan Meteorologi, Klimatologi, Dan Geofisika Tahun 2020-2024," 2020.
- [2] BNPB, "BNPB Verifikasi 5.402 Kejadian Bencana Sepanjang Tahun 2021," https://bnpb.go.id/berita/bnpb-verifikasi-5-402kejadian-bencana-sepanjang-tahun-2021 Accessed: Feb. 13, 2023. [Online]. Available: https://bnpb.go.id/berita/bnpbverifikasi-5-402-kejadian-bencana-sepanjang-tahun-2021
- [3] BMKG, "AWS Center BMKG," https://awscenter.bmkg.go.id/. Accessed: Feb. 20, 2023. [Online]. Available: https://awscenter.bmkg.go.id/
- [4] BMKG, "Peraturan Kepala Badan Meteorologi, Klimatologi, dan Geofisika Nomor 7 Tahun 2014 tentang Standar Teknis dan Operasional Pemeliharaan Peralatan Pengamatan Meteorologi, Klimatologi, dan Geofisika," 2014.
- [5] J. Zhao, C. Gao, and T. Tang, "A Review of Sustainable Maintenance Strategies for Single Component and Multicomponent Equipment," Sustainability (Switzerland), vol. 14, no. 5. MDPI, Mar. 01, 2022. doi: 10.3390/su14052992.
- [6] N. Es-sakali, M. Cherkaoui, M. O. Mghazli, and Z. Naimi, "Review of predictive maintenance algorithms applied to HVAC systems," Energy Reports, vol. 8, pp. 1003–1012, Nov. 2022, doi: 10.1016/j.egyr.2022.07.130.
- [7] WMO, "Guide to Instruments and Methods of Observation Volume I-Measurement of Meteorological Variables," 2021.

- [8] S. H. Oh and J. G. Kim, "LSTM-based PdM Platform for Automobile SCU Inspection Equipment," in International Conference on Information Networking, IEEE Computer Society, 2023, pp. 363–365. doi: 10.1109/ICOIN56518.2023.10048924.
- [9] Y. Jiang, P. Dai, P. Fang, R. Y. Zhong, X. Zhao, and X. Cao, "A2-LSTM for predictive maintenance of industrial equipment based on machine learning," Comput Ind Eng, vol. 172, Oct. 2022, doi: 10.1016/j.cie.2022.108560.
- [10] D. Dey and R. Jana, "Bearing Fault Predictive Maintenance using LSTM," in ICAN 2022 - 3rd International Conference on Computing, Analytics and Networks - Proceedings, Institute of Electrical and Electronics Engineers Inc., 2022. doi: 10.1109/ICAN56228.2022.10007139.
- [11] Y. H. Ruhiyat, S. Sumaryo, and E. Susanto, "Predictive Maintenance for a Ventilator Using LSTM Algorithm," in APWiMob 2022 - Proceedings: 2022 IEEE Asia Pacific Conference on Wireless and Mobile, Institute of Electrical and Electronics Engineers Inc., 2022. doi: 10.1109/APWiMob56856.2022.10014252.
- [12] WMO, "Guide to Instruments and Methods of Observation Volume III-Observing Systems," 2021.
- [13] B. Santoso, M. Ryan, F. Mukhlish, and D. Kurniadi, "Generating Synthetic Values on Automatic Weather Station Dataset using GAIN," in 2023 8th International Conference on Instrumentation, Control, and Automation (ICA), IEEE, Aug. 2023, pp. 218–223. doi: 10.1109/ICA58538.2023.10273082.
- [14] K. Zarzycki and M. Ławryńczuk, "LSTM and GRU neural networks as models of dynamical processes used in predictive control: A comparison of models developed for two chemical reactors," Sensors, vol. 21, no. 16, Aug. 2021, doi: 10.3390/s21165625.
- [15] N. Pudjihartono, T. Fadason, A. W. Kempa-Liehr, and J. M. O'Sullivan, "A Review of Feature Selection Methods for Machine Learning-Based Disease Risk Prediction," Frontiers in Bioinformatics, vol. 2, Jun. 2022, doi: 10.3389/fbinf.2022.927312.
- [16] M. I. Prasetiyowati, N. U. Maulidevi, and K. Surendro, "Feature selection to increase the random forest method performance on high dimensional data," International Journal of Advances in Intelligent Informatics, vol. 6, no. 3, pp. 303– 312, 2020, doi: 10.26555/ijain.v6i3.471.
- [17] R. C. Chen, C. Dewi, S. W. Huang, and R. E. Caraka, "Selecting critical features for data classification based on machine learning methods," J Big Data, vol. 7, no. 1, Dec. 2020, doi: 10.1186/s40537-020-00327-4.
- [18] P. Wellyantama and S. Soekirno, "Temperature, pressure, relative humidity and rainfall sensors early error detection system for automatic weather station (AWS) with artificial neural network (ANN) backpropagation," in The 10th International Conference on Theoretical and Applied Physics, IOP Publishing Ltd, Mar. 2020. doi: 10.1088/1742-6596/1816/1/012056.
- [19] M. Kubat, An Introduction to Machine Learning. Cham: Springer International Publishing, 2017. https://doi.org/10.1007/978-3-319-63913-0

An Automatic Internet Of Things-Based System For Breeding Rabbit in Cage

Andrian Kharisma Wijaya¹, Andini Sintawati²

1.2 Department of Computer System, Univeristas Gunadarma, Depok, Indonesia
andrian.kharisma@gmail.com, ² anies@staff.gunadarma.ac.id

Accepted on 14 November 2023 Approved on 19 December 2023

Abstract— Rabbits, low-maintenance mammals in terms of cost and space requirements, require meticulous care, encompassing disease control, feeding, and cage maintenance. To address these concerns, an automated system for feeding, drinking, temperature control, and monitoring rabbit manure gas levels within the cage was developed, all remotely accessible. The system comprises ultrasonic sensors, DHT11 sensors, MQ-135 gas sensors, a real-time clock (RTC), an Arduino Mega 2560 with built-in Wi-Fi, relays, servo motors, mini water pumps, mini fans, and a heat lamp. The feeding and drinking functions are automated, triggered by RTC sensor data or can be manually controlled through the Arduino IoT Cloud dashboard. Temperature regulation is managed based on data from the DHT11 sensor, and gas levels in the rabbit manure are monitored using the MO-135 gas sensor. Conducting 30 tests for each primary function, including automatic and manual feeding/drinking, temperature control, and disinfectant spraying, these functions performed as designed. An exception occurred three times when the DHT11 microcontroller sensors lost connection, rendering the input from these sensors unusable. To address this issue, the addition of an extra voltage supply to the Arduino Mega 2560 microcontroller is proposed, mitigating this vulnerability.

Index Terms— Internet of Things; IoT Cloud Dashboard; Rabbit; SQL Database.

I. INTRODUCTION

Rabbits belong to the mammalian order Lagomorpha, family Leporidae, and are categorized into eight genera: Bunolagus, Nesolagus, Romelagus, Brachylagus, Sylvilagus, Oryctolagus, and Poelagus[1]. Rabbits can serve as both pets and livestock. As pets, they can be trained for discipline and have stress-reducing effects on their owners[2]. They are easy to raise, requiring minimal capital and land, and they exhibit a high reproductive rate.

In a livestock capacity, rabbits offer not only consumable meat but also valuable fur, skin, and manure[3][4]. According to data from the Department of Food Security and Livestock in West Java, the rabbit population in West Java reached a total of 2,602,469

individuals from 2012 to 2020[5], with a total rabbit meat production of 18,462 tons from 2013 to 2021.

Due to its favorable meat composition, rabbit meat can be considered an alternative to chicken and beef [6]. Rabbit meat contains only 8% fat and cholesterol, which is lower than chicken and beef, with fat contents of 12% and 24%, respectively[7]. Rabbit meat also boasts a protein content of 12%, which is higher than other livestock with protein contents ranging from 17% to 20% [8].

Raising rabbits requires careful attention to various aspects, including sanitation and preventive measures, disease control, animal care, feeding practices, and cage maintenance. Rabbits are known to be prone to stress for various reasons, and emotional stress can lead to health issues such as leukopenia[9], cardiomyopathy[10], and gastric lesions[11].

Leveraging technology can significantly enhance rabbit farming practice[12], offering increased efficiency in raising rabbits as livestock or pets. One form of technological integration is the development of an Internet of Things (IoT)-based system for rabbit cages, featuring various remote control capabilities.

The Internet of Things (IoT) is a concept where devices are interconnected on a network and can communicate with each other and share data[13]. IoT is becoming an integral part of our daily lives, manifesting in various aspects of our surroundings. Essentially, IoT represents a technological advancement that integrates a wide range of intelligent devices, sensors, and smart systems[14].

In a study conducted by Nanda Budiarta Sabela and their team in 2021, a device was developed for feeding rabbits, connected to a smartphone using the ESP8266 microcontroller and relay[15]. In 2022, Dedi Hermanto designed an automated rabbit waste cleaning system connected to a waste receptacle via the Telegram application on a smartphone, utilizing the ESP8266 microcontroller[16]. Furthermore, in 2022, research by Jikti Khairina involved designing a waste cleaning and

cage temperature control system with a Raspberry Pi microcontroller, connecting to a Blynk application on a smartphone [17].

Consequently, this research introduces an IoT-based rabbit cage system with the capability to provide feed and water, regulate cage temperature, perform disinfectant spraying, and measure rabbit waste levels. This system operates automatically based on predefined schedules, can be manually controlled remotely through the Arduino IoT Cloud dashboard, and is equipped to store measurement data in a MySQL database.

II. METHODS

The method employed in this research involved several stages, including system design, encompassing block diagram system design, system flow chart design, system design, software design, and program code design.

A. Block Diagram System Design

The block diagram system design marked the initial stage in this research. The system was conceived using electronic components, represented in Figure 1 as a block diagram. These electronic components include an HC-SR04 ultrasonic sensor, DHT11 sensor, realtime clock (RTC) sensor, Arduino Mega 2560 with built-in Wi-Fi, relay, servo motor, mini pump, mini blower fan, and heat lamp. The HC-SR04 ultrasonic sensor serves as an input component for measuring remaining food and water levels in the storage containers, utilizing ultrasonic waves to measure distances ranging from 2 cm to 400 cm[18].

Another input component is the DHT11 sensor, which measures temperature and humidity in the cage environment, providing calibrated digital signal output. The RTC sensor contributes real-time data to the system.

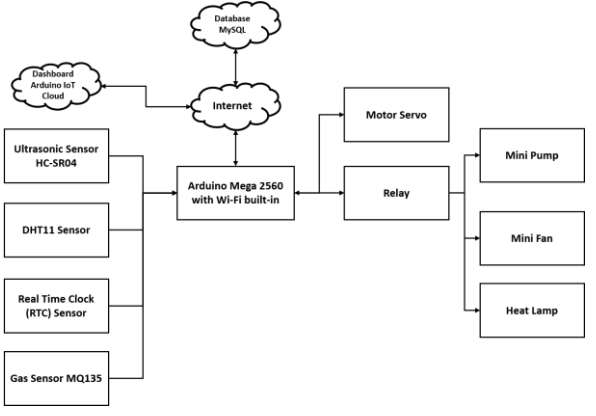


Fig. 1. Block Diagram System

In the processing section, the Arduino Mega 2560 with built-in Wi-Fi functions as the microcontroller for input and output processing, connecting the system to the Arduino IoT Cloud dashboard and the MySQL database. This component is an ATmega2560 microcontroller modified to incorporate an ESP8266 microcontroller on the same board[19].

Notably, the Arduino Mega RobotDyn offers a key distinction from the Arduino Mega 2560 as it can directly connect to the internet via serial communication with the ESP8266, eliminating the need for an additional ESP module.

The output components include the servo motor, which opens the food container cover, and the relay, serving as a switch for the mini pump, mini fan, and heat lamp. Additionally, the Arduino IoT Cloud dashboard functions as both input and output. Arduino IoT Cloud is one of the Arduino services providing cloud services for IoT platforms, enabling data transfer between IoT devices and Arduino IoT Cloud[20][21].

The MySQL database serves as an output, representing a popular open-source SQL (Structured Query Language) database management system developed, distributed, and supported by Oracle Corporation[22].

B. System Flow Chart Design

The system's operation is visually represented in the flowchart depicted in Figure 2. The system begins by initializing the ESP8266 to connect to Wi-Fi. In the event of a failed Wi-Fi connection, the initialization process repeats until successful. Upon successful Wi-Fi connection, the RTC sensor is activated. If the RTC sensor indicates that it's time for feeding, the servo motor rotates, and the water pump is activated. If it's not feeding time, DHT11 sensor is activated and checks temperature in the surrounding cage environment. If the temperature is less than 26° celcius, heat lamp and mini fan are activated. If the temperature is in the 26° - 36° celcius, heat lamp and mini fan will be deactivated. However, if the temperature is greater than 36° celcius, heat lamp turns off and mini fan is activated. The feeding process was conducted in accordance with a preset schedule, and adjustments to the cage environment temperature were automatically made by the system based on various temperature conditions that have been set. Then the ultrasonic sensor and MQ4 sensor are activated. The readings from these sensors are subsequently uploaded to both the IoT cloud dashboard and the MySQL database.

Following this, a condition is checked for input from the dashboard, encompassing button inputs like "feed," "water," "lamp," "fan," and "disinfectant." If the condition is met, each process occurs based on the

specific button input. Activating the "feed" button triggers the servo motor, the "water" button activates the water pump, the "lamp" button activates the lamp, the "fan" button engages the fan, and the "disinfectant" button initiates the water pump, this is a manual mode feature that has been programmed into the system to control several electronic components. If none of these conditions are met, the system concludes its operation.

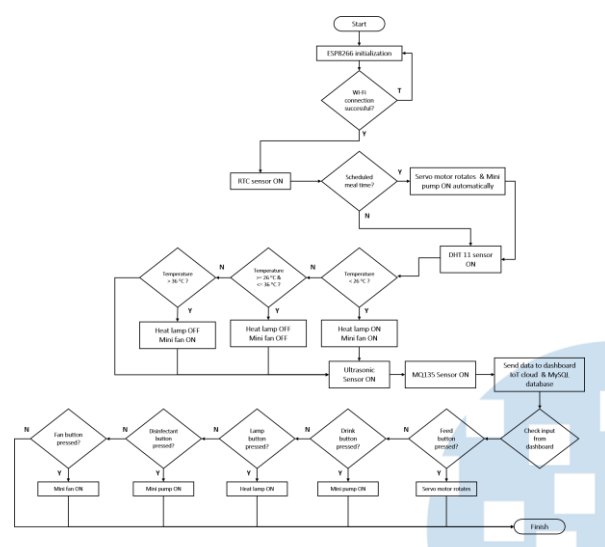


Fig. 2. System Flow Chart Design

C. System Design

The schematic diagram of the system with four main functions is presented in Figure 3. The first primary function is feed and water delivery, which can be executed automatically based on input from the RTC sensor and a pre-set schedule or manually via the "feed" and "water" buttons.

The second function involves automatic cage temperature control, relying on temperature measurements from the DHT11 sensor, or manual control through the Arduino IoT Cloud dashboard, which utilizes a heat lamp and a mini fan as outputs.

Subsequently, the system includes the capability to measure the concentration of rabbit manure gas using the MQ135 sensor and offers a disinfectant spray function that can be controlled from the dashboard, utilizing a mini water pump and a relay to operate the pump. The system's prototype is depicted in Figure 4.

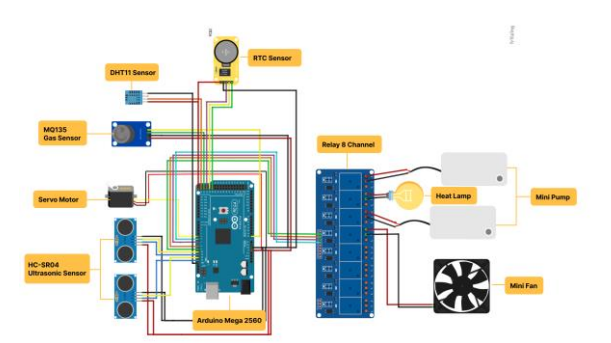


Fig. 3. System Circuit



Fig. 4. System Prototype

D. Software Design

The software design encompasses the development of the Arduino IoT Cloud dashboard, MySQL database design, program code design, and website design. The dashboard design begins by defining the variables associated with the dashboard's widgets. The layout of the dashboard is thoughtfully organized, incorporating essential widgets, as illustrated in Figure 5. Notably, this dashboard is accessible via mobile devices through the installation of the Arduino IoT Cloud application.



Fig. 5. Arduino IoT Cloud Dashboard

The MySQL database design involves creating a new database in PHPMyAdmin and establishing new tables along with their respective columns. These columns are configured with various settings, including data types, null value acceptance, and other identifiers, as depicted in Figure 6.

phpMyAdmin	- 6		Dutabase: rates		· B Tidde:							Ø 2
△■ ■①@@	(1)	rowse 🥖 Struct	re E squ	Search	14 Insert	=	Export 👼 Import	AS PONE	eges 🤌 Operations 🖂 Trigger	5		
Recent Favorites	И	Table structure	C Relation view									
- i New		# Name	7/94	Collation	Attributes	Nati	Default	Correrents	Etha	Action		
⊝ Information_achiema ⊢⊝ mysid		1 ld 🔑	H(11)			No	None		AUTO_INCREMENT		Drop	Mon
High performance_schema High phprnyadmin	D	2 tanggal_jam	tinestamp			Yes	current_timestamp()		ON UPDATE CURRENT_TRIESTAMP	() / Change	Orop	Mon
Hul pythonlogin Hul rabbit_emart_cage		3 sisa_makanan	H(11)			Yes	NULL				Orop	Mor
New data_log		4 sisa_minuman	ks(11)			Yes	NULL			🥒 Change	Orop	Mon
High text	0	5 suhu_kandang	HQ11)			Yes	MULL			/ Change	Orop	Mon
		6 kelembapan_ka	ndang in(11)			Yes	NULL				Orop	Mon

Fig. 6. MySQL Database Preview

Next, the program code is developed using the C## programming language through the Arduino IDE software. The overall program flow of the system is illustrated in Algorithm 1.

The website design in this system employs the Bootstrap framework and the PHP programming language. The website design process initiates with customizing the visual template from Bootstrap, transforming the appearance of web pages designed to display the system's data history into a layout resembling Figure 7.



Fig. 7. Website Appearance

III. TESTING AND RESULTS

The testing of the primary functions of the system is divided into several stages. The initial stage encompasses the testing of automated feeding and watering, wherein feed and water dispensing was scheduled at three specific times: 12:50-12:55, 13:00-13:05, and 13:10. The test results demonstrate that the system operates in accordance with the designed program, as evidenced by the servo motor's rotation and the activation of the mini water pump according to the predefined schedule.

The test results are visually presented in Figure 8, where a value of 0 indicates that the water pump and servo motor are in an "off" state, while a value of 1 signifies that the water pump and servo motor are in an operational state.

Subsequently, a manual feed and water dispensing test was conducted 30 times, revealing that the system effectively responds to inputs provided via the dashboard. The outcomes of this test are summarized in Table 1.

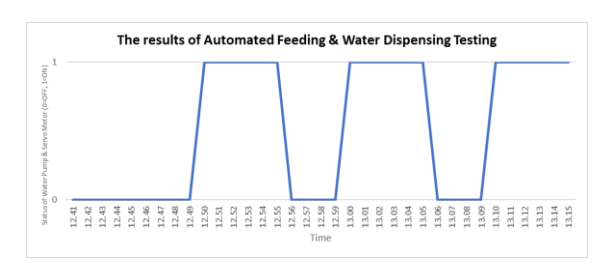


Fig. 8. Chart of Automated Feeding & Water Dispensing Test Results

TABLE I. RESULTS OF MANUAL FEEDING AND WATER DISPENSING TEST

Dashboard Input	Servo Motor Status	Mini Pump Status
Feed Button OFF & Drink Button OFF	OFF	OFF
Feed Button OFF & Drink Button ON	OFF	ON
Feed Button ON & Drink Button OFF	ON	OFF
Feed Button ON & Drink Button ON	ON	ON

Following that, an automated cage temperature control test was carried out at room temperature conditions at home, the testing process is detailed in Figure 9. Involving the design of three conditions in the program, as specified in Table 2. This ensured that the heat lamp and mini fan would activate and deactivate based on preset temperature values in the program. Of the 30 tests conducted, the results indicated that the automated cage temperature control function in the system operated successfully according to the design. The system effectively controlled the heat lamp and mini fan based on the specified temperature values. However, there were three instances of disconnection between the DHT11 sensor and the microcontroller during testing. The test results are depicted in Figure 10, where an active condition is denoted by the number 1, and an inactive condition is denoted by the number 0.



Fig. 9. Cage Environment Temperature Setting Function Testing Process

TABLE II. TEMPERATURE CONDITION SETTINGS IN THE SYSTEM

Temperature	Heat Lamp Status	Mini Fan Status
Less than 26° C	ON	ON
Greater than or equal to 26°C and less than or equal to 36°C.	OFF	OFF
Greater than 36° C	OFF	ON

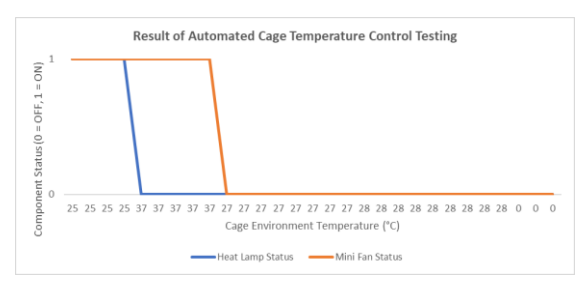


Fig. 10. Chart of Results of Automated Cage Temperature Control Testing

Subsequently, a test was performed to measure the gas content in rabbit waste. The aim of this test was to evaluate whether the MQ-135 sensor could measure the environmental conditions in the cage and detect when the rabbit waste container was full. The testing process is detailed in Figure 11, including the sensor's proximity to the gas emitted by an electric lighter and the rabbit's waste and urine. From the 30 tests conducted, the results demonstrated that the system effectively measured changes in gas levels. The test results are presented graphically in Figure 12, and the range of gas level conditions in the cage environment is documented in Table 3.

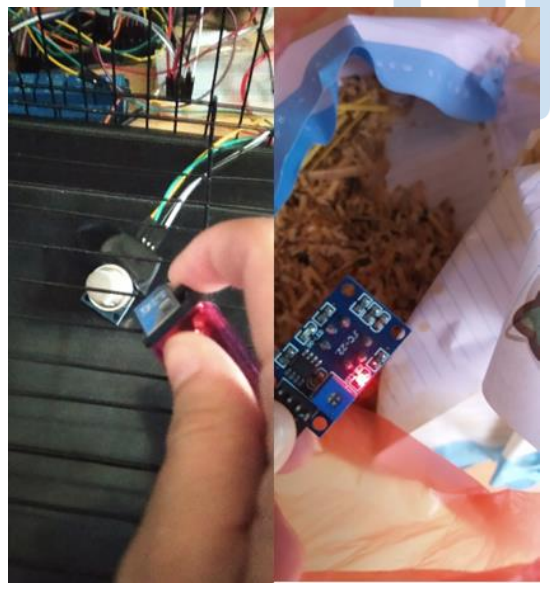


Fig. 11. Gas Content Testing Process

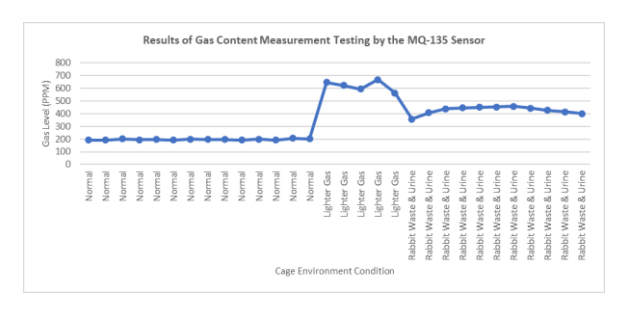


Fig. 12. Chart of Gas Content Measurement Testing Results

TABLE III. GAS LEVEL CONDITIONS IN THE CAGE ENVIRONMENT

Status	Range of Gas Levels (PPM)			
Normal	192-206			
Rabbit Waste & Urine	358-458			
Lighter Gas	564-668			

Finally, the disinfectant spraying function was tested to evaluate the system's response to inputs from the dashboard. The test was carried out by providing input from the dashboard by pressing the disinfectant button 15 times to "on" mode and 15 times to "off" mode to see whether the mini pump works according to the input given. Out of a total of 30 tests, it was observed that the system consistently produced outputs in accordance with the given inputs, the testing process is detailed in Figure 13. The test results are summarized in Table 4.



Fig. 13. Disinfectant Spracy Function Testing Process

TABLE IV. DISINFECTANT SPRAY FUNCTION TEST RESULTS

Doghhoond Innut	Mini Pump Status Count					
Dashboard Input	ON	OFF				
Disinfectant Button OFF	0	15				
Disinfectant Button ON	15	0				

IV. CONCLUSIONS

Based on the conducted tests, it can be concluded that the system has successfully achieved the expected functionality. This is evident from the automated feeding and watering tests, which operated seamlessly according to the predefined schedule, as well as the manual feed and water dispensing based on dashboard inputs.

Moreover, the system effectively measured changes in air quality with the MQ-135 sensor when there was a significant amount of rabbit waste, validating its utility. The manual disinfectant spraying function performed as designed. While the tests for both automated and manual cage temperature control were consistent with the programmed parameters, there were three instances of disconnection between the DHT11 sensor and the microcontroller, which, though tolerable, warrants attention.

Additionally, the system's response time ranged from approximately 15 seconds and beyond for processing inputs from the Arduino IoT Cloud dashboard, as the input reading process by the microcontroller was set at a 15-second interval in the program.

Throughout the design and testing phases, weaknesses in the system were identified, offering valuable recommendations for further development. These include the incorporation of backup power sources to ensure the system's optimal operation. Furthermore, the consideration of cameras can enhance the system by enabling the monitoring of rabbit activities.

REFERENCES

- M. Ren et al., "Biology of the Rabbit," Medical Journal of Peking Union Medical College Hospital, vol. 13, no. 5, pp. 880–887, 2022, doi: 10.12290/XHYXZZ.2022-0190.
- [2] R. Juliadilla and S. C. Hastuti, "Peran Pet (Hewan Peliharaan) pada Tingkat Stres Pegawai Purnatugas," *Jurnal Psikologi Integratif*, vol. 6, no. 2, pp. 153–175, Jan. 2019, doi: 10.14421/JPSI.V6I2.1488.
- [3] H. Hendriette and J. Purwono, "Strategi Pengembangan Usaha Peternakan Kelinci Pada Kampoeng Kelinci di Desa Gunung Mulya Kecamatan Tenjolaya Kabupaten Bogor," Bogor Agricultural University, 2014.
- [4] V. Cesari, M. Zucali, L. Bava, G. Gislon, A. Tamburini, and I. Toschi, "Environmental Impact of Rabbit Meat: The Effect of Production Efficiency," *Meat Sci*, vol. 145, pp. 447–454, Nov. 2018, doi: 10.1016/J.MEATSCI.2018.07.011.
- [5] Dinas Ketahanan Pangan Dan Peternakan Provinsi Jawa Barat, "Populasi Kelinci Berdasarkan Jenis Kelamin dan Kabupaten/Kota di Jawa Barat," https://opendata.jabarprov.go.id/. Accessed: Dec. 08, 2022. [Online]. Available: https://opendata.jabarprov.go.id/id/dataset/populasi-kelinci-berdasarkan-jenis-kelamin-dan-kabupatenkota-di-jawa-barat.
- [6] R. Masanto, Beternak Kelinci Potong. Penebar Swadaya, 2010.
- [7] M. Cullere and A. Dalle Zotte, "Rabbit meat production and consumption: State of knowledge and future perspectives,"

- *Meat Sci*, vol. 143, pp. 137–146, Sep. 2018, doi: 10.1016/J.MEATSCI.2018.04.029.
- [8] T.A. Ruleva, N.Y. Sarbatova, and K.Y. Shebela, "Nutritional Value of Rabbit Meat," World science, vol. 4, no. 4 (4), 2015.
- [9] L. B. Nice and H. L. Katz, "Emotional Leucopenia in Rabbits," https://doi.org/10.1152/ajplegacy.1936.117.3.571, vol. 117, no. 3, pp. 571–575, Oct. 1936, doi: 10.1152/AJPLEGACY.1936.117.3.571.
- [10] H. W. Weber and J. J. Van Der Walt, "Cardiomyopathy in Crowded Rabbits.," *Recent Adv Stud Cardiac Struct Metab*, vol. 6, pp. 471–477, 1975.
- [11] J. O. Iversen, G. L. Hoff, T. M. Yuill, and R. P. Hanson, "Gastric lesions in the snowshoe hare," *J Wildl Dis*, vol. 8, no. 1, pp. 7–9, 1972, doi: 10.7589/0090-3558-8.1.7.
- [12] G. Kartasasmita, Pembangunan untuk Rakyat: Memadukan Pertumbuhan dan Pemerataan. Jakarta: Pustaka Cidesindo, 1996
- [13] J. H. Nord, A. Koohang, and J. Paliszkiewicz, "The Internet of Things: Review and Theoretical Framework," Expert Syst Appl, vol. 133, pp. 97–108, Nov. 2019, doi: 10.1016/J.ESWA.2019.05.014.
- [14] S. Kumar, P. Tiwari, and M. Zymbler, "Internet of Things is a revolutionary approach for future technology enhancement: a review", doi: 10.1186/s40537-019-0268-2.
- [15] N. B. Sabela, A. R. Fadhillah, R. J. Sakinah, and D. Siswanto, "Implementasi Proyek Independen Melalui Inovasi Teknologi Pemberian Pakan Ternak Kelinci Berbasis IoT (Internet of Things) dalam Meningkatkan Efisiensi Kinerja Peternak," Universitas Widyagama Malang, p. 8, 2021.
- [16] D. Hermanto and D. Yendri, "Rancang Bangun Sistem Pembersih Kotoran Otomatis pada Kandang Kelinci Berbasis IoT (Internet of Things)," *Universitas Andalas*, vol. 3, no. 02, pp. 146–154, Oct. 2022, doi: 10.25077/chipset.3.02.146-154.2022.
- [17] J. Khairina and M. Nasir, "Sistem Monitoring Pembersihan Kotoran Dan Pengaturan Suhu Kandang Kelinci Berbasis Raspberry Pi," *Journal of Artificial Intelligence and Software Engineering (J-AISE)*, vol. 2, no. 1, May 2022, doi: 10.30811/JAISE.V2II.3085.
- [18] E. J. Morgan, "HC-SR04 Ultrasonic Sensor Datasheet." Accessed: Jan. 24, 2023. [Online]. Available: https://datasheetspdf.com/pdf/1380136/ETC/HC-SR04/1.
- [19] Fernando Koyanagi, "Arduino MEGA 2560 With WiFi Built-in ESP8266." Accessed: Jan. 24, 2023. [Online]. Available: https://www.instructables.com/Arduino-MEGA-2560-With-WiFi-Built-in-ESP8266/.
- [20] A. Kurniawan, "Arduino IoT Cloud," Beginning Arduino Nano 33 IoT, pp. 131–155, 2021, doi: 10.1007/978-1-4842-6446-1_5.
- [21] T. Fatema, M. A. Hakim, T. K. Mim, M. J. Mitu, and B. Paul, "IoT cloud based noise intensity monitoring system," *Indonesian Journal of Electrical Engineering and Computer Science*, vol. 30, no. 1, pp. 289–298, Apr. 2023, doi: 10.11591/IJEECS.V30.I1.PP289-298.
- [22] B. Christudas, "MySQL," Practical Microservices Architectural Patterns, pp. 877–884, 2019, doi: 10.1007/978-1-4842-4501-9_27.

Automatic Mass Waste Sorting System Using Inductive Proximity Sensor, Water Level Sensor and Image Processing using MobileNet Algorithm

Megantara Pura, Charles H. Langko, Jason Kho

Electrical Engineering Program, Universitas Multimedia Nusantara, Tangerang, Indonesia megantara.pura@umn.ac.id, charles.langko@student.umn.ac.id, jason.kho@student.umn.ac.id

Accepted on 30 November 2023 Approved on 21 December 2023

Abstract— The global municipal solid waste is predicted to increase by threefold in 2050. Indonesia's most wastes are unsorted and only end up in landfill and the waste management is less than ideal. An automatic mass waste sorting system is proposed to answer such problems. The automatic mass waste sorting system is designed to be able to identify and separate metal, plastic and organic waste using electrical sensors and image processing. The electrical sensors was able to identify waste types with 65% accuracy and the image processing system was able to identify waste types with 86.67% accuracy. The result doesn't offer much advantage compared to other research on waste management system, however it is hoped that this research may inspire other researches on mass waste sorting systems.

Index Terms— inductive proximity sensor; metal waste; MobileNet; organic waste; plastic waste; trash sorting; water level sensor.

I. INTRODUCTION

The global municipal solid waste is predicted to increase by threefold from 2.01 billion tons per year in 2050 [1]. Recycling can be one of the steps to prevent such prediction. To encourage recycling, a waste must be sorted first based on the type, such as separating plastic wastes from metal and glass [2]. However, most wastes in Indonesia are unsorted and only end up in a landfill [3]. It is also stated that the waste management in Indonesia is still not ideal; with waste reduction rate and recycling rate are only in 11% [4]. Another problem was 80% of waste management was still done by human, who are landfill workers [5]. These jobs are at risk of several diseases such as tuberculosis, bronchitis, asthma, pneumonia, dysentery, and malnutrition [6]. Therefore, an automatic waste sorting system is needed to answer such problems.

Several researches are already done in the context of waste sorting management using a technology. On

the research using electrical sensors, an example of one of the research is a prototype of smart trash bin using LDR and proximity sensors [7]. The proposed system was able to differentiate plastic and paper waste. However, the disadvantage comes with the low detection distance. Another example is the use of capacitive and inductive sensor to differentiate metal and non-metal waste [8]. The system was able to detect metal waste, but unable to sort plastic waste. Another research attempts to detect wet waste using capacitive sensor, based on the theory that wet waste will have larger dielectric constant than dry waste [9]. An alternative sensor that can be used is water level sensor, where the resistance value will change when the surface was exposed to the water [10].

On the other hand, an alternative approach for trash sorting is using image recognition technology. This is caused by limited amount of sensor types and types of wastes that can be detected. Visual analysis can be used to assist the sensors to make the trash identification become more accurate.

An example of the research that has been done is using a camera with Deep Neural Network (DNN) algorithm [11]. The algorithm was trained using VNtrash datasets to create a model, and then the model is tested for its accuracy. Another example is using CNN and transfer learning. The CNN that is used is the DenseNet Model. Other research uses MobileNet, a CNN architecture that was developed for mobile device with limited power supply. An example of the research is using MobileNet for application in Android system with limited computing capability [12]. The research states that the model reaches the accuracy of 87.2%. This architecture uses depthwise separable and pointwise convolution on the convolutional layer. Therefore, this reduces the computation value, and suitable for embedded applications [13].

The purpose of this research is to develop an automatic waste sorting system that is capable of sorting waste en masse. The waste sorting is expected to be able to separate metal waste, plastic waste, and wet organic waste from a pile of wastes. Inductive proximity sensor and water level sensor is used to detect metal and wet organic waste, while the plastic waste will be detected using image processing using MobileNet architecture.

II. METHODOLOGY

A. Design Concept

The concept of the system is a mass trash sorting system that is able to detect and sort waste types. The user placed the mass of trashes into the funnel. The funnel will open automatically to guide the trashes into the vibration machine. The vibration machine is used to make the trash fall one at a time into the detection chamber. The detection chamber contains sensors to identify and classify waste types. After then, the detection chamber opens and the trash will be guided to the separated waste bins. The system was provided with extra waste bin for the trash that was failed to be identified.

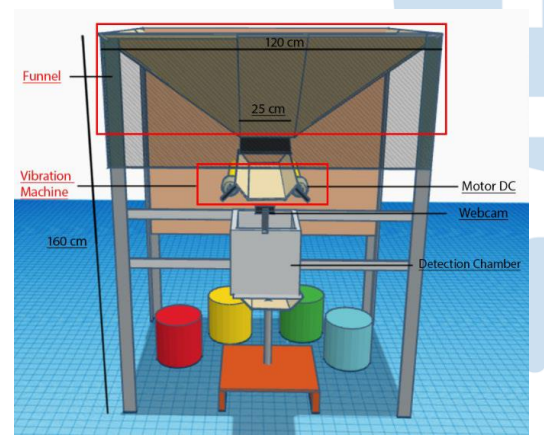


Fig. 1. The proposed design of the automatic mass waste sorting system

The proposed design is illustrated in Figure 1. The whole system has the area of 120 cm x 90 cm, with the height of 160 cm. For this research, only three types of wastes that will be tested to be identified, that is metal waste in the form of drinking cans, plastic waste in the form of drinking bottles, and organic wastes in the form of fruit peels. The size of the waste is limited to 25 cm x 25 cm. The whole system was powered using DC power supply.

There are three systems in the device; a system for trash guiding, a system for sensors, and a system for image processing. The overall block diagram is illustrated in Figure 2.

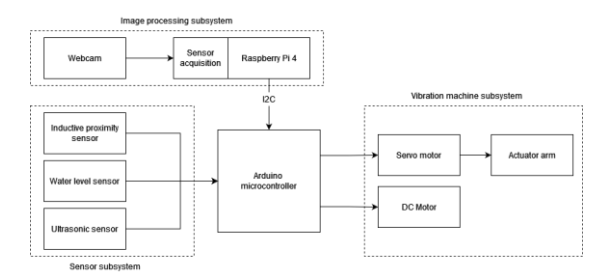


Fig. 2. The block diagram of the system

The trash was inputted to the large funnel on top. When the trash falls to the track, the vibration machine is active in order to make the trash fall to the detection chamber one at the time. When one of the trashes goes to the detection chamber, the vibration machine is inactive and the detection system starts classifying the type of waste. The detection chamber open and the trash will be guided to the waste basket according to the waste type. The process loops until there are no trashes left on the funnel. A fourth waste basket was provided in case the waste was not identified by the three types of waste already mentioned. Figure 3 provides the flowchart of the system.

The trash that fall into the detection chamber will be read by the ultrasonic sensor, stopping vibration machine to prevent more trash falling into the chamber. The image processing subsystem will start first, determining the waste types using algorithm that is stored in Raspberry Pi. If the confidence level of the image processing is below 50, the sensor subsystem will take over to determine the waste types. When the detection is done, the microcontroller will move the waste track using servo motor to the waste baskets.

B. Testing and validation method

Testing is done to evaluate how the sensors able to identify the waste type. In this system, the proximity sensor and water level sensor starts reading the data when the distance of waste and the ultrasonic sensor is less than 5 cm. 10 types of wastes, with 5 types of metallic drinking cans and 5 types of organic wastes such as fruit peels are placed one-by one in random order. Then the sensor will responds how the data is evaluated. Based on the research done on waste management system, it is expected to have 61% accuracy rate and 85% precision rate.

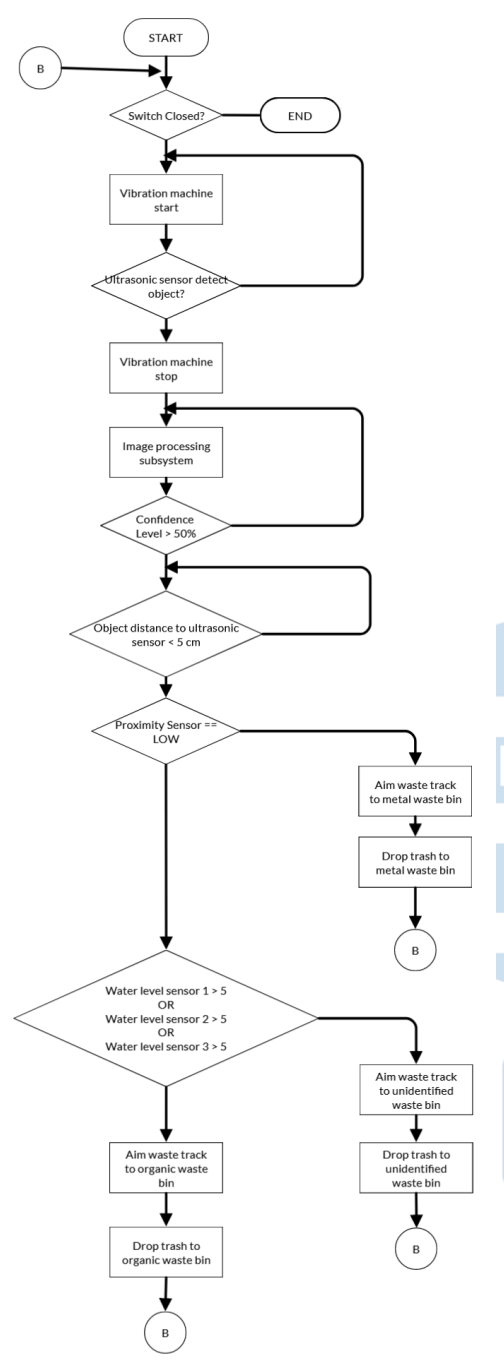


Fig. 3. The block diagram of the system

For image processing system, several testing steps were done. The first step is the preparation step, where the webcam was connected to Raspberry Pi 4. The second step is activating image processing program, object introduction in real time, and running tests on 20 different objects to evaluate the classification output from the program. The third step is the training and accuracy validations; where the datasets was put in the Teachable Machine application. In the application, the basic model that is used is *MobileNet*. This model was chosen due to its compatibility with Raspberry Pi 4. By

default, the model that is used in Teachable Machine is MobileNet version 1, or MobileNetV1. The model has the size of 224x224 pixels. The accuracy was calculated using equation (1) to (4):

$$Accuracy = \frac{TP + TN}{TP + TN + FP + FN}$$

$$Precision = \frac{TP}{TP + FP}$$

$$Recall = \frac{TP}{TP + FN}$$

$$1$$

$$F1 = \frac{1}{1 + FN}$$

$$(1)$$

$$(2)$$

$$(3)$$

$$Precision = \frac{TP}{TP + FP} \tag{2}$$

$$Recall = \frac{TP}{TP + FN} \tag{3}$$

$$F1 = \frac{1}{\frac{1}{Precision} + \frac{1}{Recall}} \tag{4}$$

Where TP is true positive, TN is true negative, FP is false positive and FN is false negative. After training, the model is converted in tflite form and run in Raspberry Pi 4.

Based on the research done on image processing for identifying waste types using similar systems; it is expected to have 90% accuracy rate and 85% precision rate.

III. ANALYSIS

Data analysis will be separated for each subsystem.

A. Trash guiding system

The whole system is constructed on a steel frame, with triplex wood as the body. The funnel part is constructed using galvanic plate. The vibration machine track was constructed using MDF plate on two PVC pipes as the frame. This vibration track will be moved using a cam driven from a 5V DC motor. On the side of the vibration track is a rack for housing the Arduino MEGA 2560, Raspberry Pi 3, and the circuitry for powering the whole system. The final track for trash separation was constructed using MDF plate on a wood, driven by MG996 servo motor. The constructed design can be seen in Figure 4.

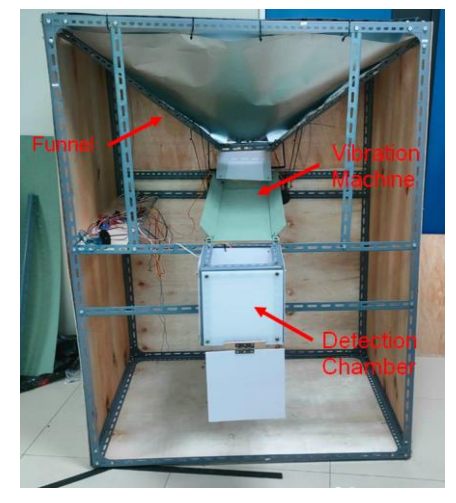


Fig. 4. Front view of the constructed system

For the detection chamber system, steel frame is used along with 5 mm acrylic glass as its body. The Logitech webcam was mounted on top of the chamber for image processing subsystem. The lid is mounted with water level sensor and inductive sensor. Placed near the lid was an ultrasonic sensor for trash detection. The inside of the chamber, along with the position of the sensors is illustrated in Figure 5.

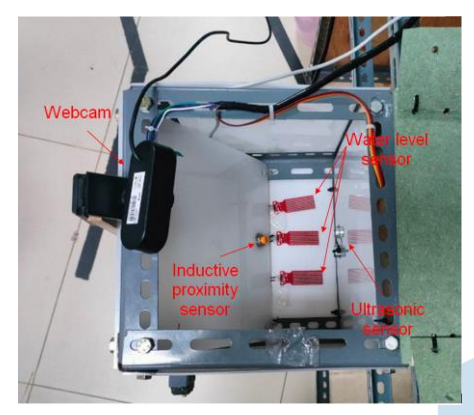


Fig. 5. The inside view of the detection chamber, showing the placement of the sensors

Testing is done to evaluate whether the system is capable of guiding the wastes into the detection chamber one by one. During the testing, the system was able to completely guide metal and plastic wastes with 100% accuracy, however it completely failed to guide organic waste to the detection chamber. One of the possible reason is the organic waste might be too sticky to the surface, and the vibration was not strong enough to move the waste.

B. Trash identification system using sensor

Testing is done to evaluate how the sensors able to identify the waste type. In this system, the proximity sensor and water level sensor starts reading the data when the distance of waste and the ultrasonic sensor is less than 5 cm. For testing purposes, the microcontroller is connected to the laptop, using Arduino IDE serial monitor to display the results from sensor reading. Figure 6 shows the output from the serial monitor.

```
distance: 1.96 cm

CLASSIFICATION = LOGAM
distance: 2.18 cm

CLASSIFICATION = LOGAM
distance: 2.28 cm

CLASSIFICATION = LOGAM
```

Fig. 6. Serial monitor output from the sensor subsystem

The random waste samples were prepared to evaluate the system accuracy. The samples are shown

in Figure 7, where M denotes metallic waste and O denotes organic wastes, and the number indicates the different waste such as drinking cans from other brand and different fruit peels. For each evaluation, the samples will be dropped inside the detection chamber in random order.



Fig. 7. Waste samples with each respective labels

Table 1 illustrates the result of random samples, "Good" indicates the sample is able to be identified correctly by the system and "Bad" indicates that the sample is failed to be identified.

TABLE I. RESULT OF THE READING FROM ELECTRICAL SENSOR SUBSYSTEM

	Test	Test set 1		set 2	Test	set 3	Test set 4		
	M1	Good	M4	Bad	O1	Good	М3	Good	
	O1	Good	О3	Bad	O2	Good	O5	Bad	
	M2	Good	M5	Good	M1	Good	О3	Bad	
	O2	Bad	O4	Bad	M3	Good	O4	Bad	
	M3	Bad	O5	Bad	O4	Bad	M4	Good	
	О3	Good	O1	Good	M4	Good	O2	Good	
1	M4	Good	M1	Good	О3	Good	M2	Good	
	O4	Bad	O2	Good	M5	Bad	M1	Good	
	M5	Good	M2	Good	M2	Good	O1	Good	
	O5	Bad	M3	Good	O5	Bad	M5	Good	
	Average accuracy = 70%			Average accuracy = 70%		ge icy =	Average accuracy = 70%		

From the results, the accuracy of the device is around 65%. On the overall score, it shows relatively no improvement to the similar researches in waste sorting systems using electrical sensors. The factors that involving such result might from the trash size that was relatively too small, therefore the ultrasonic sensor failed to recognize the object. This statement was identified by the failed result produced by the metal samples that is relatively small compared to the other samples, and the organic wastes which were relatively flat. Some metal sample also gives inconsistent results due to the metal cans might land on a different position; some of the position may not trigger the ultrasonic sensor which makes the system failed to identify the sample.

To prove this statement, an alternative script was used by bypassing ultrasonic sensor reading to identify the waste types. Sample used are the only samples that produce failed result in previous testing. Based on the alternative script testing, the successful result is 66.7%. Some organic wastes failed to be detected because the waste lands on the side where no water level sensors are present. It can be concluded that the sensor placement needs to be redesigned in order to increase its detection capability.

C. Trash identification system using image processing

During testing, the Raspberry Pi was connected to a display monitor for monitoring the result. The program was shown in figure. The display shows the image taken from the camera, along with text for displaying waste type and confidence level in percent. The program and the view of the webcam can be seen in Figure 8.



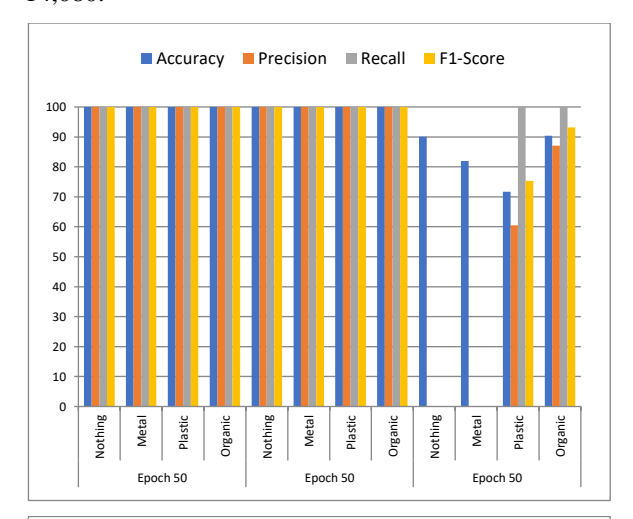
Fig. 8. View of the webcam capturing the sample image in the detection chamber, showing identification result along with the confidence level score

Using epoch value 50, batch size in range of 16-32 and learning rate value 0.001, the system works well. This is based on the score of recall, accuracy, precision and F1 score of 100%. However, using learning rate value of 0.01, the whole score decrease significantly. It is observed that a learning rate value that is too high will cause unstable model and decrease of detection capability.

On the other hand, increasing epoch value to 70 will results in stable and good score for each parameter change. However, large epoch value doesn't guarantee stability of the model. An epoch value of 80 with learning rate of 0.01 resulting in the model incapable of classifying waste types to "nothing". Therefore, an epoch value of 70 is considered optimal in this research. The summary of the model training result is illustrated in Figure 9.

After accuracy test were done, the model was downloaded in *tflite* form, and the architecture was extracted from said model. The model uses 3x3 kernel for *depthwise* layer and 1x1 for Conv2D layer. The activation used for this model is *ReLu* and *Softmax* for *Dense*, and *Linear* for other layers. From the extraction results, the total parameter is 538,608 with trainable

parameter is 524,528 and non-trainable parameter is 14,080.





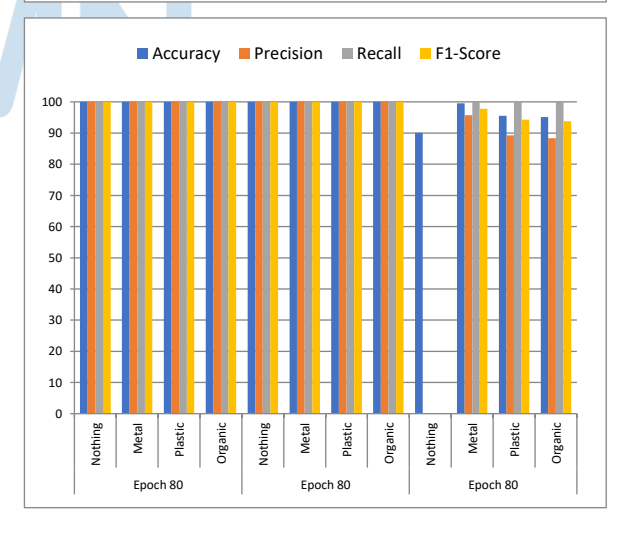


Fig. 9. Result of model training with various variables on epoch 50, 70, and 80

The created model was tested to evaluate its capability of classifying wastes in terms of shape, background, and color. Each waste identification

testing was repeated seven times, to evaluate whether the identification still accurate whether the trash lands on the detection chamber in different positions. The samples that were used is shown in Figure 10.



Fig. 10. Waste samples with each respective labels

Table 2 shows the result of the image training. "Success" indicates the samples were identified correctly, and "Fail" indicates the samples were identified wrong, regardless of confidence level score.

TABLE II. RESULT OF IMAGE PROCESSING USING TRAINED MODEL.

M	etal waste	Pla	stic waste	Organic wastes		
M1	Success 7	P1	Success 7	O1	Success 6	
	Fail 0		Fail 0		Fail 1	
M2	Success 6	P2	Success 7	O2	Success 5	
	Fail 1		Fail 0		Fail 2	
M3	Success 7	P3	Success 3	О3	Success 5	
	Fail 0		Fail 3		Fail 2	
Avera 95%	ge success =	Avera 85%	ge success =	Average success = 80%		

For waste sample testing, the average of the accuracy of the subsystem was 86.67%, with 85% precision. This accuracy was relatively low compared to other research. There are several reasons. The first one is the need to increase training data. During testing, the amount of the training data is 900 samples. The second reason is the training image variety. The images used for training are not varied enough in terms of positions, which make the failure of identification when the object is in the other positions. The third reason is the use of Tensorflow lite. This is the program that is compatible with Raspberry Pi, however the use of this program needs higher compression of the model. The compression process reduces the complexity of the model.

Another problem was found during the whole system testing. Based on the live testing, the image processing system always gives high number of confidence level, even with the wrong identification. This makes the sensor subsystem doesn't work to help image processing subsystem to give a better results. The program flow needs to be re-evaluated to solve this problem.

IV. CONCLUSIONS

The system was capable of classifying wastes with the overall accuracy of 75.83%, based on the average accuracy of the two subsystems. Several improvements needs to be done for the device, such as increasing training data, redesign sensors placement and reorganize the program flow so the subsystem can work together to improve the accuracy. Even so, it is hoped that this research may inspire future researches on mass waste sorting systems.

ACKNOWLEDGMENT

The authors would like to thank Universitas Multimedia Nusantara for supporting this research.

REFERENCES

- [1] S. Kaza, L. Yao, Perinaz Bhada-Tata, Frans Van Woerden, and Kremena Ionkova, *What a waste 2.0 : a global snapshot of solid waste management to 2050.* Washington, Dc: World Bank Group, 2018. Available: https://openknowledge.worldbank.org/handle/10986/30317.
- [2] J.-P. Lange, "Managing Plastic Waste—Sorting, Recycling, Disposal, and Product Redesign," ACS Sustainable Chemistry & Engineering, vol. 9, no. 47, Nov. 2021, doi: https://doi.org/10.1021/acssuschemeng.1c05013..
- [3] Y. A. Fatimah, K. Govindan, R. Murniningsih, and A. Setiawan, "Industry 4.0 based sustainable circular economy approach for smart waste management system to achieve sustainable development goals: A case study of Indonesia," *Journal of Cleaner Production*, vol. 269, p. 122263, Oct. 2020, doi: https://doi.org/10.1016/j.jclepro.2020.122263.
- [4] S. N. Qodriyatun, Y. Indahri, E. Andina, A. S. Suryani, "Sampah plastik dan implikasi kebijakan pembatasan plastik sekali pakai terhadap industri dan masyarakat", *Pusat Penelitian, Badan Keahlian DPR RI* bekerja sama dengan Intrans Publishing, 2019.
- [5] "Indonesia.go.id Membenahi Tata Kelola Sampah Nasional," Indonesia.go.id, 2021. https://indonesia.go.id/kategori/indonesia-dalam-angka/2533/membenahi-tata-kelola-sampah-nasional.
- [6] S. Naaz, "Health Hazards and Social Stigma Faced by Rag-Pickers in Delhi-A Review," *International Journal of Research* in Engineering, Science and Management, vol. 2, no. 5, pp. 804-807, May 2019.
- [7] Ikram et al., "Design and development of smart sorting recycle bin prototype," AIP Conference Proceedings, Nov. 2018, doi: https://doi.org/10.1063/1.5066843.
- [8] P. Aritonang, B. E.c, S. D. K, and J. Prasetyo, "RANCANG BANGUN ALAT PEMILAH SAMPAH CERDAS OTOMATIS," PROSIDING SNITT POLTEKBA, vol. 2, no. 1, pp. 375–381, Dec. 2017.

- [9] N. S. Gupta, V. Deepthi, M. Kunnath, P. S. Rejeth, T. S. Badsha, and B. C. Nikhil, "Automatic Waste Segregation," 2018 Second International Conference on Intelligent Computing and Control Systems (ICICCS), Jun. 2018, doi: https://doi.org/10.1109/iccons.2018.8663148.
- [10] R. S. Kusumadiarti and H. Qodawi, "Implementasi Sensor Water Level Dalam Sistem Pengatur Debit Air Di Pesawahan", *Jurnal PETIK*, vol. 7, no. 1, Mar. 2021.
- [11] A. H. Vo, L. Hoang Son, M. T. Vo, and T. Le, "A Novel Framework for Trash Classification Using Deep Transfer
- Learning," *IEEE Access*, vol. 7, pp. 178631–178639, 2019, doi: https://doi.org/10.1109/access.2019.2959033.
- [12] G. Kartasasmita, "Pembangunan untuk Rakyat: Memadukan Pertumbuhan dan Pemerataan". *Pustaka Cidesindo*, 1996.
- [13] S. L. Rabano, M. K. Cabatuan, E. Sybingco, E. P. Dadios, and E. J. Calilung, "Common Garbage Classification Using MobileNet," 2018 IEEE 10th International Conference on Humanoid, Nanotechnology, Information Technology, Communication and Control, Environment and Management (HNICEM), Nov. 2018, doi: https://doi.org/10.1109/hnicem.2018.8666300030.



Trajectory Planning of Spherical Pendulum Pattern for Application in Creating Batik Patterns

Indah Radityo Putri¹, Estiyanti Ekawati², Eko Mursito Budi², Alfisena Juwandana¹, Naufan Aurezan Mulyawan³, Philip Inarta Kho³, Komarudin Kudiya⁴

¹ Instrumentation and Control Graduate Program, Institut Teknologi Bandung, Bandung, Indonesia
 ² Engineering Physics Research Group, Institut Teknologi Bandung, Bandung, Indonesia
 ³ Engineering Physics Undergraduate Program, Institut Teknologi Bandung, Bandung, Indonesia
 ⁴ Rumah Batik Komar, Bandung, Indonesia

indahradityoputri@gmail.com, esti@itb.ac.id, mursito@itb.ac.id, alfisenajuwandana@gmail.com, naufanaurezan@gmail.com, philipinartakho@gmail.com, komarudinkudiya@gmail.com

Accepted on 04 December 2023 Approved on 21 December 2023

Abstract—Batik Pendulum is a new batik pattern created by Rumah Batik Komar using a single-string pendulum filled with wax. However, current production is still manual, so it is impossible to re-manufacture in large quantities. This research is part of a machine and software development project to produce Batik Pendulum, where this research focuses on software development. The designed software has a spherical pendulum trajectory planning feature through parameter changes. The spherical pendulum path was chosen because it has the same pattern as the currently produced Batik Pendulum. An algorithm that receives parameter values input has been designed to produce the spherical pendulum trajectory. These proposed parameters provide a variety of spherical pendulum patterns. After the user changes the parameters, the software requires 1-2 seconds to generate the trajectory. This duration is within the user's flow of thought when engaging with the software.

Index Terms— batik patterns; batik pendulum software; batik trajectory planning; spherical pendulum trajectory planning; trajectory planning software.

I. INTRODUCTION

Batik is a traditional Indonesian cloth designated by UNESCO as a masterpiece of the oral and intangible heritage of humanity on October 2, 2009. Batik is a detailed patterned textile made through a repetitive process, namely drawing or stamping wax on the fabric, dyeing, removing wax, washing, drying, and repeating until the desired pattern and color is achieved. The uniqueness of batik lies in its pattern. Batik has two basic patterns, geometric and nongeometric, each with characteristics [1]. Most traditional patterns are drawn by hand. Along with the growth of computer algorithms for generating patterns,

contemporary batik patterns, such as fractals, have recently been generated using software and fractal algorithms [2] and then hand-drawn on fabric and proceeding to the batik production procedure.

The batik production process occurs in eight provinces in Indonesia—Jambi, Bengkulu, Jakarta, West Java, Central Java, Yogyakarta, East Java, and Bali—which produce the majority of the country's batik [3]. However, due to social distancing health policies, the COVID-19 pandemic disrupted this business by laying off most of the workforce. Therefore, Batik Small and Medium Enterprises (SMEs) must innovate to respond to this labor shortage [4]. Automating a part of the production line is one way to compensate for the shortage of batik production workers.





Fig. 1. (a) Single-string pendulum [5] & (b) Batik Pendulum product

Rumah Batik Komar, a batik business in West Java, Indonesia, is thriving in creative patterns and automation of production processes. The latest innovation is the Batik Pendulum [5], which produces unique batik patterns using a single-string pendulum filled with wax. The pendulum is swung from a certain angle and then released to oscillate naturally. Competent craftsmen operate this pendulum to

produce artistic circular patterns. This method allows craftsmen to produce unique and exclusive batik patterns. However, batik businesses must mass produce repeating circular patterns to reach a larger market. Batik businesses want to compose pattern designs and draw them in a way that resembles pendulum oscillations to maintain image reproducibility.

Creating repetitive motifs such as Lissajous patterns has been done using tuning forks [6], oscilloscope, and pendulum [7]. In addition, a visual representation of sounds that form repeating patterns using a harmonograph has also been carried out [8]. Then, repeated Fourier decomposition patterns using ropes were created [9].

As will be done in this research, repetitive motifs can also be done using a pendulum-based machine. The use of pendulums in various studies by Galileo, Huygens, Newton, and Hooke is discussed in detail in [10]. The use of pendulums in art was carried out in [11] to stimulate the creative mind. The trajectory of a spherical pendulum was measured using a simple method [12] using a gravity ball equipped with an LED and a digital camera. Dynamic pendulum analysis on an elliptical trajectory has also been carried out [13]. Furthermore, modeling using pendulums was carried out on oscillations for slewing crane motion [14], pendulum-actuated spherical rolling robots [15], and anti-swing control on overhead cranes [16]. From these studies, this research will focus on creating repeating circular patterns close to the Batik Pendulum pattern currently made using the spherical pendulum trajectory equation approach.

In response to these challenges, a cable-driven parallel robot (CDPR) is proposed to produce Pendulum Batik. CDPR is widely used in various industries, including construction, logistics, motion simulation, production engineering, and entertainment [17]. CDPR offers a slim structure and facilitates accurate positioning [18]. Apart from that, CDPR has three advantages, namely operating in an ample working space, handling large loads, and moving dynamically [17]. This capability makes it easy to simulate pendulum movements. Initial research [19] was carried out to simulate the kinematics of a CDPR end-effector in tracking various patterns and determining the maximum cable length and area required to draw geometric patterns.

This research is part of CDPR's machine and software development project to produce Pendulum Batik, where this research will focus only on software. The proposed CDPR machine has four cables connected to an end-effector, a wax-filled pendulum. CDPR software generates the pattern and sends it to the CDPR machine to apply the wax to the fabric.

CDPR software has three modes: manual, automatic, and gallery. Manual mode allows users to maneuver the CDPR pendulum using the joystick manually. Automatic mode consists of spiral draw, pendulum draw, and execute modes. In spiral draw mode, a spiral pattern is generated, modified, combined, and saved as an image file. Meanwhile, in pendulum draw mode, the parameters are modified to produce a pattern, which will then be saved as an image file. Then, in execute mode, the image file is transferred to the CDPR machine to apply wax to the fabric. Then, gallery mode is for viewing patterns saved in image files.

In the current manual system, mass production of the same pattern is impossible because the trajectory parameters for creating the pattern are unknown. Therefore, software is needed to simplify the mass production process with the same pattern because the patterns created can be reaccessed in gallery mode for further use in execute mode. This research focuses on the pendulum draw mode. The software was created via Android Studio with KOTLIN as the main programming language.

In pendulum draw mode, craftsmen can use a range of parameters to set the pendulum trajectory parameters. The trajectory of the pendulum will form a particular pattern, which is expected to be close to the Batik Pendulum pattern that has currently been made. Research on the trajectory produced by a pendulum has been carried out in [20], [21]. Setting these pendulum parameters is part of the trajectory planning carried out in this research.

II. METHODS

A. Spherical Pendulum Equation

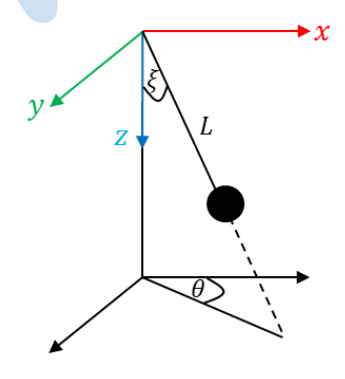


Fig. 2. Spherical pendulum parameter

Error! Reference source not found. illustrates a s pherical pendulum with string length L, and the angle formed between string L and the z-axis is the polar angle ξ , and the angle formed between string L and the x-axis is the azimuthal angle θ . The coordinates of the

spherical pendulum's position on each axis can be written as [20], [21]:

$$x_p = L \sin \xi \cos \theta$$

$$y_p = L \sin \xi \sin \theta$$

$$z_p = L \cos \xi$$
(1)

The speed on each axis can be written as the first derivative of position. The spherical speed of the pendulum can be written as:

$$\begin{split} v_{x,p} &= L\dot{\xi}\cos\xi\cos\theta - L\dot{\theta}\sin\xi\sin\theta \\ v_{y,p} &= L\dot{\xi}\cos\xi\sin\theta + L\dot{\phi}\sin\xi\cos\theta \\ v_{z,p} &= -L\dot{\xi}\sin\xi \end{split} \tag{2}$$

Next, to obtain the Lagrange equation \mathbb{L} for the equations of motion ξ and θ , it is necessary to determine the kinetic energy T and potential energy V.

$$T = \frac{1}{2}mv^{2}$$

$$= \frac{1}{2}m(v_{x,p}^{2} + v_{y,p}^{2} + v_{z,p}^{2})$$

$$= \frac{1}{2}mL^{2}(\dot{\xi}^{2} + \dot{\theta}^{2}\sin^{2}\xi)$$

$$V = -mgz_{p} = -mgL\cos\xi$$
(4)

where m is the pendulum's mass and g is the acceleration due to gravity. So, we get the Lagrange equation L as [20], [21]:

$$\mathbb{L} = T - V$$

$$= \frac{1}{2} mL^2 (\dot{\xi}^2 + \dot{\theta}^2 \sin^2 \xi) + mgL \cos \xi$$
(5)

In a damped spherical pendulum, the damping effect on the system must be considered through the Rayleigh dissipation function \mathbb{R} . [21].

$$\mathbb{R} = \frac{1}{2} \sum b_i v_i^2 = \frac{1}{2} b v^2$$

$$= \frac{1}{2} b \left(v_{x,p}^2 + v_{y,p}^2 + v_{z,p}^2 \right)$$

$$= \frac{1}{2} b L^2 (\dot{\xi}^2 + \dot{\theta}^2 \sin^2 \xi)$$
(6)

where b is the damping coefficient.

Therefore, the equation of motion for ξ and θ can be written as the Euler-Lagrange equation:

$$\frac{d}{dt} \left(\frac{\partial \mathbb{L}}{d\dot{\xi}} \right) = \frac{\partial \mathbb{L}}{d\dot{\xi}} - \frac{\partial \mathbb{R}}{d\dot{\xi}} \tag{7}$$

$$\ddot{\xi} = \frac{-mg \sin \xi + mL\dot{\theta}^2 \sin \xi \cos \xi - bL\dot{\xi}}{mL}$$

$$\frac{d}{dt} \left(\frac{\partial \mathbb{L}}{d\dot{\phi}} \right) = \frac{\partial \mathbb{L}}{d\phi} - \frac{\partial \mathbb{R}}{d\dot{\phi}}$$

$$m\ddot{\theta} \sin \xi = -2m\dot{\xi}\dot{\theta}\cos \xi - b\dot{\theta}\sin \xi$$

$$\ddot{\theta} = \frac{-2m\dot{\xi}\dot{\theta}\cos \xi - b\dot{\theta}\sin \xi}{m\sin \xi}$$

B. Proposed Equation and Parameter

The differential equations **Error! Reference s ource not found.** and **Error! Reference source not found.** can be solved when the values of b, m, L, N, and

t are known. Where N is the amount of data, and t is the duration of time the pendulum swings. In addition, to solve the differential equations in **Error! Reference s** ource not found. and **Error! Reference source not found.**, the initial value of the pendulum needs to be known. The values that determine the initial condition of the pendulum from the differential equation are ξ_0 , θ_0 , and $\mathbf{v}_{p,0}$. Here, $\mathbf{v}_{p,0} = \dot{x}_0 \hat{\mathbf{i}} + \dot{y}_0 \hat{\mathbf{j}} + \dot{z}_0 \hat{\mathbf{k}}$. Based on the initial speed value of pendulum, the speed in spherical coordinates can be derived as follows:

$$r = L = \sqrt{x_p^2 + y_p^2 + z_p^2}$$

$$\xi = \arccos\left(\frac{z_p}{r}\right)$$

$$\theta = \arctan\left(\frac{y_p}{x_p}\right)$$
(9)

Therefore,

$$\mathbf{v}_{p,0} = \frac{x_{p,0}\dot{x}_{p,0} + y_{p,0}\dot{y}_{p,0} + z_{p,0}\dot{z}_{p,0}}{L}\hat{\mathbf{r}} + \frac{z_{p,0}}{L^2} (x_{p,0}\dot{x}_{p,0} + y_{p,0}\dot{y}_{p,0} + z_{p,0}\dot{z}_{p,0}) - \dot{z}_{p,0}}{\sqrt{L^2 - z_{p,0}^2}}\hat{\boldsymbol{\xi}} + \frac{\dot{y}_{p,0}x_{p,0} - y_{p,0}\dot{x}_{p,0}}{x_{p,0}^2 + y_{p,0}^2}\hat{\boldsymbol{\theta}}$$
(10)

with

$$x_{p,0} = L \sin \xi_0 \cos \theta_0$$

$$y_{p,0} = L \sin \xi_0 \sin \theta_0$$

$$z_{p,0} = L \cos \xi_0$$

The spherical pendulum trajectory is obtained on a spherical surface with a radius from the known values and the differential equation. In order to produce a trajectory on the fabric surface, an orthogonal projection of the spherical pendulum trajectory is carried out on the xy-plane by eliminating z_p in the solution coordinates. Hence, the parameters required for planning the spherical pendulum trajectory are $v_{p,0}$, θ_0 , ξ_0 , N, t, b, m, and L.

C. Parameter Limits

The lower and upper limits of the spherical pendulum trajectory are defined in equation (11):

$$0 \le v_{p,0} \le 10$$

$$0 \le \theta_0 \le 2\pi$$

$$0 \le \xi_0 \le \frac{\pi}{2}$$

$$0 \le N \le 10000$$

$$0 \le t \le 120$$

$$0 \le b \le 2$$

$$0,1 \le m \le 10$$

$$0,1 \le L \le 5$$

D. Parameter Limits

After the software is implemented, it is necessary to evaluate its response time. Three response time

limits to consider in software applications are as follows [22]:

- 1. 0.1 seconds is the time limit when the user feels the system reacts instantaneously, which means no other info is necessary except to display the result.
- 2. 1.0 seconds is the time limit to maintain the user's flow of thought despite noticing a delay. Typically, no info is needed between 0.1 to 1.0 seconds, but the user has lost the feeling of operating directly on the data.
- 3. Ten seconds is the time limit to maintain the user's attention on the current running activity. For longer delays, users will engage in other activities while waiting for the activity to complete. Therefore, users need to see a progress indicator informing them that the activity is running and the remaining completion time.

III. RESULTS AND DISCUSSION

A. MATLAB Simulation

The spherical pendulum trajectory simulation used MATLAB's "uifigure" feature. This feature allows simulations to be carried out using the "uislider" to change trajectory parameters. Next, the spherical pendulum trajectory plot can be observed in the "uiaxes" feature. The lower and upper limits of the slider used follow equation **Error! Reference source n** ot found. The plot has the same size on the x and y axes by looking for the maximum value on both axes. The "uifigure" display that has been designed can be observed in **Error! Reference source not found.**.

Several pendulum parameters were determined to demonstrate the diversity of patterns that can be produced, as shown in Error! Reference source not f ound. and Error! Reference source not found.. Pendulum A is the pendulum trajectory in the default state. Meanwhile, pendulum B, C, and D are various patterns that can be produced by changing the pendulum parameters, as seen in Error! Reference s ource not found. with the yellow highlight. Pendulum pattern B shows a pattern that is often obtained from manual pendulum batik with one string, pendulum pattern C shows a pendulum movement that resembles a spiral, and pendulum pattern D is a new pendulum pattern that cannot be achieved on a manual system but is possible to achieve using the proposed trajectory planning system.

Error! Reference source not found. and **Error! Reference source not found.** show that the parameters proposed for planning the spherical pendulum trajectory can provide various trajectories. Next, these parameters will be used for the spherical pendulum trajectory planning process in the software draw pendulum mode.

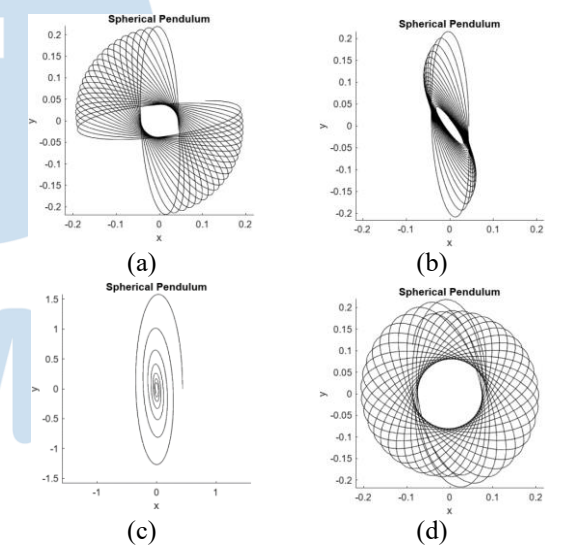


Fig. 4. Spherical pendulum pattern: (a) A, (b) B, (c) C, and (d) D

TABLE I. SPHERICAL PENDULUM PARAMETER

Pend ulum	$v_{p,0}$	θ_0	ξ_0	N	t	b	m	L
A	1	90°	5°	1000	30	0,1	10	1
В	1	90°	5°	1000	30	1	10	1
С	2.5	90°	5°	1000	30	2	10	5
D	1	90°	10°	1000	30	0.1	10	1

Fig. 3. uifigure MATLAB for spherical pendulum trajectory



Fig. 5. Pole and fabric size settings



Fig. 6. Pendulum parameters, including linear speed of the pendulum, azimuthal angle, and polar angle



Fig. 7. Pendulum parameters, including the amount of data, duration of time, and damping coefficient



Fig. 8. Pendulum parameters, including damping coefficient, mass of the pendulum, and length of the string



Fig. 9. The trajectory results from changing the pendulum parameters

B. Software Implementation

The procedure for generating spherical pendulum parameters in the implemented software is illustrated in Error! Reference source not found. - Error! Reference source not found. In pendulum draw mode, the user must define the pole size and fabric used. Next, the user can change the pendulum parameters by moving the slider on the right side of the screen. The resulting trajectory is displayed on the left side of the screen. User can save patterns in the gallery for later use.

The required time since the parameters are changed until the path is generated is 1-2 seconds. Because the required time is less than 10 seconds, it is within the user's flow of thought, and therefore, there is no need to show a progress indicator to the user.

IV. CONCLUSIONS

A trajectory planning algorithm that accepts parameter values has been designed to produce a spherical pendulum pattern. The parameters consist of $v_{p,0}$, θ_0 , ξ_0 , N, t, b, m, and L. Modifying these eight inputs between the specified lower and upper limits provides a variety of spherical pendulum patterns.

The spherical pendulum trajectory planning in the implemented software requires 1-2 seconds since the parameters are changed until the trajectory is produced. Because the response time is less than 10 seconds, there is no need to show a progress indicator to the user.

For future work, the trajectory generated from the draw pendulum mode can be saved into gallery mode for later use in the execute mode. Therefore, the user can use the saved pendulum pattern and send it to the machine to apply the wax to the fabric.

ACKNOWLEDGMENT

The authors would like to thank The Indonesia Endowment Fund for Education (LPDP) 2022-2023 supports I.R. Putri's research.

REFERENCES

- [1] I. Nurhaida, A. Noviyanto, R. Manurung, and A. M. Arymurthy, "Automatic indonesian's batik pattern recognition using SIFT Approach," in *Procedia Computer Science*, Elsevier, 2015, pp. 567–576. doi: 10.1016/j.procs.2015.07.547.
- [2] N. Margried, "Batik fractal community: Creative engagement through technology," *Procedia Soc Behav Sci*, vol. 184, pp. 214–222, May 2015, doi: 10.1016/j.sbspro.2015.05.082.
- [3] T. Ismail, L. S. Wiyantoro, Meutia, and M. Muchlish, "Strategy, interactive control system and national culture: A case study of batik industry in Indonesia," *Procedia Soc Behav Sci*, vol. 65, pp. 33–38, Dec. 2012, doi: 10.1016/j.sbspro.2012.11.087.
- [4] A. A. Rumanti, A. F. Rizana, L. Septiningrum, R. Reynaldo, and M. M. Isnaini, "Innovation capability and open innovation for small and medium enterprises (SMEs) performance: Response in dealing with the COVID-19 pandemic,"

- Sustainability, vol. 14, no. 10, p. 5874, May 2022, doi: 10.3390/su14105874.
- [5] K. Kudiya, Pendulum Batik Art. Bandung: CV. Instan Grafika Sejahtera. 2022.
- [6] J. Quereda, M. Ramón, B. Silva, J. J. Hinarejos, J. G. Rodrigo, and D. Farías, "Calibrating the frequency of tuning forks by means of Lissajous figures," *Am J Phys*, vol. 79, no. 5, pp. 517– 520, May 2011, doi: 10.1119/1.3546095.
- [7] A. P. C., "STUDY OF LISSAJOUS PATTERNS USING OSCILLOSCOPE AND PENDULUM METHOD," Kottayam, May 2022.
- [8] E. M. Kim, "Harmonograph: A Visual Representation of Sound," in 2012 IEEE International Symposium on Intelligent Signal Processing and Communication Systems (ISPACS 2012), 2012, pp. 489–494.
- [9] N. Kr. Rossing, "The Old Art of Rope Work and Fourier Decomposition," Trondheim, 2012.
- [10] M. R. Matthews, "Pendulum motion: A case study in how history and philosophy can contribute to science education," in *International Handbook of Research in History, Philosophy,* and Science Teaching, Springer Netherlands, 2014, pp. 19–56. doi: 10.1007/978-94-007-7654-8_2.
- [11] N. Mohd Isa et al., "Intertwining the Arts and Sciences to Stimulate a Creative Mind," in Proceedings of the International Conference on Student and Disable Student Development 2019 (ICoSD 2019), 2020, pp. 39–44.
- [12] H. Yang, J. Xiao, T. Yang, and C. Qiu, "A simple method to measure the trajectory of a spherical pendulum," *Eur J Phys*, vol. 32, no. 4, pp. 867–872, Jul. 2011, doi: 10.1088/0143-0807/32/4/002.
- [13] T. S. Amer, M. A. Bek, and S. S. Hassan, "The dynamical analysis for the motion of a harmonically two degrees of freedom damped spring pendulum in an elliptic trajectory," *Alexandria Engineering Journal*, vol. 61, no. 2, pp. 1715– 1733, Feb. 2022, doi: 10.1016/j.aej.2021.06.063.
- [14] A. V. Perig, A. N. Stadnik, and A. I. Deriglazov, "Spherical pendulum small oscillations for slewing crane motion," *The*

- Scientific World Journal, vol. 2014, 2014, doi: 10.1155/2014/451804.
- [15] Y. Bai, M. Svinin, and M. Yamamoto, "Dynamics-based motion planning for a pendulum-actuated spherical rolling robot," *Regular and Chaotic Dynamics*, vol. 23, no. 4, pp. 372– 388, Jul. 2018, doi: 10.1134/S1560354718040020.
- [16] G. Li, X. Liu, Y. Yu, P. Guo4, Z. Li, and X. Ma, "Modeling and Anti-swing Control for 7-DOF Overhead Crane with Double Spherical Pendulum and Varying Cable Length Effects," in *Proceedings of the 42nd Chinese Control Conference*, Tianjin, 2023, pp. 564–569.
- [17] A. Pott, "Cable-Driven Parallel Robots Theory and Application," Springer Tracts in Advanced Robotics, Springer, 2018, doi: 10.1007/978-3-319-76138-1.
- [18] C. Liu, G.-H. Cao, and Y.-Y. Qu, "Workspace Analysis of Delta Robot Based on Forward Kinematics Solution," in 2019 3rd IEEE International Conference on Robotics and Automation Sciences, 2019, pp. 1–5.
- [19] I. R. Putri, A. Juwandana, E. M. Budi, E. Ekawati, and K. Kudiya, "Simulation of cable-driven parallel robot (CDPR) for application in creating batik patterns," 2023 8th International Conference on Instrumentation, Control, and Automation (ICA), IEEE, Aug. 2023, pp. 47–52. doi: 10.1109/ICA58538.2023.10273083.
- [20] "The Spherical Pendulum." Accessed: November 01, 2023.
 [Online]. Available: http://www.maths.surrey.ac.uk/explore/michaelspages/documentation/Spherical.
- [21] M. K. Komala, "Damped Spherical Pendulum," Jan. 2023, Accessed: Nov. 01, 2023. [Online]. Available: https://www.researchgate.net/publication/367227230_Damped_Spherical_Pendulum.
- [22] J. Nielsen, *Usability Engineering*, 1st Edition. Morgan Kaufmann, 1993. Accessed: Jul. 02, 2023. [Online]. Available: https://www.nngroup.com/articles/website-response-times/.



EEG-Based Depression Detection in the Prefrontal Cortex Lobe using mRMR Feature Selection and Bidirectional LSTM

Monica Pratiwi

Computer Engineering, Universitas Multimedia Nusantara, Tangerang, Indonesia monica.pratiwi@umn.ac.id

Accepted on 04 December 2023 Approved on 27 December 2023

Abstract—Depression can induce significant anguish and impair one's ability to perform effectively in professional, academic, and familial settings. This condition has the potential to result in suicide. Annually, the number of deaths resulting from suicide exceeds 700,000. Among individuals aged 15-29, suicide has emerged as the fourth most prevalent cause of mortality. Challenges in treating depression include limited accessibility to mental health care in rural regions and misdiagnosis resulting from subjective evaluations, wherein insufficient expertise can contribute to inaccurate diagnoses. Electroencephalography (EEG) has gained popularity as a tool for the identification and study of a number of mental illnesses in the past years. Therefore, an automated technique is required to precisely distinguish between normal EEG signals and depression signals. This research focused on developing an EEG-based depression detection system in the prefrontal cortex lobe area (Fp1, Fpz, and Fp2). One of the developments carried out in this research is the implementation of Bidirectional Long Short-Term Memory (Bi-LSTM) as the model classification and minimum redundancy maximum relevance (mRMR) feature selection. The results suggest that the combination of mRMR feature selection with 25 features and the bidirectional LSTM obtained 92.83% accuracy.

Index Terms—Bidirectional LSTM; Detection Depression; EEG Signals; mRMR Feature Selection.

I. INTRODUCTION

The World Health Organization (WHO) recognized mental health and psychosocial wellbeing as essential components of health in 1978, and this definition has been discussed extensively as a UN resolution. In 2015, every nation has adopted the UN Sustainable Development Goal (SDG) point 3, which is to "ensure healthy lives and promote well-being for all at all ages." Substance misuse and mental health are directly addressed. Target 3.4 calls for countries to "promote mental health and well-being" through prevention and treatment in order to cut premature death by one-third[1].

However, since 2020, global anxiety and depression has become 25% more prevalent, with teenagers and women being the most affected. Of the 5,470 respondents, 40.9% reported having mental or behavioral health issues. TSRD (trauma- and stressorrelated disorder) symptoms associated with COVID-19 (26.3%), increased drug usage as a result of COVID-19 (13.3%), and seriously considering suicide in the last 30 days (10.7%) are among the categories that include symptoms of anxiety or depressive illness (30.9%) [2]. Among these, symptoms of anxiety or depressive illness are the most prevalent behavioral health issues. Depression differs from mild mood fluctuations and short-term emotional responses against challenges in everyday life. Repeating instances of depression at a moderate or great scale may lead to the disorder becoming a serious health condition. Depression can cause great suffering and the affected may be unable to function well at work, at school, and in the family. The disorder can lead to suicide. More than 700,000 people die from suicide annually. Suicide has become the fourth leading cause of death for people ages 15-29.

The obstacles of effective mental health treatment include the lack of resources and the social stigma against mental disorders. It is a common occurrence that people from countries of all income levels to have undiagnosed depression or to be misdiagnosed with depression and prescribed antidepressants. Doctors and psychologists are able to diagnose depressive disorders through counselling sessions and ask relevant questions to the subject, despite being vulnerable to mistakes due to the examiner's lack of experience.

For this reason, Electroencephalography (EEG) has gained popularity as a tool for the identification and study of a number of mental illnesses in the past several years, including autism, ADHD, Alzheimer's, dementia, alcoholism, and motor imagery. EEG captures electrical activity in the brain and shows how

brain signals are used. In comparison to healthy persons, depression sufferers' synapses produce less neurotransmitters and have a reduced concentration of receptors due to cell malfunction. Compared to healthy individuals, this results in extremely low levels of brain activity in depressed persons. For psychiatrists, the processes of visual interpretation and complicated, nonlinear, nonstationary EEG signal analysis are challenging, time-consuming, and inefficient[3].

In other words, an automated technique is required to precisely distinguish between normal EEG signals and depression signals as validation that helps psychiatrists or psychologists in diagnosing depression. Consequently, a number of researchers have put forth a computer-based detection system based on EEG data that use a classification technique to distinguish or identify whether the patient is in the normal or depressive category.

Wan et. al [4] proposed a machine learning technique to distinguish between Major Depressive Disorder (MDD) and normal control subjects. The EEG dataset is acquired using the Fp1 and Fp2 electrodes of a 32-channel EEG device. The findings indicate that the classification accuracy using EEG data from the Fp1 site is superior to that using EEG data from the Fp2 location. Moreover, the results suggest that analyzing single-channel EEG data can effectively differentiate Major Depressive Disorder (MDD) at a level comparable to analyzing multichannel EEG data. In addition, a portable electroencephalogram (EEG) equipment is utilized to gather the signal specifically from the Fp1 region, resulting in the acquisition of the second dataset. The genetic algorithm (GA) integrated Classification and Regression Tree obtains an impressive accuracy of 86.67% by leave-one-participant-out cross validation. This result demonstrates the potential of the singlechannel EEG-based machine learning technology in supporting the prescreening application for Major Depressive Disorder (MDD).

In a research conducted by Cai et. al [5], a psychophysiological database was created, consisting of 213 people (92 depressive patients and 121 normal The EEG signals of all subjects were recorded utilizing a prefrontal-lobe three-electrode EEG system at Fp1, Fp2, and Fpz electrode sites. The signals were collected during both resting state and sound stimulation. A total of 270 linear and nonlinear features were retrieved after using denoising techniques utilizing the Finite Impulse Response filter, which combined the Kalman derivation method, Discrete Wavelet Transformation, and an Adaptive Predictor Filter. Subsequently, the feature selection strategy known as minimal-redundancy-maximalrelevance was employed to decrease the number of dimensions in the feature space. The depressed

individuals were differentiated from the normal controls using four classification methods: Support Vector Machine, K-Nearest Neighbor, Classification Trees, and Artificial Neural Network. The performance of the classifiers was assessed using 10-fold cross-validation. The findings indicated that the K-Nearest Neighbor (KNN) algorithm achieved the highest level of accuracy, reaching 79.27%.

Similar to the two previous studies mentioned, this research also focuses on developing an EEG-based depression detection system in the prefrontal cortex lobe area (Fp1, Fpz, and Fp2) to construct a system that is more user-friendly. There are several studies that have proven the correlation between depressive disorders and activity in the prefrontal cortex lobe[6]. This research aims to increase the accuracy value of the Major Depressive Disorder classification model with normal subjects. One of the developments carried out in this research is the implementation of Bidirectional Long Short-Term Memory (Bi-LSTM) for an EEG signal-based depressive disorder classification system. Apart from applying Bi-LSTM, time segmentation of the data was also carried out in the feature extraction process.

II. RESEARCH METHODS

The research is constructed into several steps, namely dataset acquisition, signal pre-processing, feature extraction, feature selection, and classification.

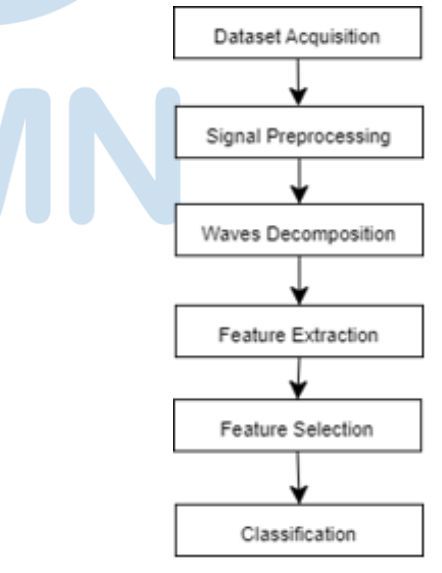


Fig. 1. Research Steps

A. Data Acquisition

This study used a publicly available dataset called MODMA, which stands for Multi-modal Open Dataset for Mental-disorder Analysis. This dataset is collected by Lanzhou University in China[7].

The EEG signal was recorded using a 24-bit analog-to-digital converter with a sampling frequency of 250Hz. The total number of participants is 55, consisting of 26 patients diagnosed with major depressive disorder (MDD) and 29 individuals in the healthy control group. Among the patients, there are 15 males and 11 females, aged 16-56. In the healthy control group, there are 19 males and 10 females, aged 18-55.

EEG data was recorded using a three-electrode complete EEG collection equipment, as the prefrontal lobe exhibits a high correlation with emotional processes and mental disorders. The device is equipped with three electrodes that are strategically placed on the prefrontal lobe, specifically at locations Fp1, Fpz, and Fp2. A 90-second segment of EEG data was recorded while the participant was in a resting state. Subsequently, the participants were directed to remain seated with their eyes closed and minimize unnecessary physical movements for an extra minute.

Several additional questionnaires were used to validate the depression level of each patient, namely the Patient Health Questionnaire (PHQ-9) is used for diagnosing, screening, tracking, and gauging the severity of depression. The average PHQ-9 score for all depressed patients is 9.6 or rounded to 10. Thus based on Table 1, the patient's condition can be categorized as moderate depressed.

TABLE I. PHQ-9 SCORING STANDARD

Depression Score	Depressive Severity
1-4	Minimal Depression
5-9	Mild Depression
10-14	Moderate Depression
15-19	Moderately Severe
	Depression
20-27	Severe Depression

B. Signal Preprocessing

The data collected as an EEG signal was recorded includes both the EEG signal and noises called artifacts. The amplitude of the clean EEG signal is about \pm 100 μV and artifacts can have an amplitude that is 10 to 100 time larger[8]. Therefore, signal preprocessing must be performed. The EEG data were filtered using Infinite Impulse Response (IIR) band pass filter. The IIR filter is recursive in nature and computes the output by incorporating current and past inputs as well as previous outputs, utilizing feedback in its structure based on the pulse transfer function to meet specified filter requirements[9].

Next, artifact data were removed using Independent Component Analysis (ICA) in order to obtain more accurate EEG data that only shows brain activity. This includes non-EEG signals such as pulse signals, muscular activity, and eye-blinking

components. The ICA stage and band pass filter were conducted using Matlab R2015b with the EEGLab plugin.

C. Waves Decomposition

EEG signal decomposition is the process of converting signals into its simpler form. This process takes place after clean signals are obtained from the artifact removal process. EEG signals are divided into several frequency subbands such as delta (δ) , theta (θ) , alpha (α) , beta (β) , gamma (γ) , alpha low, alpha high, beta low, and beta high.

A method commonly used in the decomposition process is the Butterworth Filter. This filter is first described by Stephen Butterworth in 1930. Butterworth is a type of signal processing filter that is designed to have as flat frequency response as possible, also called the maximum average magnitude filter. This filter has a better time of domain and a more stable output (with no peaks) as a result, with a better balance between smoothness and accuracy than the Chebyshev Filter. In addition to having a flatter response and no ripples in the bandpass, the Butterworth Filter also rolls toward zero as the band stops[10].

D. Feature Extraction

The goal of feature extraction is to identify important information from the signal to classify it accurately. This process is required to reduce the amount of the data, while retaining the essential details inside the signal. It is crucial to determine the fundamental characteristics that distinguish the dataset. Two types of features can be used for EEG signal analysis, namely linear features and nonlinear features.

Linear features in EEG data refer to patterns that can be studied through applying linear mathematical techniques. This study utilizes linear features such as the Hjorth activity parameter and statistical parameters including mean absolute value, maximum, and standard deviation. The Hjorth activity parameter is a method to describe spectral characteristics of EEG data within the time domain. The activity refers to how the signal varies[11]. There is a notable increase in activity during seizures, which means the signal deviates significantly in amplitude from its average value. Meanwhile, statistical parameters are used to define the spread of biological signals and can be calculated using the following formulas:

• Mean Absolute Value

$$MAV = \frac{\sum_{i=1}^{n} |xi|}{n} \tag{1}$$

• Standard Deviation

$$\sigma = \sqrt{\frac{\Sigma(xi - \mu)^2}{n}}$$
 (2)

Traditional methods such as time-domain analysis or Fourier Transform, which are often employed for signal analysis, are inadequate for a full study of EEG signals due to their non-stationary and complicated nature. The study of the brain's dynamic nature can be explored by employing nonlinear analysis, which is based on the mathematical theory of dynamical systems[12].

Detrended Fluctuation Analysis (DFA)

$$F[n] = \sqrt{\frac{1}{N} \sum_{t=0}^{N-1} (z[t] - \hat{z}[t])^2}$$
 (3)

• Sample Entropy

$$SampEn(X, m, r) = \log \phi^{m}(r) - \log \phi^{m+1}(r)$$
 (4)

• Correlation Dimension

The correlation dimension refers to the quantification of the dimensionality of the spatial extent encompassed by a collection of randomly distributed points. The estimation is obtained by calculating the slope of the correlation integral in relation to the range of radius of similarity. The utilization of correlation dimension as a characteristic metric is employed to differentiate between deterministic chaos and random noise, with the purpose of identifying potential defects.

In the feature extraction process, before being extracted, the signal was segmented into 20 miliseconds. The data collected has a duration of 90 seconds. Considering that the EEG instrument used has a sample frequency of 250Hz, the total data per participant equal to 22,500 lines of data (90 multiplied by 250).

Next, the 22,500 lines are divided into segments of 20ms or can be interpreted as taking every 5 lines for the purpose of calculating feature extraction. After applying a time segmentation of 20ms to the initial dataset of 22500 rows, the resulting dataset was reduced to 4500 data points per participant. Therefore, the total data obtained after the feature extraction process is 216,000 lines of data from a total of 48 participants' EEG signals.

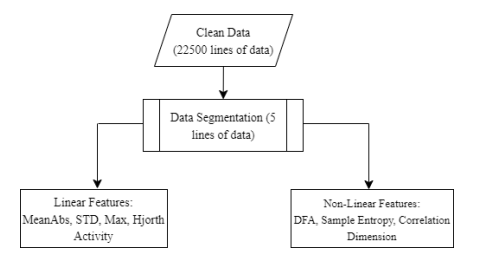


Fig. 2. Feature Extraction process using 20ms window data segmentation

E. Feature Selection

Feature selection is a crucial stage in large-scale machine learning systems. It allows developers to take advantage of the valuable feature store and address the issues and expenses that come with it. It enhances the machine learning application and system in various ways: (1) Enhanced computational efficiency: By utilizing a reduced set of features, the speed of model training and prediction is accelerated. (2) Improved prediction accuracy: This is accomplished through various methods, including the elimination of irrelevant features, prevention of overfitting, and the ability to fit a larger number of training samples into memory due to the reduced number of features. (3) Decreasing the number of features can substantially decrease the expenses associated with constructing, overseeing, and up keeping the model's feature pipeline, resulting in lower maintenance costs. (4) Simplified model interpretation and diagnosis: by exclusively using the essential feature set during the modeling process, it becomes more straightforward to comprehend the specific features and information upon which the model's prediction is founded[13].

The minimum redundancy maximum relevance (mRMR) is a feature selection approach that tends to select features with a high correlation with the class (output) and a low correlation between themselves. For continuous features, the F-statistic can be used to calculate correlation with the class (relevance) and the Pearson correlation coefficient can be used to calculate correlation between features (redundancy). Thereafter, features are selected one by one by applying a greedy search to maximize the objective function, which is a function of relevance and redundancy. Two commonly used types of the objective function are MID (Mutual Information Difference criterion) and MIQ (Mutual Information Quotient criterion) representing the difference or the quotient of relevance and redundancy, respectively[14].

This research involves three datasets that include varying numbers of selected features: 25, 50, and 75. Experiments were conducted to examine how the amount of features impacts the accuracy of the classification model. The details of the selected features are as follows:

TABLE II. NUMBER OF FEATURE SELECTED

Number of Features	Feature Details	
25	'gamma2_corrdim',	
	'theta2_sampent',	
	'delta1_sampent',	
	'beta1_corrdim', 'theta1_dfa',	
	'theta1_corrdim',	

	'gamma1_corrdim',
	'theta3_corrdim',
	'gamma3_corrdim',
	'theta2_corrdim', 'beta2_dfa',
	'theta1_sampent',
	'alpha3_sampent',
	'theta3_sampent',
	'beta2_corrdim',
	'beta1_sampent',
	'delta3_sampent',
	'beta3_sampent', 'theta2_dfa',
	'gamma3_dfa',
	'beta2_sampent',
	'delta2_mean',
	'gamma3_sampent',
	'beta3 dfa', 'delta2 sampent'
50	'gamma2_corrdim',
	'theta2_sampent',
	'delta1_sampent',
	'beta1_corrdim', 'theta1_dfa',
	'theta1_corrdim',
	'gamma1_corrdim',
	'theta3_corrdim',
	'gamma3_corrdim',
	'theta2_corrdim', 'beta2_dfa',
	'theta1_sampent',
	'alpha3_sampent', 'theta3_sampent',
	'beta2 corrdim',
	beta2_cortdini, 'beta1_sampent',
	'delta3_sampent',
	'beta3_sampent', 'theta2_dfa',
	'gamma3_dfa',
	'beta2_sampent',
	'delta2_mean',
	'gamma3_sampent',
	'beta3_dfa', 'delta2_sampent',
	'gamma2_sampent',
	'beta1_dfa', 'delta1_corrdim',
	'delta3_mean',
	'alpha3_corrdim',
	'gamma1_dfa', 'delta1_mean',
	'alpha1_corrdim', 'theta3_dfa',
	'beta3_corrdim',
	'alpha2_sampent', 'alpha2_dfa',
	'gamma1_mean',
	'delta2_corrdim',
	'gamma2_dfa', 'delta2_std',
	'delta3_corrdim', 'delta2_max',
	'delta1_std', 'alpha2_corrdim',
	'delta1_max', 'delta3_max',
	'delta3_std', 'gamma2_mean',
	'delta3 dfa'
75	'gamma2_corrdim',
	'theta2_sampent',
	'delta1_sampent',
	'beta1_corrdim', 'theta1_dfa',
	'theta1_corrdim',
	'gamma1_corrdim',
	'theta3_corrdim',
	'gamma3_corrdim',
	'theta2_corrdim', 'beta2_dfa',
	'theta1_sampent',
	'alpha3_sampent',
	'theta3_sampent',
	'beta2_corrdim',
	'beta2_corrdim', 'beta1_sampent',
	'beta2_corrdim', 'beta1_sampent', 'delta3_sampent',
	'beta2_corrdim', 'beta1_sampent', 'delta3_sampent', 'beta3_sampent', 'theta2_dfa',
	'beta2_corrdim', 'beta1_sampent', 'delta3_sampent',

'delta2_mean',
'gamma3_sampent',
'beta3_dfa', 'delta2_sampent',
'gamma2_sampent',
'beta1_dfa', 'delta1_corrdim',
'delta3_mean',
'alpha3_corrdim',
'gamma1_dfa', 'delta1_mean',
'alpha1_corrdim', 'theta3_dfa',
'beta3_corrdim',
'alpha2_sampent', 'alpha2_dfa',
'gamma1_mean',
'delta2 corrdim',
'gamma2_dfa', 'delta2_std',
'delta3_corrdim', 'delta2_max',
'delta1_std', 'alpha2_corrdim',
'delta1_max', 'delta3_max',
'delta3_std', 'gamma2_mean',
'delta3_dfa', 'delta2_hjorth',
'alpha3_dfa', 'gamma3_mean',
'delta1_hjorth', 'delta3_hjorth',
'gamma1_sampent',
'gamma1_std', 'theta2_hjorth',
'theta1_hjorth', 'theta3_hjorth',
'alpha1_sampent',
'gamma2_std', 'gamma3_std',
'alpha1_dfa', 'alpha1_hjorth',
'alpha2_hjorth',
'alpha3_hjorth',
'gamma1_hjorth',
'gamma2_hjorth',
'beta1_hjorth', 'beta2_hjorth',
'beta3_hjorth',
'gamma3_hjorth', 'delta2_dfa',
'alpha1 mean'
· -

F. Classification

Following the data processing stage, the next stage is classification. The data is divided into two groups, the group diagnosed with major depressive disorder and the healthy control group. This method utilizes binary classification through machine learning. Due to the EEG data having a sampling rate of 250Hz, each second contains 250 data samples. Therefore, a classification algorithm is required to process the large amount of data. The Long Short-Term Memory (LSTM) and bidirectional LSTM are technique models that are able to process large time-series data[8]. These models utilize memory cells that possess selfconnections and retain the temporal state of networks using a three-gate mechanism, including the input, output and forget gate. Different from one-way LSTM, Bi-LSTM adds a layer of reverse LSTM. The reverse LSTM reverses the data and the hidden layer synthesizes the forward and reverse information so that cells in the network can simultaneously obtain context information[15].

TABLE III. LSTM & BI-LSTM MODEL DETAILS

Model	Layer (type)	Output shape
LSTM	LSTM	(None, 1, 32)
	Dropout Layer	(None, 1, 32)
	(0.2)	(None, 16)
	LSTM-1	(None, 16)
	Dropout-1 (0.2)	(None, 2)

	Dense	
Bi-LSTM	LSTM	(None, 1, 32)
	Dropout Layer	(None, 1, 32)
	(0.2)	(None, 16)
	LSTM-1	(None, 16)
	Dropout-1 (0.2)	(None, 2)
	Dense	

III. RESULTS AND DISCUSSION

This section contains an explanation of the experimental scenarios that have been carried out. The study involves the evaluation of three datasets using LSTM and Bi-LSTM models to determine the impact of the amount of features and the type of classification model on the obtained results.

A. Results

TABLE IV. ACCURACY COMPARISON

Classification Model	Number of Selected Features	Accuracy (%)
LSTM	25	89.28
	50	85.04
	75	81.87
Bi-LSTM	25	92.83
	50	86.59
	75	83.74

Table 4 reveals that the LSTM and Bi-LSTM classification models achieve their maximum performance when using a dataset containing 25 features. However, with further comparison, it is evident that the dataset with 25 characteristics and a bidirectional LSTM classification model achieves a superior accuracy of 92.83%. Concurrently, the Long Short-Term Memory (LSTM) model applied to a dataset containing 25 features has an accuracy rate of 89.28%.

Subsequently, an accuracy of 85.04% was achieved with 50 features, while a number of features of 25 resulted in an accuracy of 81.87%. The same trend was observed in the Bi-LSTM model. Once the dataset with 25 features achieved the highest accuracy, the subsequent accuracy values were 86.59% for a dataset with 50 features and 83.74% for a dataset with 75 features. These results suggest that the number of affects the accuracy characteristics categorization model. Machine learning algorithms will achieve superior performance when provided with data that has pertinent features and optimal amounts.

When comparing Figures 3 and 4, which depict the accuracy of the LSTM and Bi-LSTM models, it can be observed that the disparity in accuracy between the two models is rather small. Nevertheless, the conspicuous disparity is in the quantity of epochs. For the LSTM model, reaching an accuracy of 89.28% necessitates 50 epochs. By using Bi-LSTM, an accuracy of 92.83% may be achieved with just 30 epochs. Applying a Bi-

LSTM for classification enables the sequential processing of input data in both forward and backward directions, allowing for the accumulation of relevant information while discarding irrelevant data. This approach can yield good results with reduced training time.

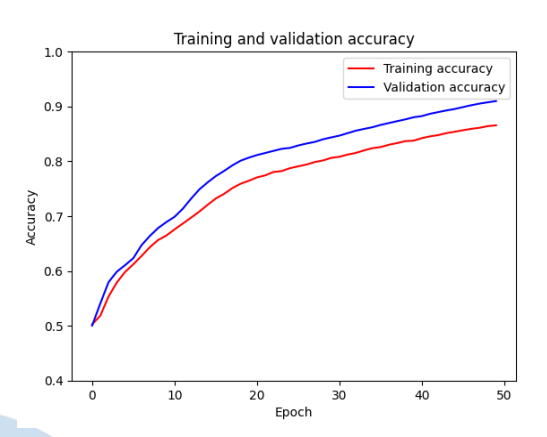


Fig. 3. The Accuracy Plot from LSTM with 25 Selected Features

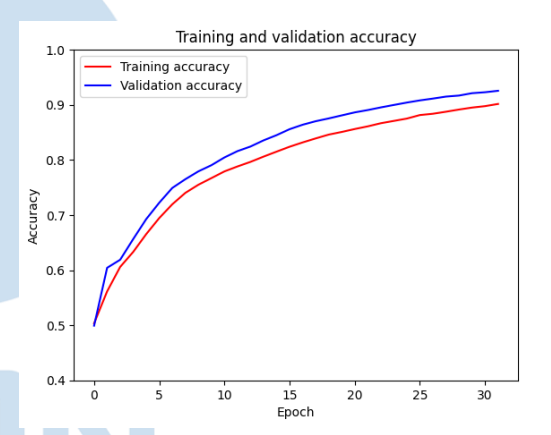


Fig. 4. The Accuracy Plot from Bi-LSTM with 25 Selected Features

However, evaluations entirely reliant on accuracy can be considered as biased. It is essential to assess additional aspects, including the number of True Positives (TP), True Negatives (TN), False Positives (FP), and False Negatives (FN). This evaluation will determine the accuracy of the predictions by assessing the proportion of testing data that was correctly predicted and the proportion that was not. This will enhance the assessment of the model.

According to the results presented in figures 5 and 6, the Bi-LSTM model has a higher number of true positives (TPs) compared to the LSTM model. Specifically, the Bi-LSTM model has 20,596 TPs, whereas the LSTM model has 20,000 TPs. According to this, the Bi-LSTM classification model has a relatively low amount of false negatives (1658) and false positives (1512). The recall, precision, and F1-

Score values in Table 5 are derived from the TP, TN, FP, and FN counts acquired from pictures 5 and 6.

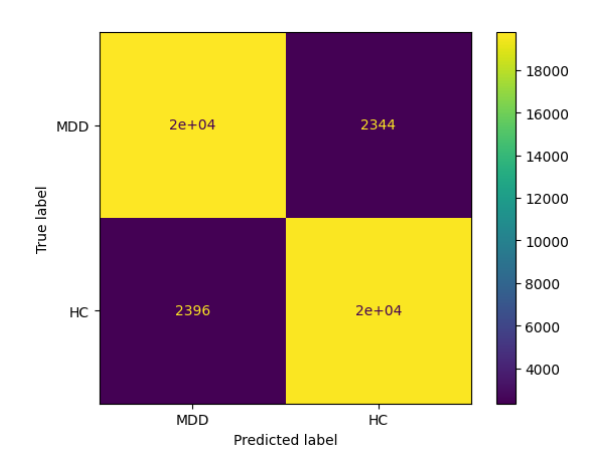


Fig. 5. Confusion Matrix from LSTM with 25 Selected Features

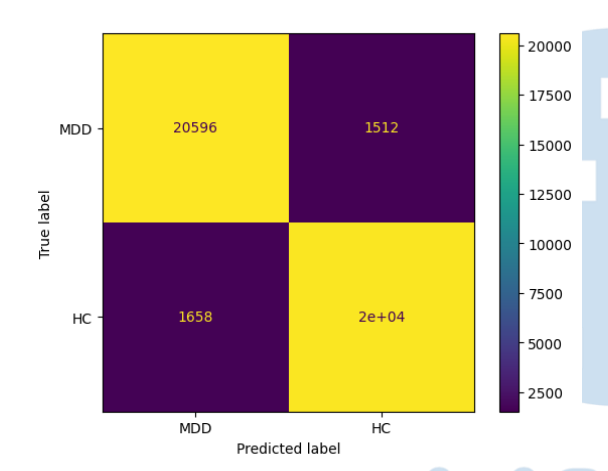


Fig. 6. Confusion Matrix from Bi-LSTM with 25 Selected Features

TABLE V. RECALL, PRECISION, & F1-SCORE

	LSTM (%)	Bi-LSTM (%)
Recall	89.3	92.5
Precision	89.5	93.2
F1-Score	89.4	92.8

Based on the recall, precision, and F1-Score findings of the LSTM and Bi-LSTM models, it is apparent that these three parameters have similar values or a small difference compared to the accuracy value. The trained LSTM and Bi-LSTM models can accurately differentiate between the EEG signals of patients with Major Depressive Disorder (MDD) and those of Healthy Control (HC).

B. Discussions

Several tests were conducted in this study with the objective of enhancing the precision of the depression detection system. Prior research in this field has utilized classification methods to distinguish EEG

signals of patients with Major Depressive Disorder (MDD) from those without the disorder (HC). Cai et. al [5] study, which also focused on analyzing the prefrontal cortex, achieved an accuracy rate of approximately 79%. Approaches for improving accuracy in this research include comparing the amount of selected features and evaluating the performance of LSTM and Bi-LSTM classification models.

The dataset with 25 features yields the highest accuracy value when comparing the number of features in both LSTM and Bi-LSTM models. The research applies the minimum redundancy maximum relevance (mRMR) algorithm for feature selection. The algorithm yields feature rankings based on their highest level of importance. The relevance of a feature increases proportionally with its rating. In contrast, features that receive low rankings are deemed to be less relevant. Based on the obtained results, it can be inferred that the dataset with the selected features has a higher accuracy value compared to the datasets with 50 and 75 selected features. This suggests that the dataset with the selected features has a more relevant feature set.

Another finding obtained is that the accuracy value of Bi-LSTM is higher when compared to LSTM. Not only is the accuracy higher but the epochs required for the training process are fewer compared to LSTM. This is caused by the advantages of Bi-LSTM where BLSTM allows information flow in both directions, adding a new LSTM layer that inverts the sequence, and the outputs of both layers are combined, for example, with average, sum, multiplication, or concatenation. The possibility of two flow directions enables a better learning process[16].

Numerous research had demonstrated that in some classification cases, Bi-LSTM exhibits superior performance in comparison to LSTM. Some examples of research areas include text classification[17], power load forecasting[15], and financial data forecasting[18]. The comparison of Bi-LSTM and LSTM has also been shown from several studies that use EEG signals as classification data such as emotion classification[8][19] and response classification to music and sound[20]. In the domain of EEG signal classification, similar to text classification and other types of classifications, Bi-LSTM demonstrates superior performance compared to LSTM.

IV. CONCLUSIONS

This study aimed to classify EEG patterns in individuals diagnosed with major depressive disorder (MDD) and healthy controls (HC). Classification is conducted through multiple situations, specifically by considering the quantity of selected features and the

classification model used. The study assessed a total of 25, 50, and 75 selected attributes. The highest accuracy value was achieved by utilizing 25 selected characteristics in both the LSTM and Bi-LSTM models, out of the three features that were chosen. Regarding the investigation comparing the LSTM and Bi-LSTM classification models, the Bi-LSTM model achieved the highest accuracy value of 92.83%. In addition to offering superior precision, it utilizes a lower epoch value compared to LSTM. These results suggest that the combination of mRMR feature selection with 25 features and the Bidirectional LSTM classification model can be employed to categorize the EEG signals of patients with Major Depressive Disorder (MDD) and healthy control (HC) individuals. In order to enhance future study, it is desirable to incorporate supplementary attributes into the EEG signal and investigate alternative techniques for feature selection.

ACKNOWLEDGMENT

The author would like to acknowledge the research funding by Universitas Multimedia Nusantara under the grant of numbers 0037-RDLPPM-UMN/P-INT/II/2023.

REFERENCES

- [1] J. Heymann and A. Sprague, "Meeting the UN Sustainable Development Goals for mental health: why greater prioritization and adequately tracking progress are critical," World Psychiatry, vol. 22, no. 2, pp. 325–326, May 2023, doi: https://doi.org/10.1002/wps.21090.
- [2] M. É. Czeisler, "Mental Health, Substance Use, and Suicidal Ideation during the COVID-19 Pandemic," MMWR. Morbidity and Mortality Weekly Report, vol. 69, no. 32, Aug. 2020, doi: https://doi.org/10.15585/mmwr.mm6932a1.
- [3] H. Akbari, M. T. Sadiq, M. Payan, S. S. Esmaili, H. Baghri, and H. Bagheri, "Depression Detection Based on Geometrical Features Extracted from SODP Shape of EEG Signals and Binary PSO," *Traitement du Signal*, vol. 38, no. 1, pp. 13–26, Feb. 2021, doi: https://doi.org/10.18280/ts.380102.
- [4] W. Zhang, H. Zhang, J. Huang, H. Zhou, J. Yang, and N. Zhong, "Single-Channel EEG-Based Machine Learning Method for Prescreening Major Depressive Disorder," *International Journal of Information Technology and Decision Making*, vol. 18, no. 05, pp. 1579–1603, Sep. 2019, doi: https://doi.org/10.1142/s0219622019500342.
- [5] H. Cai et al., "A Pervasive Approach to EEG-Based Depression Detection," Complexity, vol. 2018, pp. 1–13, 2018, doi: https://doi.org/10.1155/2018/5238028.
- [6] D. A. Pizzagalli and A. C. Roberts, "Prefrontal cortex and depression," *Neuropsychopharmacology*, vol. 47, no. 1, Aug. 2021, doi: https://doi.org/10.1038/s41386-021-01101-7.
- [7] H. Cai et al., "A multi-modal open dataset for mental-disorder analysis," *Scientific Data*, vol. 9, no. 1, p. 178, Apr. 2022, doi: https://doi.org/10.1038/s41597-022-01211-x.

- [8] M. Pratiwi, Adhi Dharma Wibawa, and Mauridhi Hery Purnomo, "EEG-based Happy and Sad Emotions Classification using LSTM and Bidirectional LSTM," Jul. 2021, doi: https://doi.org/10.1109/icera53111.2021.9538698.
- [9] I. Grout, "Introduction to Digital Signal Processing," in *Digital Systems Design with FPGAs and CPLDs*, Elsevier Ltd, 2008.
- [10] M. Shouran and E. Elgamli, "Design and Implementation of Butterworth Filter," *Int. J. Innov. Res. Sci. Eng. Technol.*, vol. 9, 2020.
- [11] P. Boonyakitanont, A. Lek-uthai, K. Chomtho, and J. Songsiri, "A review of feature extraction and performance evaluation in epileptic seizure detection using EEG," *Biomedical Signal Processing and Control*, vol. 57, p. 101702, Mar. 2020, doi: https://doi.org/10.1016/j.bspc.2019.101702.
- [12] H. Nee. Oon, A. Saidatul, and Z. Ibrahim, "Analysis on Non-Linear Features of Electroencephalogram (EEG) Signal for Neuromarketing Application," 2018 International Conference on Computational Approach in Smart Systems Design and Applications (ICASSDA), Aug. 2018, doi: https://doi.org/10.1109/icassda.2018.8477618.
- [13] Z. Zhao, R. Anand, and M. Wang, "Maximum Relevance and Minimum Redundancy Feature Selection Methods for a Marketing Machine Learning Platform," *IEEE Xplore*, Oct. 01, 2019. https://ieeexplore.ieee.org/abstract/document/8964172.
- [14] M. Radovic, M. Ghalwash, N. Filipovic, and Z. Obradovic, "Minimum redundancy maximum relevance feature selection approach for temporal gene expression data," BMC Bioinformatics, pp. 1–14, 2017, doi: 10.1186/s12859-016-1423-9.
- [15] J. Du, Y. Cheng, Q. Zhou, J. Zhang, X. Zhang, and G. Li, "Power Load Forecasting Using BiLSTM-Attention," *IOP Conference Series: Earth and Environmental Science*, vol. 440, no. 3, p. 032115, Feb. 2020, doi: https://doi.org/10.1088/1755-1315/440/3/032115.
- [16] Silva and A. Alvarenga, "Comparing Long Short-Term Memory (LSTM) and bidirectional LSTM deep neural networks for power consumption prediction," *Energy Reports*, vol. 10, pp. 3315–3334, Nov. 2023, doi: https://doi.org/10.1016/j.egyr.2023.09.175.
- [17] P. Zhou, Z. Qi, S. Zheng, J. Xu, H. Bao, and B. Xu, "Text Classification Improved by Integrating Bidirectional LSTM with Two-dimensional Max Pooling," ACLWeb, Dec. 01, 2016..
- [18] S. Siami-Namini, N. Tavakoli, and Akbar Siami Namin, "A Comparative Analysis of Forecasting Financial Time Series Using ARIMA, LSTM, and BiLSTM," arXiv (Cornell University), Nov. 2019.
- [19] J. Yang, X. Huang, H. Wu, and X. Yang, "ScienceDirect ScienceDirect EEG-based classification based on Bidirectional International emotion Knowledge in the Long Short-Term Memory Network EEG-based classification based Bidirectional Jinru emotion Wu on Short-Term Memory Network," Procedia Comput. Sci., vol. 174, no. 2019, pp. 491– 504, 2020, doi: 10.1016/j.procs.2020.06.117.
- [20] I. Ariza, A. M. Barbancho, L. J. Tardón, and I. Barbancho, "Energy-based features and bi-LSTM neural network for EEG-based music and voice classification," *Neural Computing and Applications*, Oct. 2023, doi: https://doi.org/10.1007/s00521-023-09061-3.

AUTHOR GUIDELINES

1. Manuscript criteria

- The article has never been published or in the submission process on other publications.
- Submitted articles could be original research articles or technical notes.
- The similarity score from plagiarism checker software such as Turnitin is 20% maximum.
- For December 2021 publication onwards, Ultima Computing: Jurnal Sistem Komputer will be receiving and publishing manuscripts written in English only.

2. Manuscript format

- Article been type in Microsoft Word version 2007 or later.
- Article been typed with 1 line spacing on an A4 paper size (21 cm x 29,7 cm), top-left margin are 3 cm and bottom-right margin are 2 cm, and Times New Roman's font type.
- Article should be prepared according to the following author guidelines in this <u>template</u>.
 Article contain of minimum 3500 words.
- References contain of minimum 15 references (primary references) from reputable journals/conferences

3. Organization of submitted article

The organization of the submitted article consists of Title, Abstract, Index Terms, Introduction, Method, Result and Discussion, Conclusion, Appendix (if any), Acknowledgment (if any), and References.

Title

The maximum words count on the title is 12 words (including the subtitle if available)

Abstract

Abstract consists of 150-250 words. The abstract should contain logical argumentation of the research taken, problem-solving methodology, research results, and a brief conclusion.

Index terms

A list in alphabetical order in between 4 to 6 words or short phrases separated by a semicolon (;), excluding words used in the title and chosen carefully to reflect the precise content of the paper.

Introduction
 Introduction commonly contains the background, purpose of the research,

problem identification, research methodology, and state of the art conducted by the authors which describe implicitly.

Method

Include sufficient details for the work to be repeated. Where specific equipment and materials are named, the manufacturer's details (name, city and country) should be given so that readers can trace specifications by contacting the manufacturer. Where commercially available software has been used, details of the supplier should be given in brackets or the reference given in full in the reference list.

• Results and Discussion

State the results of experimental or modeling work, drawing attention to important details in tables and figures, and discuss them intensively by comparing and/or citing other references.

Conclusion

Explicitly describes the research's results been taken. Future works or suggestion could be explained after it

- Appendix and acknowledgment, if available, could be placed after Conclusion.
- All citations in the article should be written on References consecutively based on its' appearance order in the article using Mendeley (recommendation). The typing format will be in the same format as the IEEE journals and transaction format.

4. Reviewing of Manuscripts

Every submitted paper is independently and blindly reviewed by at least two peer-reviewers. The decision for publication, amendment, or rejection is based upon their reports/recommendations. If two or more reviewers consider a manuscript unsuitable for publication in this journal, a statement explaining the basis for the decision will be sent to the authors within six months of the submission date.

5. Revision of Manuscripts

Manuscripts sent back to the authors for revision should be returned to the editor without delay (maximum of two weeks). Revised manuscripts can be sent to the editorial office through the same online system. Revised manuscripts returned later than one month will be considered as new submissions.

6. Editing References

Periodicals

J.K. Author, "Name of paper," Abbrev. Title of Periodical, vol. x, no. x, pp. xxx-xxx, Sept. 2013.

Book

J.K. Author, "Title of chapter in the book," in Title of His Published Book, xth ed. City of Publisher, Country or Nation: Abbrev. Of Publisher, year, ch. x, sec. x, pp xxx-xxx.

Report

J.K. Author, "Title of report," Abbrev. Name of Co., City of Co., Abbrev. State, Rep. xxx, year.

Handbook

Name of Manual/ Handbook, x ed., Abbrev. Name of Co., City of Co., Abbrev. State, year, pp. xxx-xxx.

Published Conference Proceedings

J.K. Author, "Title of paper," in Unabbreviated Name of Conf., City of Conf., Abbrev. State (if given), year, pp. xxx-xxx.

Papers Presented at Conferences

J.K. Author, "Title of paper," presented at the Unabbrev. Name of Conf., City of Conf., Abbrev. State, year.

Patents

J.K. Author, "Title of patent," US. Patent xxxxxxx, Abbrev. 01 January 2014.

Theses and Dissertations

J.K. Author, "Title of thesis," M.Sc. thesis, Abbrev. Dept., Abbrev. Univ., City of Univ., Abbrev. State, year. J.K. Author, "Title of dissertation," Ph.D. dissertation, Abbrev. Dept., Abbrev. Univ., City of Univ., Abbrev. State, year.

Unpublished

J.K. Author, "Title of paper," unpublished. J.K. Author, "Title of paper," Abbrev. Title of Journal, in press.

On-line Sources

J.K. Author. (year, month day). Title (edition) [Type of medium]. Available: http://www.(URL) J.K. Author. (year, month). Title. Journal [Type of medium]. volume(issue), pp. if given. Available: http://www.(URL) Note: type of medium could be online media, CD-ROM, USB, etc.

7. Editorial Adress

Jl. Scientia Boulevard, Gading Serpong Tangerang, Banten, 15811 Email: ultimacomputing@umn.ac.id

Paper Title

Subtitle (if needed)

Author 1 Name¹, Author 2 Name², Author 3 Name²

¹ Line 1 (of affiliation): dept. name of organization, organization name, City, Country Line 2: e-mail address if desired

²Line 1 (of affiliation): dept. name of organization, organization name, City, Country Line 2: e-mail address if desired

Accepted on mmmmm dd, yyyy Approved on mmmmm dd, yyyy

Abstract—This electronic document is a "live" template which you can use on preparing your Ultima Computing paper. Use this document as a template if you are using Microsoft Word 2007 or later. Otherwise, use this document as an instruction set. Do not use symbol, special characters, or Math in Paper Title and Abstract. Do not cite references in the abstract.

Index Terms—enter key words or phrases in alphabetical order, separated by semicolon (;)

I. INTRODUCTION

This template, modified in MS Word 2007 and saved as a Word 97-2003 document, provides authors with most of the formatting specifications needed for preparing electronic versions of their papers. Margins, column widths, line spacing, and type styles are built-in here. The authors must make sure that their paper has fulfilled all the formatting stated here.

Introduction commonly contains the background, purpose of the research, problem identification, and research methodology conducted by the authors which been describe implicitly. Except for Introduction and Conclusion, other chapter's title must be explicitly represent the content of the chapter.

II. EASE OF USE

A. Selecting a Template

First, confirm that you have the correct template for your paper size. This template is for Ultima Computing. It has been tailored for output on the A4 paper size.

B. Maintaining the Integrity of the Specifications

The template is used to format your paper and style the text. All margins, column widths, line spaces, and text fonts are prescribed; please do not alter them.

III. PREPARE YOUR PAPER BEFORE STYLING

Before you begin to format your paper, first write and save the content as a separate text file. Keep your text and graphic files separate until after the text has been formatted and styled. Do not add any kind of pagination anywhere in the paper. Please take note of the following items when proofreading spelling and grammar.

A. Abbreviations and Acronyms

Define abbreviations and acronyms the first time they are used in the text, even after they have been defined in the abstract. Abbreviations such as IEEE, SI, MKS, CGS, sc, dc, and rms do not have to be defined. Abbreviations that incorporate periods should not have spaces: write "C.N.R.S.," not "C. N. R. S." Do not use abbreviations in the title or heads unless they are unavoidable.

B. Units

- Use either SI (MKS) or CGS as primary units (SI units are encouraged).
- Do not mix complete spellings and abbreviations of units: "Wb/m2" or "webers per square meter," not "webers/m2." Spell units when they appear in text: "...a few henries," not "...a few H."
- Use a zero before decimal points: "0.25," not ".25."

C. Equations

The equations are an exception to the prescribed specifications of this template. You will need to determine whether or not your equation should be typed using either the Times New Roman or the Symbol font (please no other font). To create multileveled equations, it may be necessary to treat the equation as a graphic and insert it into the text after your paper is styled.

Number the equations consecutively. Equation numbers, within parentheses, are to position flush right, as in (1), using a right tab stop.

$$\int_{0}^{r_2} F(r,\phi) dr d\phi = [\sigma r_2 / (2\mu_0)]$$
 (1)

Note that the equation is centered using a center tab stop. Be sure that the symbols in your equation have been defined before or immediately following the equation. Use "(1)," not "Eq. (1)" or "equation (1)," except at the beginning of a sentence: "Equation (1) is ..."

D. Some Common Mistakes

- The word "data" is plural, not singular.
- The subscript for the permeability of vacuum μ_0 , and other common scientific constants, is zero with subscript formatting, not a lowercase letter "o."
- In American English, commas, semi-/colons, periods, question and exclamation marks are located within quotation marks only when a complete thought or name is cited, such as a title or full quotation. When quotation marks are used, instead of a bold or italic typeface, to highlight a word or phrase, punctuation should appear outside of the quotation marks. A parenthetical phrase or statement at the end of a sentence is punctuated outside of the closing parenthesis (like this). (A parenthetical sentence is punctuated within the parentheses.)
- A graph within a graph is an "inset," not an "insert." The word alternatively is preferred to the word "alternately" (unless you really mean something that alternates).
- Do not use the word "essentially" to mean "approximately" or "effectively."
- In your paper title, if the words "that uses" can accurately replace the word using, capitalize the "u"; if not, keep using lower-cased.
- Be aware of the different meanings of the homophones "affect" and "effect," "complement" and "compliment," "discreet" and "discrete," "principal" and "principle."
- Do not confuse "imply" and "infer."
- The prefix "non" is not a word; it should be joined to the word it modifies, usually without a hyphen.
- There is no period after the "et" in the Latin abbreviation "et al."
- The abbreviation "i.e." means "that is," and the abbreviation "e.g." means "for example."

IV. USING THE TEMPLATE

After the text edit has been completed, the paper is ready for the template. Duplicate the template file by using the Save As command, and use the naming convention as below

ULTIMATICS_firstAuthorName_paperTitle.

In this newly created file, highlight all of the contents and import your prepared text file. You are

now ready to style your paper. Please take note on the following items.

A. Authors and Affiliations

The template is designed so that author affiliations are not repeated each time for multiple authors of the same affiliation. Please keep your affiliations as succinct as possible (for example, do not differentiate among departments of the same organization).

B. Identify the Headings

Headings, or heads, are organizational devices that guide the reader through your paper. There are two types: component heads and text heads.

Component heads identify the different components of your paper and are not topically subordinate to each other. Examples include ACKNOWLEDGMENTS and REFERENCES, and for these, the correct style to use is "Heading 5."

Text heads organize the topics on a relational, hierarchical basis. For example, the paper title is the primary text head because all subsequent material relates and elaborates on this one topic. If there are two or more sub-topics, the next level head (uppercase Roman numerals) should be used and, conversely, if there are not at least two sub-topics, then no subheads should be introduced. Styles, named "Heading 1," "Heading 2," "Heading 3," and "Heading 4", are prescribed.

C. Figures and Tables

Place figures and tables at the top and bottom of columns. Avoid placing them in the middle of columns. Large figures and tables may span across both columns. Figure captions should be below the figures; table heads should appear above the tables. Insert figures and tables after they are cited in the text. Use the abbreviation "Fig. 1," even at the beginning of a sentence.

TABLE I. TABLE STYLES

Table	Table Column Head			
Head	Table column subhead	Subhead	Subhead	
copy	More table copy			

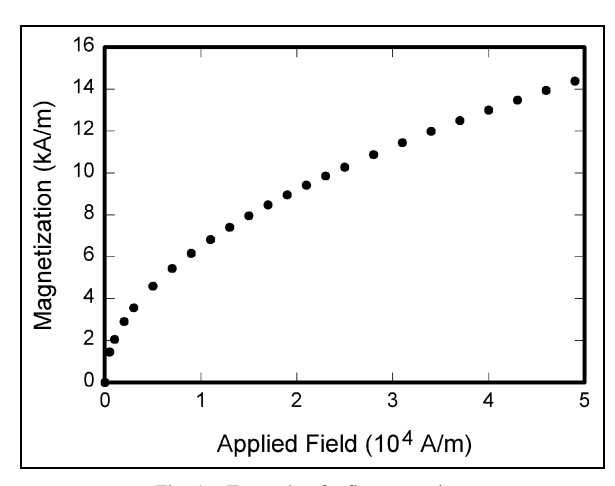


Fig. 1. Example of a figure caption

V. CONCLUSION

A conclusion section is not required. Although a conclusion may review the main points of the paper, do not replicate the abstract as the conclusion. A conclusion might elaborate on the importance of the work or suggest applications and extensions.

APPENDIX

Appendixes, if needed, appear before the acknowledgment.

ACKNOWLEDGMENT

The preferred spelling of the word "acknowledgment" in American English is without an "e" after the "g." Use the singular heading even if you have many acknowledgments. Avoid expressions such as "One of us (S.B.A.) would like to thank" Instead, write "F. A. Author thanks" You could also state the sponsor and financial support acknowledgments here.

REFERENCES

The template will number citations consecutively within brackets [1]. The sentence punctuation follows the bracket [2]. Refer simply to the reference number, as in [3]—do not use "Ref. [3]" or "reference [3]" except at the beginning of a sentence: "Reference [3] was the first ..."

Number footnotes separately in superscripts. Place the actual footnote at the bottom of the column in which it was cited. Do not put footnotes in the reference list. Use letters for table footnotes.

Unless there are six authors or more give all authors' names; do not use "et al.". Papers that have not been published, even if they have been submitted for publication, should be cited as "unpublished" [4]. Papers that have been accepted for publication should be cited as "in press" [5]. Capitalize only the first word in a paper title, except for proper nouns and element symbols.

For papers published in translation journals, please give the English citation first, followed by the original foreign-language citation [6].

- G. Eason, B. Noble, and I.N. Sneddon, "On certain integrals of Lipschitz-Hankel type involving products of Bessel functions," Phil. Trans. Roy. Soc. London, vol. A247, pp. 529-551, April 1955. (references)
- [2] J. Clerk Maxwell, A Treatise on Electricity and Magnetism, 3rd ed., vol. 2. Oxford: Clarendon, 1892, pp.68-73.
- [3] I.S. Jacobs and C.P. Bean, "Fine particles, thin films and exchange anisotropy," in Magnetism, vol. III, G.T. Rado and H. Suhl, Eds. New York: Academic, 1963, pp. 271-350.
- [4] K. Elissa, "Title of paper if known," unpublished.
- [5] R. Nicole, "Title of paper with only first word capitalized," J. Name Stand. Abbrev., in press.
- [6] Y. Yorozu, M. Hirano, K. Oka, and Y. Tagawa, "Electron spectroscopy studies on magneto-optical media and plastic substrate interface," IEEE Transl. J. Magn. Japan, vol. 2, pp. 740-741, August 1987 [Digests 9th Annual Conf. Magnetics Japan, p. 301, 1982].
- [7] M. Young, The Technical Writer's Handbook. Mill Valley, CA: University Science, 1989.



ISSN 2355-3286



Universitas Multimedia Nusantara Scientia Garden Jl. Boulevard Gading Serpong, Tangerang Telp. (021) 5422 0808 | Fax. (021) 5422 0800